Model studies of plasma heating in the continuous casting tundish.

BARRETO SANDOVAL, Jose de Jesus.

Model Studies of Plasma Heating in the Continuous Casting Tundish

José de Jesús Barreto Sandoval

A thesis submitted in partial fulfilment of the requirements of
Sheffield Hallam University
for the degree of Doctor of Philosophy

April 1993

Collaborating Organisation: BOC

To: *Adriana and Daniel*

Who sometimes wondered what I did all day

ACKNOWLEDGEMENTS

I would like to acknowledge the influence of Professor A W D Hills for his contagious enthusiasm for the subject, originality, superb teaching skills, continuous guidance and encouragement. Dr. D M Allen-Booth for his receptivity, encouragement, and his valuable ideas. Who as supervisors, both have a great share of my acknowledgements concerning to this work.

Particular thanks to Mr. N. Dziemidko for his continuous assistance and help during the experimental work, and for his friendship during the completion of this thesis.

I also would like to thank Mr. B. Palmer and Mr. R. Wilkinson for their ready availability and assistance during the experimental work.

To my fellow students, at the School of Engineering for their help and friendship at various stages of the work. Particular thanks to C. Brashaw for his friendship, long discussions and his help during the writing-up stage.

Technicians, administrative staff, secretaries, librarians, and other members of the staff at Sheffield Hallam University for their prompt and efficient services.

CONACYT - Mexico, for the financial support.

I am grateful to my wife Adriana for her constant encouragement, patience, toleration of odd working hours and putting me through. And thanks to Daniel for waking me up early every morning.

ABSTRACT

A room temperature water model of a tundish was design, constructed and operated. The model was equipped with a steam heating system that simulates that simulates the tundish plasma heating systems operated by some of the more modern continuous casting plants. Similarity between steam heating in the water model and plasma heating in the tundish has been established. A dimensionless criterion was developed to validate the simulation experiments and its represented by the plasma heating number. Using this similarity criterion plasma heating can be simulated by steam heating in an appropriately designed water model.

A theoretical dispersion model has been formulated for the flow through the tundish and the parameters in this model determined from the results obtained from residence time distribution measurements. A conductivity method was used, a highly conducting species being injected at the inlet point and changes in conductivity monitored at the exit. Measurements were also made of the changes in temperature at the exit resulting both from changes in temperature of the inlet stream and from the use of steam heater system.

A stable inverse heat conduction method has been developed in which the measured and estimated temperature are analysed in terms of a steady components of short duration. A finite difference method has been used to predict the effect on a thermocouple temperature of the deviatory components of the liquid steel temperature. The incorporation of these predictions into look-up tables has allowed an algorithm to be developed thet can deduce the current deviatory component of the steel temperature from the thermocouple response.

CONTENTS

LIST OF SYMBOLS

SYMBOL	MEANING	SI UNITS
A	area	m^2
C	concentration	kmol m^{-3}
C_p	heat capacity	J kg^{-1} $°K^{-1}$
C_θ	dimensionless concentration	[-]
C_{mean}	mean concentration	kmol m^{-3}
D_i	longitudinal dispersion coefficient	m^2 s^{-1}
d	distance	m
d	nozzle diameter	m
d_f	depth of fluid in the tundish	m
d_p	depth of penetration of the heat wave	m
F	flow rate of molten steel	kg Sec^{-1}
F_θ	dimensionless fractional temperature	[-]
g	acceleration due to gravity	m s^{-2}
h	fluid depth	m
h	heat transfer coefficient	W m^{-2} $°K^{-1}$
K	total kinematic energy	J
k	thermal conductivity	W m^{-1} $°K^{-1}$
L	characteristic length	m
L_D	plasma heater "dog-house" length	m
l	Prandtl mixing length	m
l_f	length scale factor	
$\dot{Q}$"	flow rate	m^3 s^{-1}

SYMBOL	MEANING	SI UNITS
$\dot{Q}"_f$	flow rate scale factor	[-]
$\dot{q}"$	heat flux	W m^{-2}
r	distance from the centre line	m
T	temperature	°C
t	time	s
t_f	time scale factor	[-]
t	mean residence time	s
u	velocity	m s^{-1}
V	stream velocity	m s^{-1}
V_f	velocity factor	m s^{-1}
V	volume	m^3
V_{dead}	dead volume of the tundish	m^3
V_{mixed}	mixed volume of the tundish	m^3
V_{plug}	plug flow volume of the tundish	m^3

Greek Characters

α	thermal diffusivity	m^2 s^{-1}
β	constant	
β_θ	temperature coefficient of volume expansion	$°K^{-1}$
ε	rate of dissipation of turbulence kinematic	J $Kg^{-1}s^{-1}$
	energy/unit mass of fluid	or m^2 s^{-3}
μ	molecular viscosity	m^2 s^{-1}
μ_t	turbulent viscosity	Pa s
μ_{eff}	effective viscosity	Pa s

SYMBOL	MEANING	SI UNITS
υ	kinematic viscosity	Pa s
Θ^S	"steady state" surface temperature	°C
Θ^M	measured temperature	°C
Θ^i	current partial temperature	°C
Θ^i_M	deviatory temperature measured	°C
Θ_{SURF}	current estimate of surface temperature	°C
θ	temperature	°C
$\Delta\theta$	average rise in fluid temperature resulting from heat input	°C
Θ	dimensionless sampling time	[-]
ρ	mass density	Kg m^{-1}
σ	variance	[-]
σ	surface tension	N m^{-1}
$\Delta\tau$	temperature pulse duration - time interval	s
τ	dimensionless time	[-]
τ_p	characteristic dwell time by the fluid beneath the plasma heater "dog-house"	s

1

INTRODUCTION

1.1 FOREWORD

The temperature of liquid steel during the continuous casting is one of the basic indicators of operation and quality control. In the past decade, the requirements for high quality steel have increased dramatically, with more emphasis on superheat control and an ever need for better automation. Auxiliary heating and continuous temperature measurement in the tundish have become indispensable technologies for the modern continuous casting process.

It has been long recognized that superheat plays a key role in determining the structure and properties of continuously cast products, therefore to achieve quality and ease of operation the casting temperature must be controlled as closely as possible.

Low temperatures of tundish superheat promotes fine equiaxed grains in the largest part of the section, consequently the segregated areas are small in size and distributed in the volume, thus preferred microstructures can be achieved with low tundish superheat. On the other hand, as the tundish superheat is increased, the index of micro-inclusions is reduced, this effect might be assumed to be due to the decrease in viscosity at higher temperatures. An optimum tundish superheat is one that tends to minimize chemical segregation and the occurrence of inclusions in the product yet avoids freezing-off problems.

1.2 THE OBJECTIVE OF THE INVESTIGATION

The basic objective of the present work is to investigate whether the temperature at which liquid steel enters the mould of a continuous casting machine can be controlled dynamically from indirect measurements of liquid steel temperature at a point of entry to the tundish.

This consist of:

(i) Studying the fluid flow of liquid steel through a tundish using water modelling techniques.

(ii) Modelling plasma heating using a steam jet in the water analogue model.

(iii) Measuring residence times distribution from tundish inlet to outlet.

(iv) Measuring residence times distribution from heater to tundish outlet.

(v) Matching applied heat to input "steel" temperature to maintain constant output temperature.

(vi) Developing a device sensor system to monitor input and output temperatures continuously.

2

LITERATURE SURVEY

2.1. GENERAL OVERVIEW

In the past couple of decades, it has been recognized that tundish superheat and the melt flow in tundishes has a marked influence on the quality of steel. Thus many steel companies and research laboratories have employed mathematical and physical modelling to simulate melt flow in tundishes. An importan recente development in tundish design has been the consideration of plasma heating and continuous temperature measurement to control tundish superheat.

In order to understand the effectiveness of providing thermal energy supplied at the top of the steel flowing in the tundish and to study its response and controllability, it is important to appreciate the key developments of previous works.

The objective of the present literature survey is not to be an exhaustive review of the literature, but rather to enable the experimental results and conclusions to be considered in their right perspective, and to serve as a basis on which the new ideas and theories will be developed.

(a) Development of continuous casting.

Continuous casting has become an increasingly important step in the manufacture of steel in the past two decades. The continuous casting process is increasingly replacing the conventional ingot casting route for the manufacture of finished steel products worldwide, because of the inherent advantages. They are, principally:

i).- Energy savings and the potential for reducing energy consumption through hot charging of continuously cast products to the rolling mill furnace.

ii).- Increased productivity, 10% and more higher yield compared to conventional ingot casting.

iii).- Higher quality and more uniform final product.

iv).- Reduced operating, capital and depreciation costs.

v).- Improved safety and working conditions for the operators.

vi).- Good environmental conditions.

vii).- Process suited for integral automation.

Because of the increased productivity and the operating costs benefits, it is expected that the continuous casting process will dominate the production scheduled of most steelmaking plants in the near future, especially in the view of the technological development under way.

(b) Quality requirements for the continuously cast products.

Concurrent with the development of the continuous casting technology, the quality requirements of the final steel product have become very stringent. These quality aspects - mainly surface finish and internal cleanness - have become determining with the gradually increasing machine throughputs and larger products dimensions. Therefore, steel cleanness, tundish superheat and strict composition control are now the primary concern of steelmakers. After investigation, it has been recognized that the interaction between the three processing parameters: temperature, composition, and fluid flow, determine the processing response in terms of both quality and productivity. Several authors have found that the melt flow in tundishes has a marked influence on the quality of cast steel products.

2.2. FLUID FLOW ASPECTS OF TUNDISH OPERATIONS

Fluid flow behaviour plays an important role in the whole process of continuous casting with regard to the quality of the final product, the ease of operation and productivity. Fluid flow in steelmaking tundish vessels has been the subject of extensive study, the approaches used have included mathematical modelling, physical modelling and radioactive tracer studies.

(a) Mathematical modelling

Mathematical modelling has been stimulated in recent years by the ready availability of computer facilities and software packages to predict flow patterns in tundish systems.

However, the fundamental equations which describe fluid flow are often too complex to be solved even using large computers, since the computations require the simultaneous solution of a number of highly non-linear equations. For instance, the continuity and the three components of the Navier-Stokes equations fully describe fluid flow behaviour, but they are extremely complex and their solution requires simplifications and assumptions to be made about a number of aspects, for example the choice of a turbulence model to represent the effective viscosity and the treatment of the boundary conditions and numerical methods of solution. The fundamental equations and the simplifications and assumptions chosen, make up a mathematical model. It is obvious that such mathematical models need to be validated against experimental measurements.

Several such models have been developed to represent fluid flow in continuous casting tundishes, involving the solution of two and three-dimensional Navier-Stokes and the continuity equations.

The model developed by Debroy and Sychterz[1] is a two-dimensional one, the flow being assumed isothermal, incompressible and steady. Flow predictions are based on

the Navier-Stokes equations in two-dimensions. For the computation of the turbulent viscosity, μ_t, the hypothesis of mixing length given by Prandtl is used, which is written as:

$$\mu_t = \rho l^2 \left(\frac{\partial u}{\partial y}\right) \tag{2.1}$$

Where: ρ: density of the medium

μ_t: turbulent viscosity

l: Prandtl mixing length

$(\partial u/\partial y)$: Absolute value of the velocity gradient along a direction perpendicular to the direction of flow

The mixing length is defined as:-

$$l = 0.4d \tag{2.2}$$

Where: d: is distance to the nearest wall

The effective viscosity is expressed as:-

$$\mu_{eff} = \mu_t + \mu \tag{2.3}$$

Where: μ_{eff}: Effective viscosity

μ: Molecular viscosity of the medium

A three dimensional mathematical model was introduced by Tanaka et. al.[2] to predict fluid flow patterns in tundish systems. The fundamental equations used were the continuity and the three-dimensional turbulent Navier-Stokes equations, incorporating the K-ϵ turbulence model of Jones and Launder[3,4] to calculate the turbulent viscosity. There, turbulence is expressed by two transport equations for the turbulence kinematic energy K and its rate of dissipation ϵ. The relation between μ_t and the two turbulence characteristics is:-

$$\mu_t = K_1 \rho K^2 / \epsilon \tag{2.4}$$

The governing equations for K and ϵ are, respectively:-

$$\frac{\partial}{\partial x_i}\left(\rho u_i K - \frac{\mu_{eff}}{\sigma_K}\frac{\partial K}{\partial x_i}\right) = G - \rho\epsilon \tag{2.5}$$

$$\frac{\partial}{\partial x_i}\left(\rho u_i \epsilon - \frac{\mu_{eff}}{\sigma_\epsilon}\frac{\partial \epsilon}{\partial x_i}\right) = \left(K_2 G - K_3 \rho \epsilon\right)\frac{\epsilon}{K} \tag{2.6}$$

Where:

$$G = \mu_t \frac{\partial u_j}{\partial x_i}\left(\frac{\partial u_j}{\partial x_i} + \frac{\partial u_i}{\partial x_j}\right) \tag{2.7}$$

K: Turbulent kinetic energy

ϵ: Rate of dissipation of turbulent kinetic energy

G: Generation of turbulent energy

μ_{eff}: Effective viscosity

μ_t: Turbulent viscosity

K_1, K_2, K_3, σ_K, σ_ϵ: Empirical constants

The above equations were solved together with boundary conditions. The results were found to be in good agreement with the experimental results obtained from a one-sixth scale water model.

Similar mathematical models have been developed by Lai et. al.[5] and by Szekely, Ilegbusi and El-Kaddah[6,7] to study fluid flow in tundishes when flow control devices, such as dams and weirs, were employed. Another one was developed by He and Sahai[8,9] to study the effect of tundish wall inclination on the fluid flow and mixing, the results found were in good agreement with those measured experimentally in a one-third scale water model. More recently, Sahai and co-workers[10] have shown the influence of the finite difference grid spacing on the predicted fluid flow and the residence time distribution by comparison of computed results from the K-ϵ model of turbulence and water model experiments in the tundish systems.

The solution procedures of the mathematical models of fluid flow in steelmaking tundishes are mainly through the solution of finite difference equations which are derivided from the governing differential equations. Thus the methods involve the derivation of finite difference formulations from the differential equations and boundary conditions as well as methods for solving the resulting set of simultaneous non-linear equations. Nowadays, some of the methods for the solution of the fundamental equations of turbulent two and three-dimensional flow, such as those encountered in tundish operations, have been embodied in computational fluid dynamics packages, such as **PHOENICS, TEACH(2D,3D), FLUENT, FLOW3D, FLOW-3D, FLOWDIA, etc.**

(b) Physical modelling

The flow of liquid steel in a steelmaking tundish systems is very difficult to observe directly, with the exception of open pouring streams. The application of mathematical modelling is often too complicated by the occurrence of turbulence in some regions of the system. Thus, physical modelling, using water models, is an attractive alterative for the study of fluid flow in the tundish and mould. The key requirement for the physical model to represent the real system, or the prototype is to achieve the criteria for similarity.

There exist many states of similarity; however, to obtain similarity between two flowing systems the following four conditions must satisfied:

i) Geometric similarity

Geometric similarity is the similarity of shape. Systems are geometrically similar when the ratio of any length in one system to the corresponding length in the other system is everywhere the same. This ratio is usually termed the scale factor.

ii) Kinematic similarity

Kinematic similarity represents the similarity of motion. The streamlines in one system are geometrically similar to the streamlines of the other system.

iii) Dynamic similarity

Dynamic similarity represents the similarity of forces. The magnitude of forces at corresponding location in each system is in a fixed ratio.

iv) Thermal similarity

The dimentionless numbers involving heat transfer are equal in both systems.

Kinematic similarity between prototype and model is ensured if geometric and dynamic similarities are observed. The principal forces to be considered in obtaining dynamic similarity in the tundish are inertial, gravitational, viscous and surface tension forces.

The principal dimentionless groups which involve these forces are given by:

$$Froude\ No \quad Fr = \frac{V^2}{gL} = \frac{inertial\ force}{gravitational\ force}$$

$$Reynolds\ No \quad Re = \frac{VL}{\upsilon} = \frac{inertial\ force}{viscous\ force}$$

$$Weber\ No \quad We = \frac{\rho V^2 L}{\sigma} = \frac{inertial\ force}{surface\ tension\ force}$$

Where:
- V: Stream velocity
- g: Gravity
- L: Characteristic length
- ν: Kinematic viscosity
- σ: Surface tension
- ρ: Density

Absolute dynamic similarity requires that each of the dimensionless groups listed above have the same value in both the model and the prototype. Due to the difference of the physical properties of water at room temperature and molten steel, table 2.1, it is impossible to satisfy simultaneously all of the requirements for similarity which applies to fluid flow in the same model of a given particular scale. Reynolds-Froude similarity

requires a full scale model. The Weber-Froude similarity requires a model of 0.6 scale. Some numerical values for the applicable dimensionless groups are presented in table 2.2.

TABLE 2.1 Physical properties of water at 20°C and steel at 1600°C.

Property	Water (20°C)	Steel (1600°C)
Absolute Viscosity (cp)	1	6.40
Density (g/cm^3)	1	7.08
Kinematic Viscosity (cs)	1	0.90
Surface Tension (dyne/cm)	7.3	1600

TABLE 2.2 Calculated values for various dimensionless grups in the steel and water model systems.

Number	Steel System	Full Scale Water Model
Reynolds	1	1.1
Froude	1	1.0
Weber	1	3.1
Morton	1	44.0
Modified Froude	1	7.0

It has been demonstrated by Heaslip et. al.[11] that the Froude number can be satisfied at any scale in a tundish water model as long as all metering orifices and fluid hydraulic heads in the system are varied in accordance with a single scaling parameter. To decide

requires a full scale model. The Weber-Froude similarity requires a model of 0.6 scale. Some numerical values for the applicable dimensionless groups are presented in table 2.2.

TABLE 2.1 Physical properties of water at 20°C and steel at 1600°C.

Property	Water (20°C)	Steel (1600°C)
Absolute Viscosity (cp)	1	6.40
Density (g/cm^3)	1	7.08
Kinematic Viscosity (cs)	1	0.90
Surface Tension (dyne/cm)	7.3	1600

TABLE 2.2 Calculated values for various dimensionless grups in the steel and water model systems.

Number	Steel System	Full Scale Water Model
Reynolds	1	1.1
Froude	1	1.0
Weber	1	3.1
Morton	1	44.0
Modified Froude	1	7.0

It has been demonstrated by Heaslip et. al.[11] that the Froude number can be satisfied at any scale in a tundish water model as long as all metering orifices and fluid hydraulic heads in the system are varied in accordance with a single scaling parameter. To decide

what scale of model should be used, the extent to which similitude is necessary in modelling the actual system must be considered.

(i) Experimental methods.

The experimental methods used to study fluid flow in the continuous casting tundish via water modelling are the stimulus-response method and the elapsed-time photographic technique.

The residence time distribution, this is the departure of actual residence times from the mean, of the fluid flowing through a tundish can be determined by the use of the stimulus-response method. Basically, this involves the addition of a tracer, such as a dye or a chemical substance, to the stream entering the tundish and then measurement of the concentration at the exit. Several techniques have been developed for introducing the tracer material into the system, but the most important are the step input and the pulse input. These have been described by Levenspiel[41].

When taking pictures of the fluid flow pattern in water models, the following techniques are available for fluid flow visualization:

i) Particle-addition into the water system

ii) Dye injection into the stream

iii) Use of a slit light source to illuminate the fluid flow domain two-dimensionally.

For the quantitative description of the fluid flow pattern, the following methods can be used to measure the flow velocity at certain points of the domain:

i). Impact tube and static pressure tap with manometer.

ii). Form drag strain gauge system with strain amplifier and recorder.

iii). Laser doppler anemometry

iv). Thermistor probe.

v). Hot film anemometry

vi). Stroboscopic photography.

The literature describing water modelling using the above experimental methods to describe fluid flow in tundishes is extensive.

A full scale water model of a slab caster tundish has been used by Kemeny et al.[12] so that Reynolds and Froude similarity criteria could be satisfy simultaneously. It was found that flow into a tundish from a poured ladle stream was not beneficial to product quality owing to air and slag entrapment within steel. Stagnant regions were present which prevented a significant portion of the tundish volume being usefully used. This naturally lowered mean residence times within the tundish from those nominally expected, hindering effective separation of buoyant non-metallic particles from the molten steel before draining into the mould.

Weirs were found to be effective in confining the turbulence generated by the ladle stream to the impingement zone itself. The liquid surface in the remainder of the

tundish was smooth, allowing the presence of a coherent protective layer of slag. It was also shown that with proper weir placement, stagnant areas could be eliminated and mean residence time within the tundish could increased. Dams were shown to be more effective than weirs in damping surges in metal flow. As these methods successfully increased the retention time greatly, the authors argued that the separation of non-metallic particles would be greatly enhanced.

A one-third scale water model of a typical slab tundish was used by Sahai and Ahuja[13] to investigate the effects of various flow control devices, such dams, weirs, slotted dams and submerged gas injection, on the flow characteristics. In this study, the Froude number similarity was maintained between the model and the prototype.

It was shown that in open stream pouring, the plunging jet entrains significant volume of air or gas, in an inert gas shrouded stream. The entrained air causes a strong upward buoyancy force and the liquid flow in this region is reversed. The liquid stream loses its downward momentum on entering the tundish and reverses to the free surface, where it flows downstream towards the tundish-mould nozzle.

It was found that in a tundish without any flow control devices a stagnant volume of about 23%. Whilst the use of a weir helped to push the liquid down, thus reducing the dead region found in the previous case. Nevertheless, this weir created a dead region behind it, and the stagnant volume was calculated as 17%. The addition of a dam further increased the dead volume to about 27% and a similar situation was created by

the use of one or two slotted dams. Each of this physical control devices created a slow secondary recirculation in the downstream region behind the device. The use of gas injection in conjunction with the physical control devices decreased the dead volume by activating the slow recirculating liquid and considerably increased the dispersed plug/dead volume ratio. Gas injection, however, did not have much effect on the mixed volume fraction. The gas stream acted as a barrier to longitudinal mixing but contributed to fluid mixing in the vertical direction. The completely mixed volume fraction varied from approximately 0.45 to 0.52 for various configuration studied.

This study also shows that during submerged stream pouring, liquid enters the pool with sufficient downward momentum to carry it right to the bottom. The configurations with no flow control devices have a slightly smaller dead zone of about 17%. Addition of a weir or a dam at the given positions increased the dead volume for reasons similar to those of open stream pouring. Again, it was found that the gas injection did not increase substantially the mixed volumes in the tundish.

Similar approaches towards improving flows in the tundish of a slab caster at the Kashima works of Sumitomo, were suggested, based on water model experiments by Hashio et. al.[14], a variation of shapes and depths of liquid tundishes were proposed. Dobson et. al.[15] also carried out similar experiments in reduced and full scale water models of two different tundishes in use by BHP, Australia. They solved the three-dimensional Navier-Stokes equation in a transient mode to describe the fluid flow, incorporating the physical model results into the mathematical treatment to predict

improved flow control device placements and geometries in actual plant tundishes. Significant improvements are reported.

(c) Radioactive tracer studies

In contrast to the large number of reported investigations concerned with mathematical and physical modelling studies, the open literature available on the radioactive tracer studies in operating tundishes is rather scanty. Measurements on a plant scale are highly desirable, but not straightforward.

Martinez et. al.[16] presented a comparison between water modelling test results and tracer measurements in real systems. The pulse input technique was used to determine residence time diagrams, for water models and for the experiments with Cu^{64} in the real tundish. The residence time distribution curves obtained from a one-third scale water model and from a 12-tonnes tundish of a five-strand billet caster machine are presented in figure 2.1, where it is shown to give good agreement in one case and moderately good agreement in the other between the water model and the real system.

Van der Heiden and co-workers[17] carried out similar experiments to study the flow behaviour of liquid steel in a boat-shaped tundish with a capacity of 60 ton, in order to improve the separation of inclusion particles. Copper tracer was added using step input techniques, for this the copper content in an intermediate ladle in a sequence casting was raised to a level significantly different from the preceding and succeeding ladles

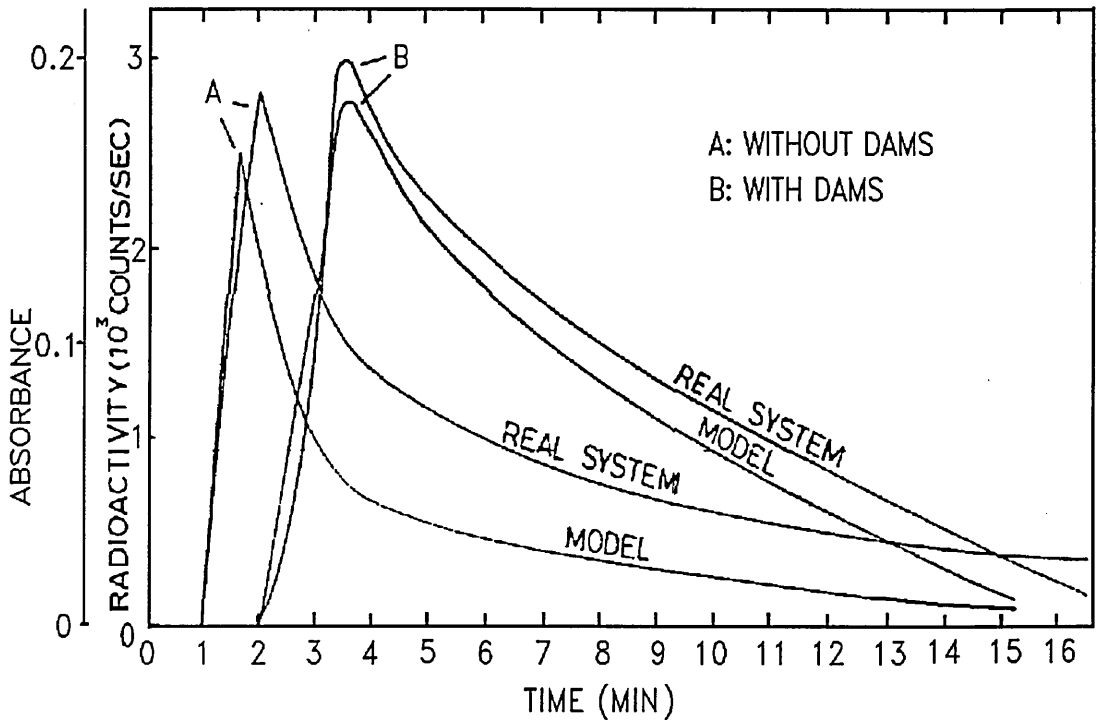

Figure 2.1. Residence time diagrams for real system and model (⅓ scale). (From Martinez et. al. 1986)

in the period near the ladle change. The copper concentration was determined by sampling the mould at 15 seconds intervals, the residence time distributions are presented in figures 2.2 and 2.3, for the absence of flow control arrangements and in the presence of flow control arrangements, respectively. In this real system it was also found that applying dam and weirs the minimum residence is increased, and it was argued that the separation of oxide particles may be improved.

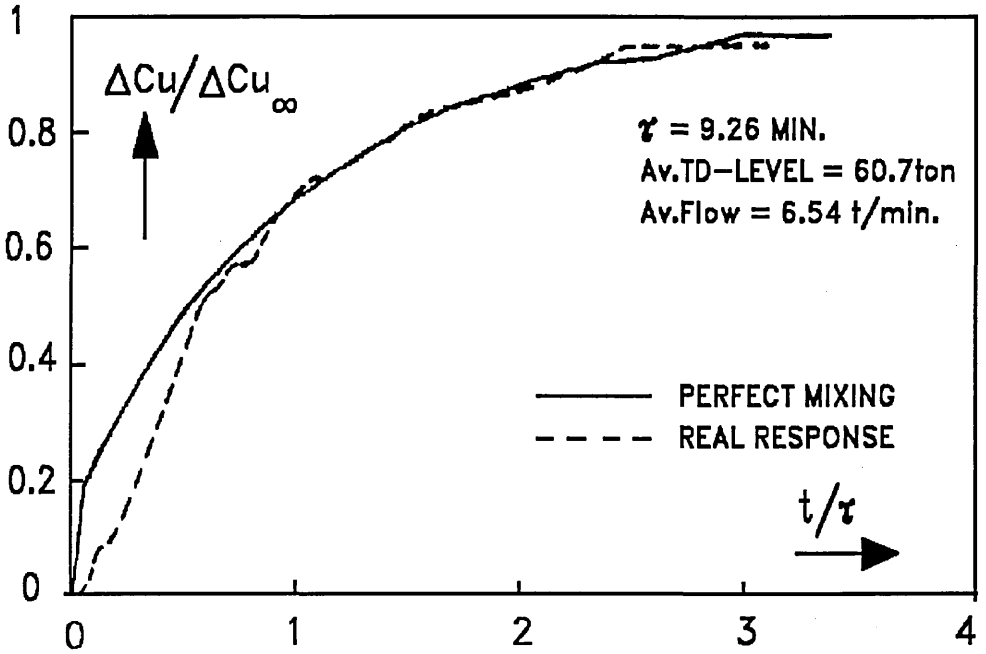

Figure 2.2. Step response of the tundish without obstacles; Cu (tracer): 0.012% to 0.070%. (From Van der Heiden et.al. 1986)

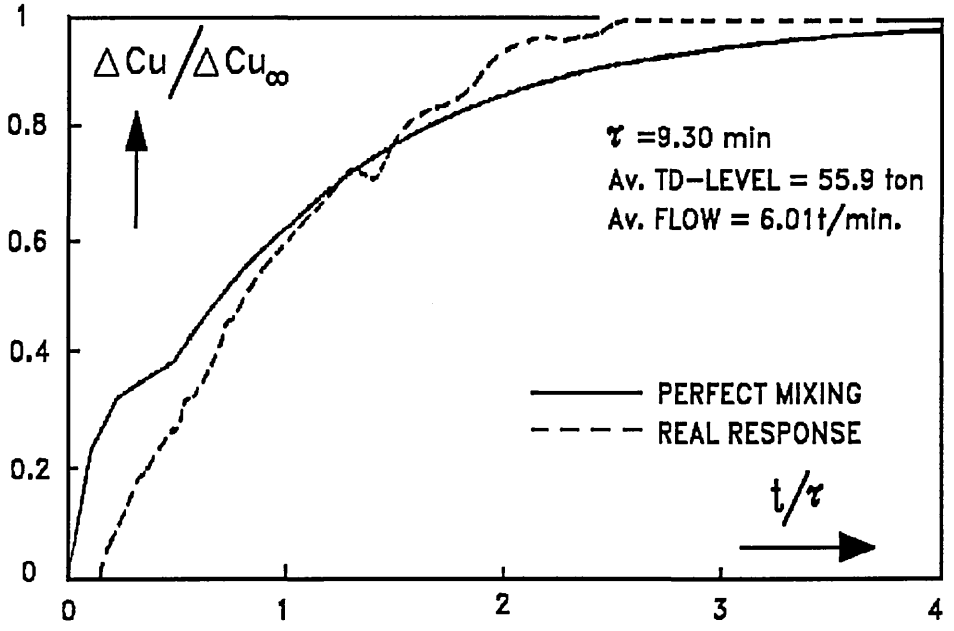

Figure 2.3. Response of the tundish with weirs and dams; Cu (tracer): 0.010% to 0.070%. (From Van der Heiden et.al. 1986)

The results of this investigation have been compared to theoretical predictions by Ilegbusi and Szekely[18]. The K-ϵ model was employed and the results were generated using the PHOENICS code. Figures 2.4 and 2.5 show the comparison between the experimentally measured and the theoretically predicted "F" curves, that is the response of the system to a step change of tracer concentration. It is seen that reasonably good agreement is obtained in both cases.

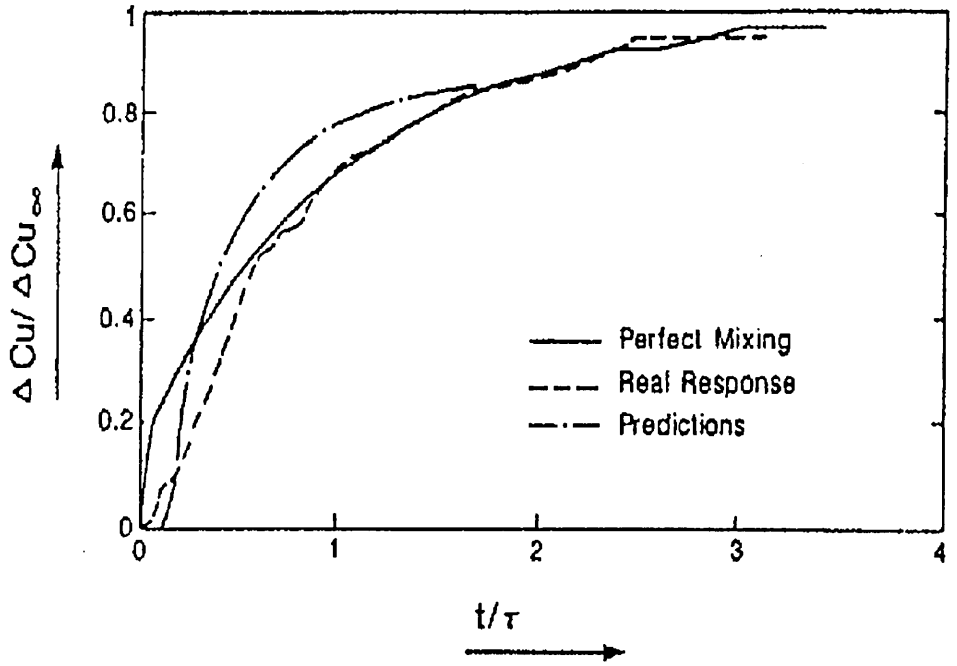

Figure 2.4. Measured and predicted response of steel system to a step change in a tracer concentration in the absence of the flow control. (From Ilegbusi et.al. 1988)

More recently Lowry and Sahai[19] investigated the effect of multiple-hole baffles on the steel flow in a six-strand tundish using tracer measurements, mathematical and water modelling. The research concentrated on measurements and calculation of the residence time distribution in a real "T"-shaped tundish, in a one-third water analogue model of

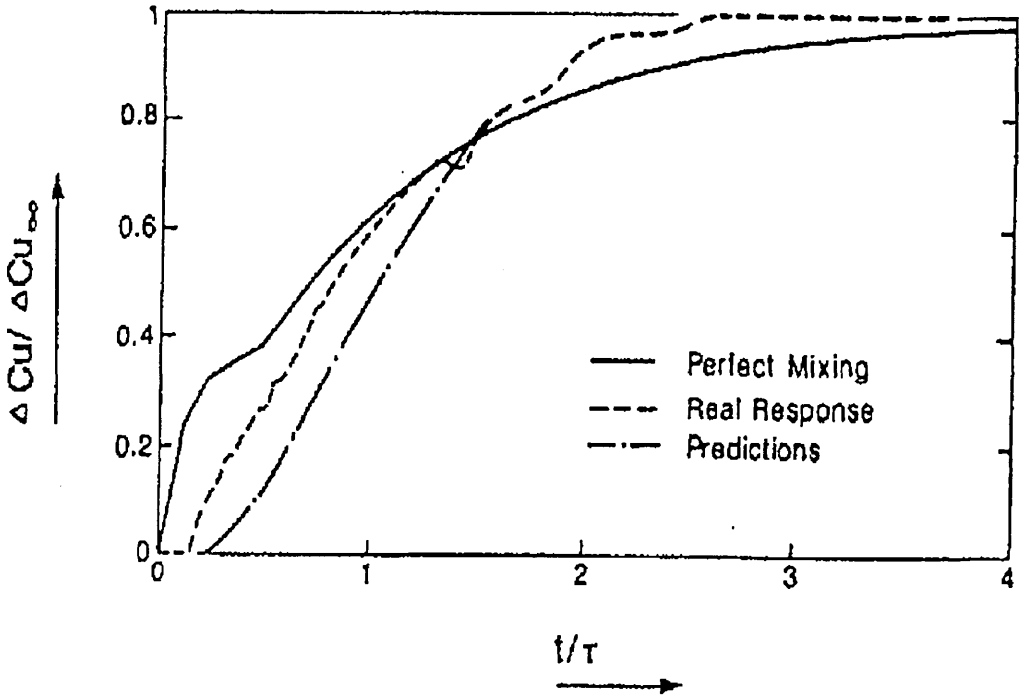

Figure 2.5. Measured and predicted response of steel system to a step change in tracer concentration in the presence of flow control. (From Ilegbusi et.al. 1988)

the real system and by calculation using the K-ϵ turbulence model equations. A symmetrical half of the "T"-shaped tundish was considered for the computations.

The results presented from the actual tundish trials show that adding baffles to the system alters the flow in the tundish, increasing the mean residence time for the steel to the inside nozzle, accompanied by a slight decrease in residence time to the outside nozzle. This effects on the flow produced a more uniform distribution of liquid steel to different nozzles in the tundish.

Good similarity was found between the results obtained by tracer studies and mathematical and water modelling. However, comparing the mean residence time for the nozzles, the mathematical model results were somewhat different quantitatively, especially for the outside nozzles. The results of the water model and that of the actual tundish are in better agreement with the mathematical model, which predicted higher residence times in both inner and outer nozzles.

Lowry and Sahai argue that the discrepancies among the water model, mathematical model and the actual tundish are that the tracers used had higher density than the fluid, and tended to flow closer to the bottom, reaching the nozzle faster. For the mathematical model the density is constant changing the concentration only. Also, the temperature of molten steel is higher close to the ladle stream and therefore its density is lower. This density difference in the liquid produces a buoyancy force which acts to modify the fluid flow in the tundish.

For the inner nozzles a smaller discrepancy among tracer experiments and the theoretical model was shown, which was explained by the combination of effects in the real tundish not characteristic of the model, the incoming steel is hotter and less dense than the melt in the tundish, causing it to flow up towards the free surface, and the dense copper tracer would have the tendency to bring the copper-containing melt down. These two effects seem to neutralize each other and the residence time distribution predicted by the mathematical model is very close to that of the actual tundish.

The main discrepancy was found in the residence time distribution in the outer nozzles. The combination of effects described above were not seen, mainly because the temperature gradient in the molten steel is considerably reduced by the time the melt reaches the end of the tundish.

2.3. HEAT TRANSFER IN TUNDISH OPERATIONS.

The temperature of liquid steel plays one of the most important roles in determining the structure and properties of continuously cast products. It is well established fact that heat losses occur in the ladle during transfer operations, so that the temperature of metal stream entering and leaving the tundish will vary with time, a precise knowledge of heat losses in the tundish itself is highly desirable. Mathematical modelling has been used to quantify the heat transfer process and its effects on the melt flow; and recently water models have been used to visualize thermal effects on the flow pattern during the tundish operations.

(a) Mathematical Modelling

Recently, computational modelling has become a useful tool to study heat transfer in steelmaking tundish vessels. In order to describe heat transfer in industrial tundishes, the relevant partial differential equations requiring numerical solution are:

-Equation of continuity

-Momentum balance equation

-Energy conservation equation

-Turbulent kinematic equation

-Dissipation rate of turbulent energy equation

Using the above fundamental equations together with the boundary conditions and simplifications Ilegbusi and Szekely[20,21] developed a mathematical representation to describe the temperature profile in tundishes, as affected by both flow control and auxiliary heating arrangements.

The governing equations with the boundary conditions were solved with a finite domain, fully implicit iterative procedure embodied in the Phoenics computer code. Computation required about five hours of CPU time on a microVAX II.

The principal findings were as follows:

-When no auxiliary heating was provided, more significant heat losses occurred in the absence of flow control devices.

-Auxiliary heating was found to be a potentially attractive way of compensating the heat lose in the tundish and for providing a rather more precise temperature control of these systems.

-Plasma heating is an effective way of providing thermal energy where there is strong mixing and high turbulence, in order to obtain higher dispersion of the thermal energy supplied at the top. The provision of flow control arrangements

reduces mixing and thus interferes with the ready absorbtion of the thermal energy provided by the thermal jet. In contrast, Induction heating and the associated stirring would be an effective way of rising the tundish temperature in the presence of flow control devices.

Similar mathematical models were developed by Joo and Guthrie[22,23] assuming steady state flows and heat losses, and by Chakraborty and Sahai[24,25,26] for both steady and unsteady state conditions, to predict the effect of varying ladle stream temperature conditions on the melt flow and heat transfer in steelmaking tundish vessels.

(b) Physical Modelling

Water modelling has improved understanding of the way in which liquid steel flows in tundishes and interacts with different flow control devices. Most of the research published on physical simulation of fluid flow in tundishes has assumed isothermal conditions. Very recently, hot-water models have been used to visualize the effects on the flow profile that take place during the ladle change operation when hotter steel is poured into the tundish containing a relatively cooler melt.

To study the changes in melt flow characteristics during ladle changes, and whether hot and cold water can be used to simulate thermal changes taking place in actual tundish, Lowry and Sahai[27] measured the residence time distribution for an actual six-strand bloom caster tundish and for its one-third scale water model.

It was found that the measured residence time distributions using copper tracers in an actual tundish indicated that the flow following a ladle change is radically different from the flow under isothermal, steady state conditions in the late half of the ladle cast. Following a ladle change, the new steel entering the tundish at a higher temperature than the present steel actually reaches the nozzle at the end of the tundish before it reaches the nozzle closest to the pouring stream, except for a brief interval immediately after the ladle change.

It was also concluded that a water model in which the temperature of the inlet water may be changed to simulate a ladle change-over produces a residence time distribution similar to the actual tundish and a similar difference when compared to the model residence time distribution under isothermal conditions.

It was observed in the water model that the density difference in the fluids due to temperature provides a buoyancy force component which is sufficient to reverse the steady state flow. Lowry and Sahai showed how during the ladle change the steel entering the tundish flows across the surface over the colder steel present in the tundish and descends near the end wall to reach the outermost nozzles first. The process of re-establishing steady state was calculated to be about 2.5 times the mean residence time for the tundish, which represents a significant portion of the casting time.

In another hot-water model Mori et. al.[28] evaluated the flow pattern including natural convection for an "H"-shaped tundish. The main concern for this study was whether the

liquid steel on the non-pouring side of the first vessel might stagnate and partly solidify owing to heat loss through the tundish refractory walls.

They presented the results of fluid flow analysis made for this non-isothermal system which showed that natural convection causes the higher temperature fluid to be supplied to the non-pouring side of the first vessel. This was compared to temperature distribution predicted using a three dimensional mathematical representation of the isothermal and non-isothermal system, the higher-temperature liquid steel was found to flow in the upper stratum to be supplied to the non-pouring side of the first vessel. From this the authors concluded that there is no steel solidification problem on the non-pouring side of the first vessel.

2.4. THE ROLE OF AUXILIARY HEATING.

Steel temperature control in the tundish is essential for the production of high quality steel with maximum productivity. It is being increasingly recognized that each steel grade has a narrow range of ideal casting temperatures where the ease of casting and internal quality are optimized.

An important recent development in tundish design has been the consideration of auxiliary heating, either by induction coils or through the application of a plasma jet impinging onto the steel surface. A schematic diagram of a plasma tundish heater is

shown in figure 2.6. Plasma tundish heating is a very attractive way of compensating for heat losses during tundish operations, installations of various types are rapidly proliferating around the world. A partial list of these installations are given in table 2.3.

TABLE 2.3 Industrial plasma tundish heating installations.

START-UP	POWER CAPACITY	PLANT LOCATION
1987	1 MW, 14-ton	Nippon Steel, Hirohata
1988	300 KW, 5-ton	Aichi Steel
1988	2.0 MW, 20-ton	Deltasdar, Oasta Works
1988	4.0 MW, 27-ton	Chaparral, TX
1989	1.4 MW, 35-ton	NKK, Keihin
1989	2.4 MW, 80-ton	Kobe, Kakogawa Works
1990	1.4 MW, 40-ton	NKK, Keihin
1990	1.4 MW, 17-ton	NKK, Fukuyama
1990	800 KW, 6-ton	Anval Nyby AB
1990	1.5 MW	First Miss, PA

The open literature on tundish plasma heating is based on the development and application of the systems. Kuwabara et.al.[29] published their experience of the development of a 1 MW DC plasma system installed in the 14-ton of a slab caster at Hirohata Works. They reported that it is possible to obtain about 10°C increase in temperature of liquid steel by adding 200 kW/tonne/min, with a heat efficiency between 70-80%.

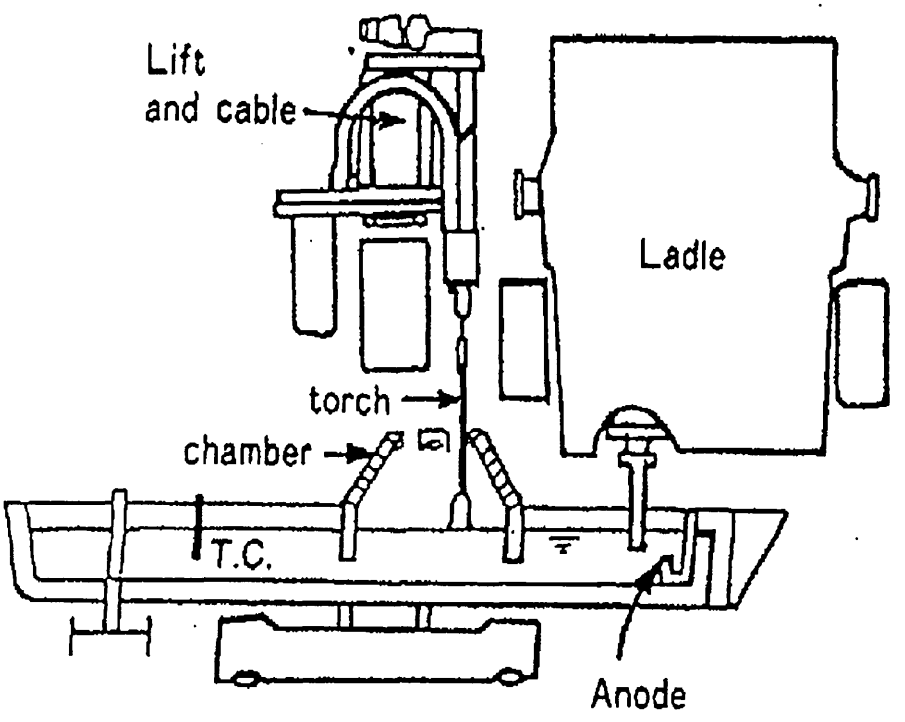

Figure 2.6. Schematic diagram of tundish plasma heater. (From Matsumoto et.al. 1990)

In relation to temperature response and controllability, it is reported that the temperature of molten steel starts to increase in the 2-3 minutes following ignition and becomes constant in about 8 minutes. Figure 2.7 shows the temperature changes of molten steel at the tundish inlet and outlet side respectively. The temperature at inlet side dropped by 0.35°C/min after the start of teeming and abruptly dropped by 3-4°C/min during the ladle change period. Plasma heating was applied for 20-25 minutes before ladle changes. Temperatures rose by 7-8°C at steady-state and 18-20°C during the ladle change period. As a result the casting temperature could be controlled within 5°C by manual control of input power during the ladle exchange. It was considered that the accuracy can be improved by using a computer control system.

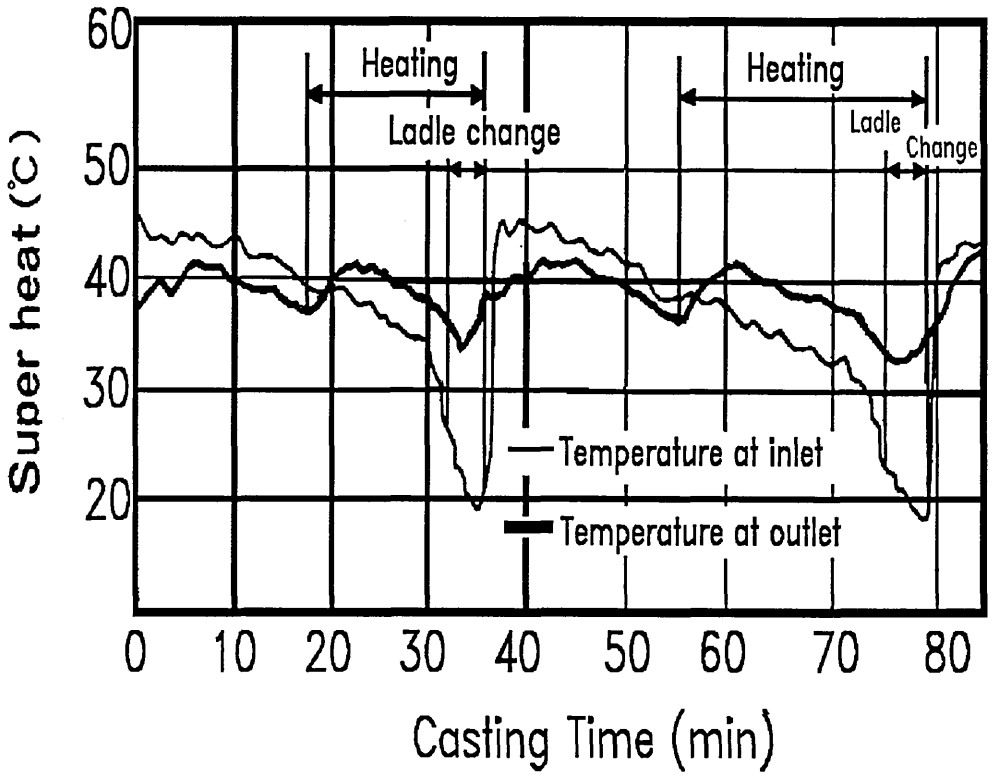

Figure 2.7. Temperature change of molten steel during casting. (From Umezawa et. al. 1989)

Recently, Matsumoto et.al.[30] reported on the implementation and application of the above tundish system at Hirohata works. Using the experimental data on thermal response of plasma heating evaluated in the previous paper, a semi-empirical mathematical model was developed to predict the change in molten steel temperature in the tundish.

The tundish was separated into three zones according to the location of the flow control devices. The first zone considered was the area downstream from the entry nozzle, the second zone the plasma heating area under the "dog-house", and the third zone the area

outside the plasma heating chamber. The first and second zones are assumed to contain perfect mixing, and the third zone plug flow. The heat balance is modelled on the above assumptions for each zone respectively by using the following equations:

$$\textit{Zone I} \qquad \frac{\partial}{\partial t}(V_1 \cdot \rho \cdot Cp \cdot T_1) = F(t) \cdot Cp\,(T_0 - T_1) - Q_{L_1} \tag{2.11}$$

$$\textit{Zone II} \qquad \frac{\partial}{\partial t}(V_2 \cdot \rho \cdot Cp \cdot T_2) = F(t) \cdot Cp\,(T_1 - T_2) - Q_{L_2} + Q_P \tag{2.12}$$

$$\textit{Zone III} \qquad \frac{\partial}{\partial t}(V_3 \cdot \rho \cdot Cp \cdot T_3) = F(t) \cdot Cp \cdot (T_2 - T_3) - Q_{L_3} \tag{2.13}$$

$$T_3 = T_2 - \frac{Q_{L_3}}{F(t) \cdot Cp} \tag{2.14}$$

Where:

Cp:	Specific heat (Kcal/Kg°C)
ρ:	Density of molten steel (Kg/m^3)
F:	Flow rate of molten steel (Kg/min)
Q_p:	Plasma calorie input (Kcal/min)
V_1, V_2, V_3:	Volume of each zone (m^3)
T_0, T_1, T_2, T_3:	Molten steel temperature in each zone (°C)
Q_{L1}, Q_{L2}, Q_{L3}:	Heat loss in each zone (Kcal/min)

For this model the heat loss from the refractory and into the refractory are given as time function on the basis of practical measurements. They argue, that with the use of this model the temperature of molten steel (T_3) at the outlet side of the tundish can be controlled by varying plasma calorie input (Q_p).

During operation, the temperature of molten steel is monitored continuously at a location near the middle of the third zone. This temperature, together with selected temperature and ladle conditions are entered into the computer to determine plasma input power. Figure 2.8 shows actual results of temperature measurements; however, using this method temperature control to within $\pm 5°C$ was achieved.

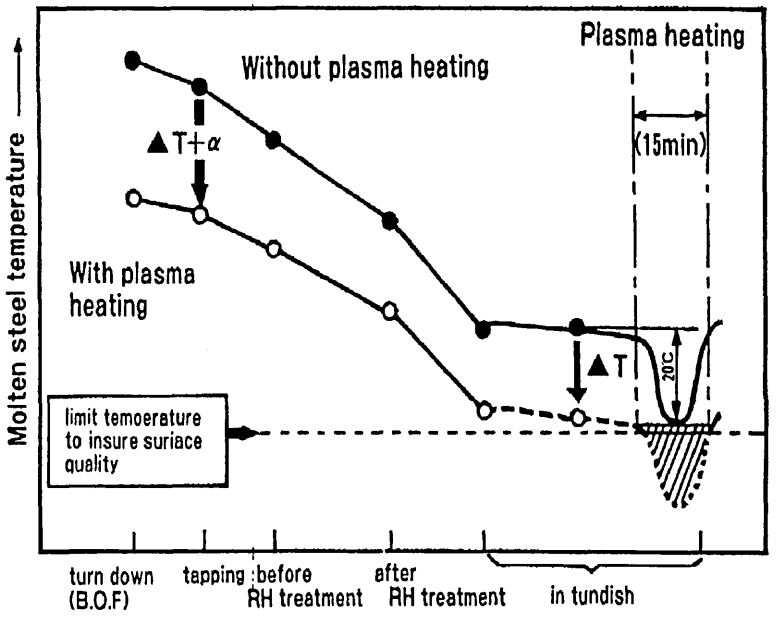

Figure 2.8. Effect of tundish plasma heater on tapping temperature. (From Umezawa et.al. 1989)

Mizushina et. al.[31] reported on the development of a 1.4 MW tundish plasma heating system, where the temperature of the molten steel in the tundish could be maintained to within $\pm 1\,^{\circ}C$ of the required steady state value using the control system, shown in figure 2.9. The system is based on a computing unit which provides feedback so that the molten steel temperature on the outlet side of the tundish heating chamber corresponds to the present value of the desk-top set point station setter. The results obtained by using the plasma heating system have been a reduction on segregations due to variations from the targeted superheat, and improvements in the reduction of abnormal solidification patterns due to a drop in temperature during transient-state operation. The required plasma heating power is set based on variations in the tapping temperature, therefore, reduction in the tapping temperature is possible, extending the service life of the converter and increasing its heat allowance.

Moore et.al.[32,33,34] have also reported on the development, installation, uses and advantages of the plasma heating systems in operation at the above steelmaking plants.

In order to control the tundish exit temperature reliably a system to monitor the input temperature continuously needs to be developed as a basic element of the control system.

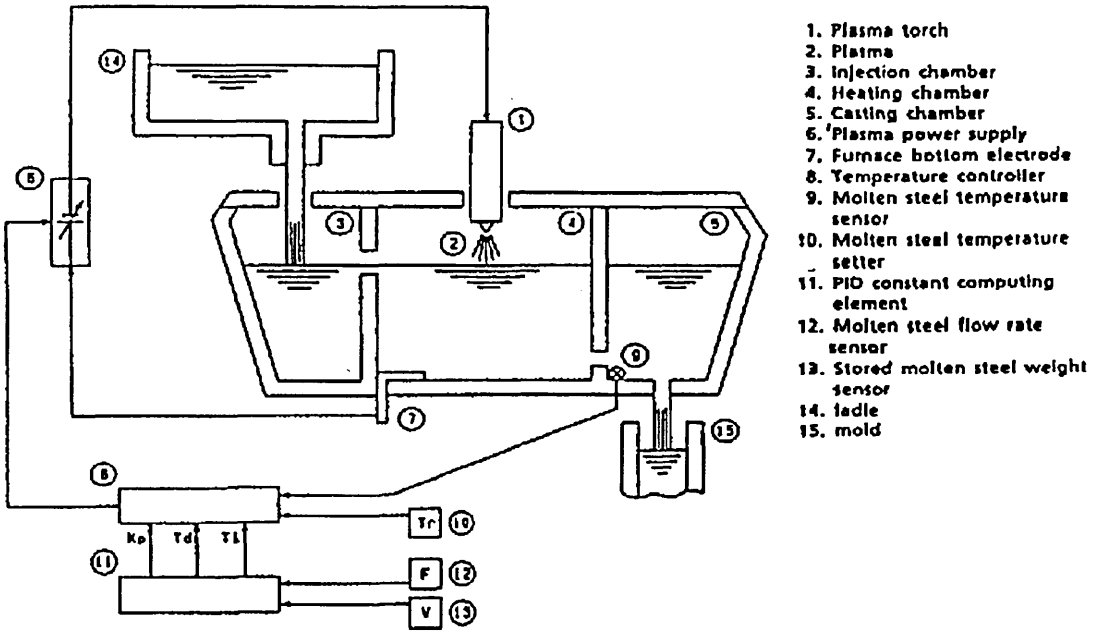

Figure 2.9. Typical example of a temperature control system using plasma heating. (From Mizushina et.al. 1990)

2.5. CONTINUOUS TEMPERATURE MEASUREMENT OF LIQUID STEEL IN THE TUNDISH.

In the steelmaking processes, liquid steel temperature is one of the basic indicators of operation and quality control. The requirements for high quality steel have increased dramatically, with more emphasis on superheat control and an ever increasing need for better automation. Continuous temperature measurement in the tundish has become an indispensable technology for the continuous casting process.

The systems developed include immersion probes consisting of a either a classical thermocouple protected by a ceramic tube or multiple thermocouple embedded in a refractory section at varying displacements.

Choi and Mucciardi[35] developed a heat transfer model to monitor liquid steel temperature continuously. The system is based on multiple thermocouple embedded in a refractory section, the model analyzes the transient heat transfer behaviour started once liquid steel is poured in the vessel in order to infer the temperature of liquid steel.

This mathematical model is based on the finite difference formulation of Fourier's heat conduction equation. The refractory section was divided into discrete nodes to fulfil the requirements of the finite difference technique. Then Fourier's equation was applied to each node, assuming one dimensional conditions.

The mathematical model was tested in a low temperature water model, and in a high temperature laboratory experiments. Results showing actual measurements of bath temperature were compared with computed bath temperature and were found to be in good agrement.

Some steelmaking plants have developed continuous temperature devices which consist basically in protecting the thermocouple with a ceramic insulator. Russo and Phillippi[36] have used an alumina-graphite isopressed composite to protect a type B thermocouple against the liquid steel and slag. The protection tube is designed to survive a full

tundish campaign. At the end of each campaign the old protection tube is discarded and the platinum thermocouple assembly is then reused with a new protection tube. However, they report that premature failure of the protective tube can occur, slag skulling being the main contributor.

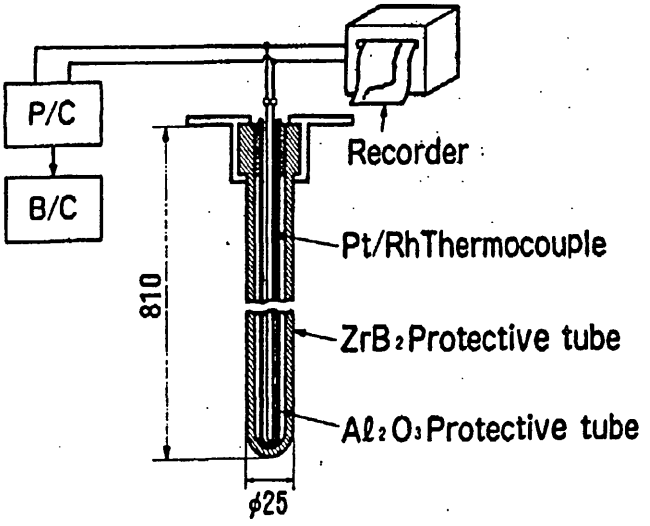

Figure 2.10. Construction of continuous measuring thermometer. (From Mori et.al. 1990)

Mori et.al.[37] developed a similar system, their research started by studying the advanced ceramic to be used as the protective tube, various ceramics were selected, tested by immersion into liquid steel, and evaluated for resistance to liquid steel and slag. Zirconium diboride (ZrB_2) was found to be the best suited.

The life of the continuous measuring thermometer is reported to be affected by operating conditions, such as the molten steel temperature, steel product mix and the

number of times it is immersed and withdrawn. It measures the temperature of liquid steel for an average of 40 hours and maximum of more than 100 hours during the casting of carbon steel at Nippon Steel.

Similar continuous temperature measuring devices are reported to be in use in European plants[38,39].

3

EXPERIMENTAL TECHNIQUES

3.1 DEVELOPMENT OF WATER MODEL SYSTEMS

The diversity of the fluid flow phenomena and the limitations of water as a modelling fluid make it impossible to satisfy all of the requirements for similarity which apply to fluid flow in a model of a given particular scale. Reynolds-Froude similarity requires a full scale model. The Weber-Froude similarity requires a model of 0.6 scale. Some numerical values for the applicable dimensionless groups are presented in chapter two, table 2.2. It is important to determine to what extent similarity in the absolute sense is necessary in modelling the actual system.

(a) Model design calculations

Heaslip et.al.[11] demonstrated that Froude number alone can be satisfied at any scale in a tundish water model as long as all metering orifices and fluid hydraulic heads in the system are sized in accordance with a single scaling parameter. This fortuitous results arises as a consequence of the fact that all flows in the continuous casting system are gravity driven.

Therefore, for the simulation of gravity driven flow in a steelmaking tundish it is is is required that: $Fr_m = Fr_p$

Where: The subscripts **m** and **p** refer to the model and prototype, respectively.

Thus:

$$\frac{V_m^2}{g \cdot L_m} = \frac{V_p^2}{g \cdot L_p} \tag{3.1}$$

or

$$\frac{L_m}{L_p} = \frac{V_m^2}{V_p^2}$$

$$L_f = \frac{L_m}{L_p} \quad \textit{is the length factor} \tag{3.1}$$

$$V_f^2 = \frac{V_m^2}{V_p^2} \quad \textit{is the velocity factor}$$

Therefore, the length scale factor, L_f, is:

$$L_f = V_f^2 \tag{3.3}$$

For gravity driven flow depth above the orifice:

$$V = \sqrt{2gh} \tag{3.4}$$

Where: h is the fluid depth above the orifice

Therefore, the fluid velocity V, for the model and prototype can be written as:

$$\begin{aligned} V_m^2 &= 2 \cdot g \cdot h_m \\ &\vdots \\ V_p^2 &= 2 \cdot g \cdot h_p \end{aligned} \tag{3.5}$$

The velocity scale factor is given by:

$$\frac{V_m^2}{V_p^2} = \frac{h_m}{h_p} \qquad \textit{Thus,} \qquad V_f^2 = h_f \tag{3.6}$$

or

$$L_f = h_f \tag{3.7}$$

Therefore, hydraulic heads and linear dimensions must be reduced in the same ratio.

The time scale factor, t_f, can be found from the following equation:

$$t_f = \frac{L_f}{V_f} \quad \rightarrow \quad \textit{time scale factor} \tag{3.8}$$

Which can be written in terms of the length factor by substituting:

$$L_f = V_f^2 \quad \rightarrow \quad V_f = \sqrt{L_f} \quad \rightarrow \quad t_f = \frac{L_f}{\sqrt{L_f}} = \sqrt{L_f} \tag{3.9}$$

The scale factor for flow rate, $\dot{Q}''_f$, can be derived from the factors for length and time as follows:

$$\dot{Q}''_f = \frac{L_f^3}{t_f} = \frac{L_f^3}{\sqrt{L_f}} \rightarrow \quad \dot{Q}''_f = \sqrt{L_f^5} \tag{3.10}$$

In general, for flow through an orifice area, **A**, the flow rate, Q_f, is given by:

$$\begin{aligned} \dot{Q}'' &= V \cdot A \\ &\vdots \\ \textit{Thus,} \qquad \dot{Q}''_m &= V_m \cdot A_m \\ &\vdots \\ \dot{Q}''_p &= V_p \cdot A_p \end{aligned} \tag{3.11}$$

Rewriting this equations in terms of orifice diameter d, and dividing:

$$\frac{\dot{Q}''_m}{\dot{Q}''_p} = \frac{V_m}{V_p} \cdot \frac{d_m^2}{d_p^2} \tag{3.12}$$

Or, in terms of scale factors:

$$\dot{Q}''_f = V_f \cdot d_f^2 \tag{3.13}$$

Therefore:

$$d_f^2 = \frac{\dot{Q}_f''}{V_f} = \frac{\sqrt{L_f^5}}{\sqrt{L_f}} = L_f^2 \tag{3.14}$$

giving

$$d_f = L_f \tag{3.15}$$

The nozzle scale must thus be reduced in accordance with the linear dimensions.

Therefore, for a gravity driven flow, Froude No. equivalence is maintained if all dimensions are scaled according to single scaling factor. The important relationships are:

$$L_m = X\, L_p \tag{3.16}$$

$$V_m = X^{\frac{1}{2}} V_p \tag{3.17}$$

$$\dot{Q}_m'' = X^{\frac{5}{2}} \dot{Q}_p'' \tag{3.18}$$

Where: **X** is the scaling factor

(b) The tundish model

A one-sixth scale water model of a typical slab caster tundish, including the ladle collector nozzle and the mould submerged entry nozzle, was constructed using the Froude model design calculations.

Important parameters for the model and the prototype are given in table 3.1. A schematic representation is shown in figure 3.1.

TABLE 3.1. Parameters for model and prototype

Parameter	Model	Prototype
Tundish width	0.13 m	0.79 m
Tundish length	1.18 m	7.10 m
Tundish depth	0.13 m	0.79 m
Wall inclination	9 Deg	9 Deg
Vol. flow rate	12 L Min^{-1}	8200 Kg Min^{-1}
Ladle nozzle diam.	13 mm	80 mm
Mould SEN diam.	13 mm	80 mm

6 mm thick perspex sheet was used to construct the water analogue tundish model. The ladle collector nozzle was machined from perspex blocks, the thickness of the nozzle wall was 18 mm, with 13 mm internal diameter, it was attached to a two-way change over valve. It was also equipped with a syringe injector to add the tracer to the incoming water stream. For the conductivity test, the tundish exit nozzle was made

from 19 mm outside diameter perspex pipe with 13 mm internal diameter. For the remote temperature experiments the nozzle wall thickness was 18 mm with 13 mm internal diameter. They were attached to the bottom of the tundish by a screw thread so they could be inter-changeable.

(c) The ladle

The ladles were simple plastic tanks of 20 litres capacity, supported above the tundish water level. One contained hot water and the other cold. Overflow pipes in the tanks allowed control of the water level. The ladles were connected by a two-ways interchangeable valve, so that water at changing temperatures could be supplied to the tundish model.

(d) Water heating system

One of the ladles contained hot water for that it was equipped with a water heating system. Because the hot water had to be supplied continuously, a 8 kW continuous electric heater was connected to the main water supply. This water was mixed with tap water before entering the tank by a "Y" junction, to make up the flow rate required.

The second ladle contained only tap water, which was supplied directly. The two ladles were connected by a two way diversion valve beneath them, and simply by changing its direction, hot or cold water was poured to the tundish through the sub-ladle entry

nozzle. The valve was manually operated and sufficiently fast to introduce a step input.

(e) Steam heating system

A pressurized steam generator was constructed, to simulate a plasma heater system. It was made of aluminium and in the inside three 2.75 kW electric heating elements were fitted. It was supported above the tundish water level and the steam was blown onto the surface of the water passing under the "dog house". The pressure vessel had a capacity of 30 litres of water, which was sufficient to allow steam to be blown for about 15 minutes continuously. The cover of the vessel was also equipped with a pressure release valve and a two-way diversion valve, one way to the tundish and the other to a vessel full of water to condense the steam. This manually operated diversion valve allowed the steam supply to the surface of the water to be almost instantaneously switched on and off.

The steam nozzle was fitted with a syringe injection point, so that the steam could be used as carrier of the tracer injected at the "dog house".

The "dog house" was made of glass, the inside chamber had a dome shape covered with aluminium foil, in order to minimise radiation heat loss from the top of the chamber.

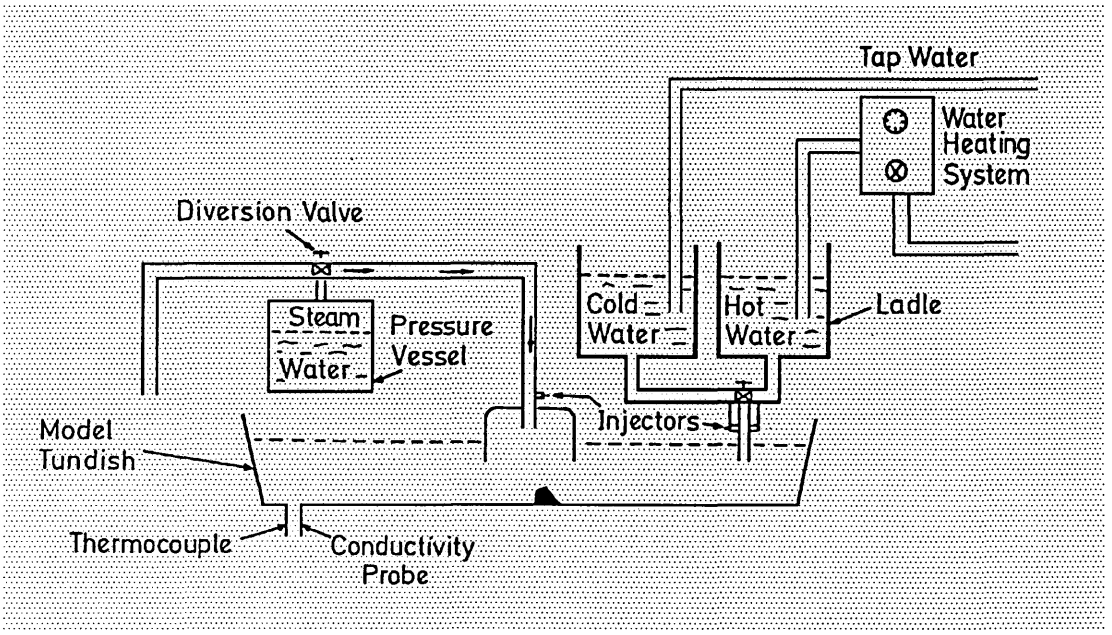

Figure 3.1 Schematic diagram of apparatus.

3.2 EXPERIMENTAL TECHNIQUES TO DETERMINE RESIDENCE TIME DISTRIBUTIONS

Techniques used to determine residence time distribution of a fluid flowing through a vessel have mainly involve the addition of a tracer material - such as a dye, a radioactive material or a chemical substance - to the stream entering the vessel, followed by measurement of the concentration at the exit.

Two methods were used to determine residence time distribution of the water flowing through the tundish model:

(i) Conductivity method, a highly conducting species being injected as a pulse at the inlet point and changes in conductivity monitored at the exit. Two sets fo

measurements were made, one set from the flow between the inlet stream and the exit of the tundish and one set for flow between the steam heater chamber and the exit.

(ii) Temperature change method, measurement of the changes in temperature at the exit resulting from the step changes in the inlet stream and from the use of the steam heating system.

(a) Choice of tracers.

Several material have been used as the tracers. Some of them are too dense and sink to the bottom of the tundish, flowing close to lower surface towards the exit nozzle. Hydrochloric acid (HCl) did not show that behaviour and mixed well with the water flowing in the tundish. Because it is also highly conductive, it was chosen as the tracer for the conductivity measurements.

(b) Preparation and addition of the tracers.

The concentrated hydrochloric acid used as a tracer was diluted to 90 per cent by volume with water. The solution was analyzed and the concentration found to be 9.3 moles dm^{-3}.

20 ml of hydrochloric acid solution was injected as a pulse, at the injection points,

using a syringe.

(c) Conductivity measurements.

Platinum electrodes were attached on the inside walls, facing each other, close to the exit of the outlet nozzle, creating a conductivity cell.

The electrodes were approximately half centimetre square and coated in platinum black. The cell was connected to a laboratory conductivity meter, and the output was recorded on an oscilloscope.

(d) Temperature measurements.

Two Copper-Copper/Nickel, type "T", thermocouples were placed at the entry and outlet stream nozzles to measure the changes in temperature resulting both from changes in the temperature of the inlet stream and from the use of the steam heater system.

The flowing water in the tundish was left to get a steady state temperature before imposing a step input, of higher or lower temperature water, on the stream entry nozzle. The temperature of this sudden change was measured as it passed through the tundish nozzles by the thermocouples, and the output was amplified and recorded on an oscilloscope.

3.3 EXPERIMENTAL TECHNIQUES FOR REMOTE TEMPERATURE SENSING

In order to develop a temperature control system able to function reliably during the continuous casting of steel, a remote method of liquid steel temperature sensing at the inlet stream to the tundish and in the submerge entry nozzle was investigated.

(a) Method of temperature measurement

This method involved the incorporation of three thermocouples into the walls of the ladle and tundish nozzles tubes. As the temperature of liquid steel in either tube changes, the temperature indicated by the thermocouples will also change, but at later time and to a lesser extent. The liquid steel temperatures must be estimated from these measured changes.

The analogue water tundish model was used investigate this remote sensing method. The ladle and the submerged entry nozzles were made of perspex, the wall thickness was 18 mm with a 13 mm internal diameter. Three needle type "T" thermocouples were embeded in nozzle wall two, four, and six millimetres away from the internal surface.

The thermocouples were conected to a 386 PCSX computer with an analog connection card, which provided cold juntion compensation and linearization for 10 thermocouples types, including type "T".

The data acquisition computer package "WorkBench PC™" for IBM computers was used to read the temperatures from the three sensors at 40 seconds intervals. WorkBench is a data acquisition program, with data logging and display sofware enviroment. Using this facilities the data for each thermocouple was logged to a disk for later analysis.

The temperature reading of each thermocouple was then read into a Power Basic code which included the algorithm to estimate internal surface temperature. This algorithm is formulated in chapter four.

4

THEORETICAL DEVELOPMENT

4.1. THEORETICAL DISPERSION MODEL

When a fluid flows through a vessel in which it undergoes a chemical change, it is important to establish the time spent in the system by individual fluid elements. The mean time of the fluid in the system is calculated from the definition:

$$t_{mean} = \frac{Volume\ of\ the\ vessel}{Volumetric\ rate\ of\ fluid\ flow}$$

However, it is frequently found that some individual fluid elements may spend longer, and others a shorter, period of time in the system. This departure of actual residence times from the mean, that is, the distribution of residence times, is an important characteristic of the system and influences appreciable its performance as a reactor.

The residence time distribution of a fluid flowing through a vessel can be determined by means of tracer techniques. Basically, these involve the addition of a tracer to the stream entering the vessel, and then measurement of the concentration at the exit.

Several methods have been developed for introducing the tracer material into the vessel, but the two most important are:

(i) Pulse input technique:

This is the addition of a tracer over a short time interval, the duration of which is negligible in comparison with the mean residence time of fluid in the vessel.

The normalized response is then called the **C** curve, figure 4.1 shows a typical curve and its properties.

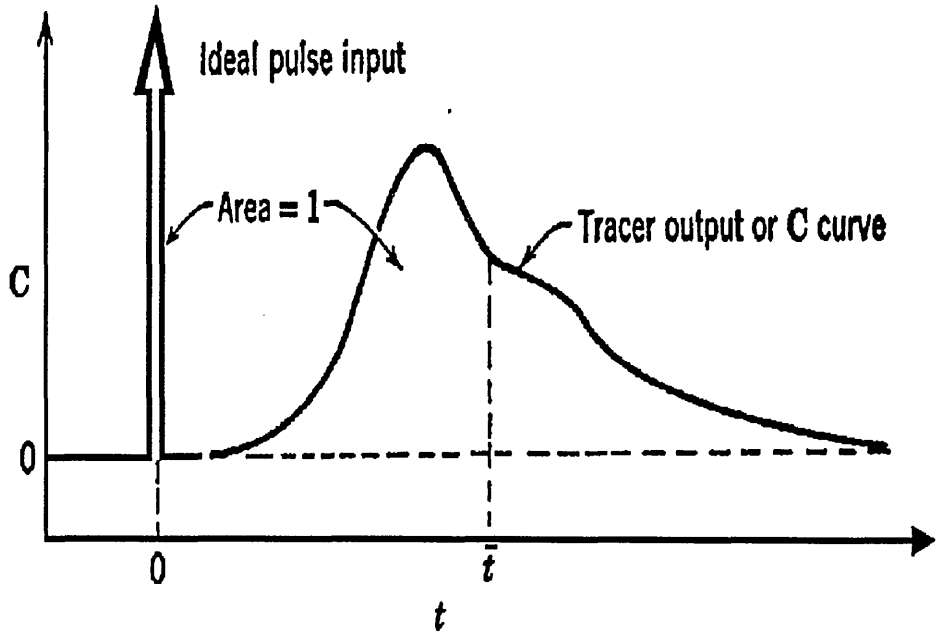

Figure 4.1 Typical downstream signal, called the **C** curve, in response to pulse input. (From Levenspiel 1972)

(ii) Step input technique:

This is the imposition of a sudden step input of tracer of concentration C_0 on the fluid stream entering the vessel. Then a time record of tracer in the exit stream from the vessel, measured as C/C_0, is called the **F** curve. Figure 4.2 sketches this curve and it shows that it always rises from 0 to 1.

Many type of models can be used to characterize fluid flow within the vessel by analysis of the experimentally obtained residence time distribution curves.

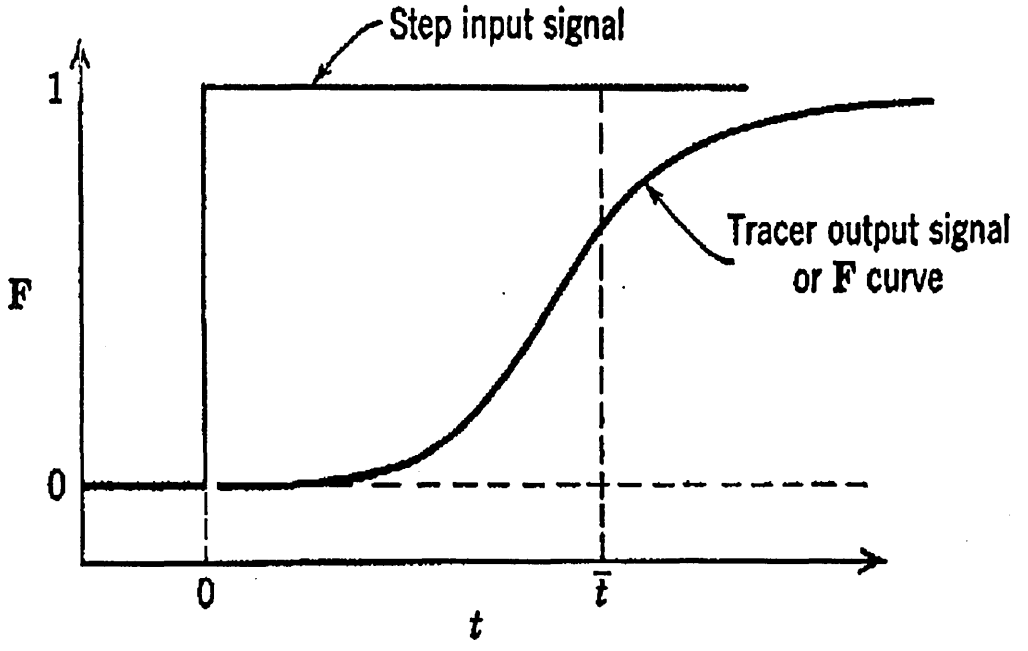

Figure 4.2 Typical downstream signal, called the F curve, in response to a step input. (From Levenspiel, 1972)

(a) The dispersion model

The mixing process involves a re-distribution of tracer materials by eddies, this is repeated a considerable number of times during the flow of fluid through the vessel. Therefore, this disturbances can be considered to be statistical in nature, similar as in molecular diffusion. According to this, the dispersion of the tracer in a continuous flow system, such as the tundish, may be expressed:

$$\frac{\partial C_i}{\partial t} - D_i \frac{\partial^2 C_i}{\partial x^2} \qquad (4.1)$$

Where: D_i is the longitudinal dispersion coefficient

x is measured from a co-ordinate system that moves through the tundish at the mean flow velocity.

(i) Pulse input in tracer concentration

With no tracer initially present anywhere an instantaneous pulse of tracer is imposed on the stream entering the vessel.

The boundary conditions for **pulse input** of the tracer are:

$t = 0$; $x = 0$: $C_i = [C_i]_0$

$t = 0$; $x \neq 0$: $C_i = 0$

$t > 0$; $x = \infty$: $C_i = 0$

The concentration of **i** at the outlet is the measure of the number of fluid elements that have left the vessel. If the fluid mixing is considered to be at random, it would be expected that the concentration distribution would bear a likeness to the distribution of random errors. This curve is described by the mathematical expression:

$$N = \frac{A}{\sigma} \exp\left\{-\frac{e^2}{2\sigma^2}\right\} \qquad (4.2)$$

Where: A: is a constant

σ^2: is the variance of the distribution

e: is the ramdom error

These concentration distribution can be described by a similar equation, but the variance replaced by a monotonically increasing function of time:

$$[C_i]_{(x,t)} = \frac{A}{\sqrt{\beta t}} \exp\left\{\frac{-x^2}{\beta t}\right\} \qquad (4.3)$$

Where: β: is a constant

Provided that $\beta = 4D_i$ this equation is the required solution.

Thus, the concentration distribution due to longitudinal dispersion from a pulse input is given by:

$$[C_i]_{(x,t)} = \frac{A}{\sqrt{4D_i t}} \exp\left\{\frac{-x^2}{4D_i t}\right\} \qquad (4.4)$$

This equation also satisfies the boundary conditions. Substitution into this equation gives:

$[C_i]_{(0,0)}$ = an indeterminative constant

$[C_i]_{(x,0)} = 0$

$[C_i]_{(\infty,t)} = 0$

This equation becomes indeterminated under the conditions corresponding to the first boundary condition. In order to determine the value of A, the initial boundary conditions must be used in a different way. A fourth boundary condition, expressing conservation of mass is:

$$S_i'' = \int_{-\infty}^{\infty} [C_i]_{(x,t)} dx \qquad (4.5)$$

Where: S''_i is the amount of tracer material per unit area.

Substituting for $[C_i]_{(x,t)}$:

$$S_i'' = \frac{A}{\sqrt{4D_i t}} \int_{-\infty}^{\infty} \exp\left\{\frac{-x^2}{4D_i t}\right\} dx \qquad (4.6)$$

simplifying the integral, by defining a new variable:

$$\eta^2 = \frac{x^2}{4D_i t} \qquad \rightarrow \qquad \partial\eta = \frac{\partial x}{\sqrt{4D_i t}}$$

and as $x = \infty , \eta = \infty$; $x = -\infty , \eta = -\infty$

Thus the equation can be rewritten as:

$$S_i'' = A \int_{-\infty}^{\infty} \exp(-\eta^2)\partial\eta \qquad (4.7)$$

And the integral is:

$$\int_{-\infty}^{\infty} \exp(-\eta^2)\, \partial\eta = \sqrt{\pi}$$

and the particular solution is:

$$[C_i]_{(x,t)} = \frac{S_i''}{\sqrt{4D_i\pi t}} \exp\left\{\frac{-x^2}{4D_i t}\right\} \qquad \textbf{(4.8)}$$

Which becomes:

$$[C_i]_{(x,t)} = \frac{QL}{V}\frac{1}{\sqrt{4D_i\pi t}} \exp\left\{\frac{-x^2}{4D_i t}\right\} \qquad \textbf{(4.9)}$$

and

$$C_\Theta = \frac{[C_i]_{(x,t)}V}{Q} = \frac{L}{\sqrt{4D_i\pi t}} \exp\left\{\frac{-x^2}{4D_i t}\right\} \qquad \textbf{(4.10)}$$

Defining an ordinate x' measured from the tundish point, it can be written:

$$x' = x + ut$$

Representing Θ as the fraction of the mean residence time, allows the dispersion time "t" to be written as:

$$t = \frac{\Theta L}{u}$$

Thus the equation is modified to yield:

$$C_\theta = \frac{L}{\sqrt{4D_i\pi t}} \exp\left\{\frac{-(x'-ut)^2}{4D_i t}\right\} \tag{4.11}$$

Substituting the dimensionless parameters:

$$C_\theta = \frac{L}{\sqrt{4D_i\pi\left(\frac{\Theta L}{u}\right)\frac{L}{L}}} \exp\left\{\frac{-(x'-\Theta L)^2}{4D_i\left(\frac{\Theta L}{u}\right)\frac{L}{L}}\right\} \tag{4.12}$$

$$C_\theta = \frac{L}{\sqrt{4\left(\frac{D_i}{uL}\right)\Theta\pi L^2}} \exp\left\{\frac{-(x'-\Theta L)^2}{4\left(\frac{D_i}{uL}\right)L^2\Theta}\right\} \tag{4.13}$$

When x' = L :

$$C_\theta = \frac{1}{\sqrt{4\Theta\pi\left(\frac{D_i}{uL}\right)}} \exp\left\{\frac{-(L-\Theta L)^2}{4\left(\frac{D_i}{uL}\right)L^2\Theta}\right\} \tag{4.14}$$

$$C_\theta = \frac{1}{\sqrt{4\Theta\pi\left(\frac{D_i}{uL}\right)}} \exp\left\{\frac{-L^2(1-\Theta)^2}{4\left(\frac{D_i}{uL}\right)\Theta L^2}\right\} \tag{4.15}$$

The concentration change from **pulse input** of a tracer is given by:

$$C_\Theta = \frac{1}{\sqrt{4\pi\Theta\left(\frac{D_i}{uL}\right)}} \exp\left\{\frac{-(1-\Theta)^2}{4\Theta\left(\frac{D_i}{uL}\right)}\right\} \qquad (4.16)$$

The tracer plot of the concentration distribution (C_Θ) against time (Θ) is a unique function of the dimensionless dispersion parameter (D_i/uL).

(ii) Step change in tracer concentration

Assume that at some instant of time $t = 0$, one starts labelling a constant fraction of $[C_i]_0$ of the particles and then measures the fraction of the labelled particles $[C_i]_{(x,t)}$ at the exit:

$$[C_i]_{(x,t)} = F_{(x,t)} \cdot [C_i]_0 \quad \therefore \quad F_{(x,t)} = \frac{[C_i]_{(x,t)}}{[C_i]_0}$$

To represent the tracer material on a small increment in the concentration the following equation will apply:

$$\delta\{[C_i]_{(x,t)}\} = \frac{[S_i'']_\xi}{\sqrt{4D_i\pi t}} \exp\left\{\frac{-(x-\xi)^2}{4D_i t}\right\} \qquad (4.17)$$

Where: $[S''_i]$: is the amount of tracer material at ξ per unit area normal to the longitudinal direction

ξ: is the distance from the tundish entry point

if $[C_i]$ is the initial concentration,

$$\left[S_i''\right]_\xi = \left[C_i\right]_0 \delta\xi$$

Therefore:

$$\delta\left\{\left[C_i\right]_{(x,t)}\right\} = \frac{\left[C_i\right]_0}{\sqrt{4D_i\pi t}} \exp\left\{\frac{-(x-\xi)^2}{4D_i t}\right\}$$

$$\vdots \qquad \textbf{(4.18)}$$

$$\left\{\left[C_i\right]_{(x,t)}\right\} = \frac{\left[C_i\right]_0}{\sqrt{4D_i\pi t}} \int \exp\left\{\frac{-(x-\xi)^2}{4D_i t}\right\} \delta\xi$$

In order to evaluate the integral, the variables must be changed:

$$\frac{x-\xi}{\sqrt{4D_i t}} = \zeta \quad \therefore \quad -\frac{\partial\xi}{\sqrt{4D_i t}} = \partial\zeta$$

and the limits when:

$$\xi = 0 \quad ; \quad \zeta = \frac{x}{\sqrt{4D_i t}}$$

With these changes of variables the equation becomes:

$$\left\{\frac{[C_i]_{(x,t)}}{[C_i]_0}\right\} = -\frac{1}{\sqrt{\pi}}\int_{\infty}^{\frac{x}{\sqrt{4D_i t}}} \exp(-\zeta^2)\partial\zeta$$

$$= \frac{1}{\sqrt{\pi}}\left\{\int_0^{\infty}\exp(-\zeta^2)\partial\zeta - \int_0^{\frac{x}{\sqrt{4D_i t}}}\exp(-\zeta^2)\partial\zeta\right\} \qquad \textbf{(4.24)}$$

The integral $\int_0^{\frac{x}{\sqrt{4D_i t}}} \exp(-\zeta^2)\partial\zeta$ *is only function of* $\frac{x}{\sqrt{4D_i t}}$

It must be evaluated numerically, and so a new function must be defined. This is known as the error function, and is expressed by the equation:

$$erf(y) = \frac{2}{\sqrt{\pi}}\int_0^{y}\exp(-\zeta^2)d\zeta \qquad \textbf{(4.25)}$$

The erf(y) has three useful properties:

$$\text{erf}(0) = 0 \quad ; \quad \text{erf}(-y) = -\text{erf}(y) \quad ; \quad \text{erf}(\infty) = 1$$

With these definitions in mind the equation becomes:

$$\left\{\frac{[C_i]_{(x,t)}}{[C_i]_0}\right\} = \frac{1}{2}\left\{erf(\infty) - erf\left(\frac{x}{\sqrt{4D_i t}}\right)\right\} \qquad \textbf{(4.26)}$$

and

$$F_\Theta = \left\{\frac{[C_i]_{(x,t)}}{[C_i]_0}\right\} = \frac{1}{2}\left\{1 - erf\left(\frac{x}{\sqrt{4D_{it}}}\right)\right\} \qquad (4.27)$$

Using the definition of x' measured from the tundish point:

$$x' = x + ut$$

And representing Θ as the fraction of the mean residence time, allows the dispersion time "t" to be written as:

$$\Theta = \frac{t}{t_{mean}} = \frac{tu}{L} \quad \therefore \quad t = \frac{\Theta L}{u}$$

Then:

$$F_\Theta = \frac{1}{2}\left\{1 - erf\left(\frac{x' - ut}{\sqrt{4D_i t}}\right)\right\} \qquad (4.28)$$

$$F_\Theta = \frac{1}{2}\left\{1 - erf\left(\frac{x' - u\left(\frac{\Theta L}{u}\right)}{\sqrt{4D_i\left(\frac{\Theta L}{u}\right)\frac{L}{L}}}\right)\right\} \qquad (4.29)$$

$$F_\theta = \frac{1}{2}\left\{1 - erf\left(\frac{x' - \Theta L}{\sqrt{4\Theta\left(\frac{D_i}{uL}\right)L^2}}\right)\right\} \qquad (4.30)$$

When x' = L , the fractional concentration change for **step input** of a tracer is given by:

$$F_\Theta = \frac{1}{2}\left\{1 - erf\left(\frac{1-\Theta}{\sqrt{4\Theta\left(\frac{D_i}{uL}\right)}}\right)\right\} \qquad (4.31)$$

(b) Temperature compensation by the application of heat

It is well established fact that heat losses occur in the ladle during transfer operations, and when molten steel enters the tundish inevitable heat losses will also occur, causing a temperature drop. So that the temperature of the metal stream entering and leaving the tundish will vary with time. Plasma tundish heating has been used to compensate this heat losses during tundish operations, allowing a more precise control of the steel temperature entering the mould of the continuous casting machine.

This temperature drop can be estimated by applying the dispersion model. By analogy with the step input in tracer concentration, the fractional temperature drops from 1 to 0, and the compensating heat is applied at a time $\Theta_{A,H}$ later.

Thereafter, the fractional fluid temperature drop before heat is applied is given by:

$$T_\Theta = \frac{1}{2}\left\{1 + erf\left(\frac{1 - \Theta_A}{\sqrt{4\Theta_A\left(\frac{D_i}{uL_A}\right)}}\right)\right\} \tag{4.32}$$

And the fractional fluid temperature compensation after heat is applied is given by:

$$T_\Theta = \frac{1}{2}\left\{1 + erf\left(\frac{1 - \Theta_A}{\sqrt{4\Theta_A\left(\frac{D_i}{uL_A}\right)}}\right)\right\} + \frac{1}{2}\left\{1 - erf\left(\frac{1 - \Theta_B}{\sqrt{4\Theta_B\left(\frac{D_i}{uL_B}\right)}}\right)\right\} \tag{4.33}$$

Where:

$\left(\frac{D_i}{uL_A}\right)$: *is the dispersion parameter for route A*

$\left(\frac{D_i}{uL_B}\right)$: *is the dispersion parameter for route B*

and

$$\Theta_B = \frac{L_A}{L_B}\left(\Theta_A - \Theta_{A,H}\right)$$

For this the pulse input analysis have to be carried out twice:

-Once from the sub-ladle entry nozzle → residence path A.

-Once from the plasma heating chamber → residence path B.

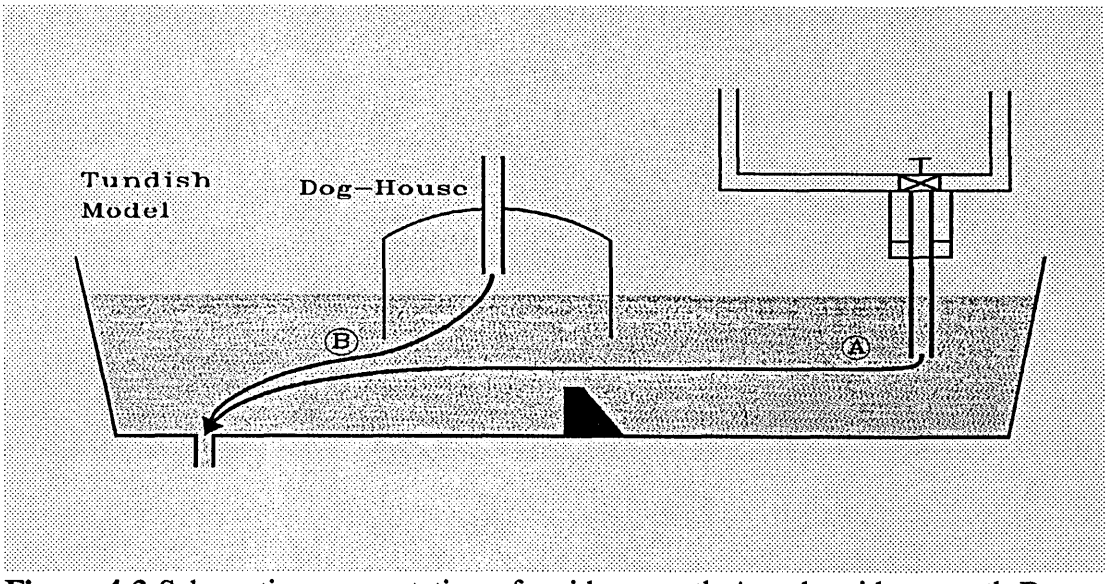

Figure 4.3 Schematic representation of residence path A and residence path B.

In order to monitor the molten steel temperature at a point of entry to the tundish, a continuous temperature sensor system has been developed. The system consists on a series of thermocouples embedded in the wall of a ladle nozzle. The molten steel temperature is estimated from varying thermocouple temperature by solving a difficult inverse heat conduction problem.

4.2. NEW APPROACH TO THE INVERSE HEAT CONDUCTION PROBLEM

The inverse heat conduction problem is the estimation of the surface temperature and heat flux history given one or more measured temperature histories inside a heat-conducting body. If the heat flux or temperature histories at a surface of a solid are known as function of time, then the temperature distribution can be found. This is termed a direct problem. However, in many dynamic heat transfer situations, the

surface heat flux and temperature histories of a solid must be determined from transient temperature measurement at one or more interior locations.

To estimate the surface heat flux and temperature it is necessary to have a mathematical model. Heat flow, along with many other diffusion processes, can be modelled using the general heat conduction equation, for which numerical solutions can almost always be produced. Even where an analytical solution exists, it is usually quicker to produce the results for a particular situation using a numerical technique.

(a) The general equation of heat conduction.

Figure 4.3 shows a cubic differential control volume in a region of moving fluid, in which unsteady state heat transfer is taking place.

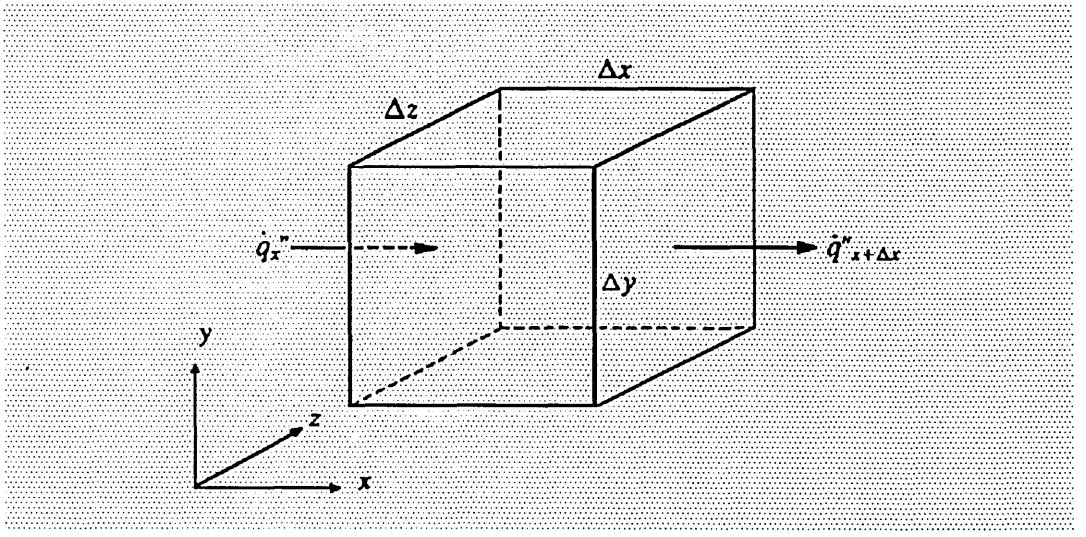

Figure 4.3 Elemental volume through which heat flows in the X direction.

$\dot{q}''_x$ is the heat flux per unit area into the cubic element shown.

$\dot{q}''_{x+\Delta x}$ is the heat flux per unit area out of the cubic element shown.

Not shown are the corresponding fluxes per unit area $\dot{q}''_y$, $\dot{q}''_{x+\Delta x}$, and $\dot{q}''_z$, $\dot{q}''_{z+\Delta z}$ along the directions y and z respectively.

Considering the x direction only:

If Δx is small, the variation of $\dot{q}''_x$ over Δx may be regarded as approximately linear.

Thus:

$$\dot{q}'''_{x+\Delta x} = \dot{q}'''_x + \left(\frac{\partial \dot{q}'''_x}{\partial x}\right)\Delta x \qquad \textbf{(4.34)}$$

And the net energy inflow:

$$- \left(\dot{q}'''_x - \dot{q}'''_{x+\Delta x} \right)\Delta y \, \Delta z \qquad \textbf{(4.35)}$$

rewritten as:

$$= - \left(\frac{\partial \dot{q}'''_x}{\partial x}\right) \Delta x \cdot \Delta y \cdot \Delta z \qquad \textbf{(4.36)}$$

By a similar argument, the net energy inflow along y:

$$= - \left(\frac{\partial \dot{q}'''_y}{\partial y}\right) \Delta x \cdot \Delta y \cdot \Delta z \qquad \textbf{(4.37)}$$

Whilst that along z is:

$$= -\left(\frac{\partial \dot{q}_z''}{\partial z}\right) \Delta x \cdot \Delta y \cdot \Delta z \qquad \textbf{(4.38)}$$

Assuming that there is not internally generated heat, the total rate of energy increase within the volume $\Delta x, \Delta y, \Delta z$ is given by:

$$-\left(\frac{\partial \dot{q}_x''}{\partial x} + \frac{\partial \dot{q}_y''}{\partial y} + \frac{\partial \dot{q}_z''}{\partial z}\right) \Delta x \cdot \Delta y \cdot \Delta z \qquad \textbf{(4.39)}$$

By the principle of conservation of energy, this may be equated to the rate of increase of internal energy.

If θ is the internal temperature, then the rate of rise of temperature is $(\partial\theta/\partial t)$ and the thermal capacity is given by:

$$(\rho \; Cp \;) \; \Delta x \cdot \Delta y \cdot \Delta z \qquad \textbf{(4.40)}$$

Where: ρ: density

Cp: specific heat

Hence the rate of increase of internal energy:

$$= \rho Cp \left(\frac{\partial \theta}{\partial t}\right) \Delta x \cdot \Delta y \cdot \Delta z \qquad \textbf{(4.41)}$$

Whilst equating this to the rate of inflow of energy yields:

$$-\left(\frac{\partial \dot{q}_x''}{\partial x} + \frac{\partial \dot{q}_y''}{\partial y} + \frac{\partial \dot{q}_z''}{\partial z}\right) \Delta x\ \Delta z\ \Delta y - \rho Cp\left(\frac{\partial \theta}{\partial t}\right) \Delta x\ \Delta y\ \Delta z \qquad \textbf{(4.42)}$$

or

$$\rho Cp\left(\frac{\partial \theta}{\partial t}\right) = -\left(\frac{\partial \dot{q}_x''}{\partial x} + \frac{\partial \dot{q}_y''}{\partial y} + \frac{\partial \dot{q}_z''}{\partial z}\right) \qquad \textbf{(4.43)}$$

The fluxes $\dot{q}''_x$, $\dot{q}''_y$, $\dot{q}''_z$ may be related to temperature using Fourier's Law of heat conduction namely:

$$\dot{q}_n'' = -k\left(\frac{\partial \theta}{\partial n}\right) \qquad \textit{For } n\text{-}x,y,z \qquad \textbf{(4.44)}$$

The negative sign shows that the heat flows down the temperature gradient, whilst k is the thermal conductivity.

Substituting this Law into the heat flow equation gives:

$$\rho Cp\left(\frac{\partial \theta}{\partial t}\right) = \frac{\partial}{\partial x}\left(k\frac{\partial \theta}{\partial x}\right) + \frac{\partial}{\partial y}\left(k\frac{\partial \theta}{\partial y}\right) + \frac{\partial}{\partial z}\left(k\frac{\partial \theta}{\partial z}\right) \qquad \textbf{(4.45)}$$

Which may be written in terms of vector operators:

$$\rho Cp \left(\frac{\partial \theta}{\partial t}\right) = \nabla (k \cdot \nabla \theta) \tag{4.46}$$

In most practical applications, It may be assumed that the medium is isotropic. Then k may be treated as a constant, giving:

$$\rho Cp \left(\frac{\partial \theta}{\partial t}\right) = k \cdot \nabla^2 \theta \tag{4.47}$$

This is the general equation for heat flow in an isotropic medium.

It may be simplified by written:

$$\alpha = \frac{k}{\rho Cp} \tag{4.48}$$

giving:

$$\left(\frac{\partial \theta}{\partial t}\right) = \alpha \cdot \nabla^2 \theta \tag{4.49}$$

Where: α is the thermal diffusivity

For a cylinder of infinite length, the operator $\nabla^2\theta$ reduces to:

$$\left(\frac{\partial^2\theta}{\partial r^2} + \frac{1}{r} \cdot \frac{\partial\theta}{\partial r}\right) \tag{4.50}$$

Giving the following form of heat flow equation:

$$\alpha\left(\frac{\partial^2\theta}{\partial r^2} + \frac{1}{r} \cdot \frac{\partial\theta}{\partial r}\right) - \left(\frac{\partial\theta}{\partial t}\right) \tag{4.51}$$

Where: r: distance from the centre line

t: time

θ: temperature

Since the thermal diffusivity (α) has the dimensions [L^2 t^{-1}] it is possible to render the above equation in dimensionless form by the following substitutions:

Let $r = a\,f$

Where a is the outer diameter of the nozzle.

Then $\partial r = a\,\partial f$ and

$$\left(\frac{\partial^2\theta}{\partial r^2}\right) - \left(\frac{1}{a^2} \cdot \frac{\partial^2\theta}{\partial f^2}\right) \tag{4.52}$$

Similarly

$$\left(\frac{1}{r}\cdot\frac{\partial\theta}{\partial r}\right) = \left(\frac{1}{a^2}\cdot\frac{1}{f}\frac{\partial\theta}{\partial f}\right) \qquad \textbf{(4.53)}$$

Where: f is a dimensionless parameter

Also, the substitution

$$\tau = \frac{\alpha t}{a^2} \qquad \textbf{(4.54)}$$

gives a dimensionless time parameter.

Then

$$\left(\frac{\partial\theta}{\partial t}\right) \rightarrow \left(\frac{\alpha}{a^2}\cdot\frac{\partial\theta}{\partial\tau}\right)$$

and then the conduction equation is:

$$\frac{\alpha}{a^2}\left(\frac{\partial^2\theta}{\partial f^2} + \frac{1}{f}\frac{\partial\theta}{\partial f}\right) = \left(\frac{\alpha}{a^2}\cdot\frac{\partial\theta}{\partial\tau}\right) \qquad \textbf{(4.56)}$$

or

$$\left(\frac{\partial^2\theta}{\partial f^2} + \frac{1}{f}\frac{\partial\theta}{\partial f}\right) = \left(\frac{\partial\theta}{\partial\tau}\right) \qquad \textbf{(4.57)}$$

Although analytical solutions are available for this equation, it is much easier to handle in terms of net analysis using finite difference techniques. Such an approach makes it possible to cope with the complex boundary conditions often encountered.

(b) The finite difference analysis.

The nozzle is divided into a series of concentric, thin walled tubes, each have the same thickness specified by (a Δf), where **a** is the tube outer radius and Δf is the fractional increment in fractional radius for each element.

With this geometry a incremental graph of temperature versus step radius can be produced. The labelling of the temperature increment is such that θ_n is the temperature at a point $n\Delta f$ from the axis of the nozzle when considering dimensionless heat flow.

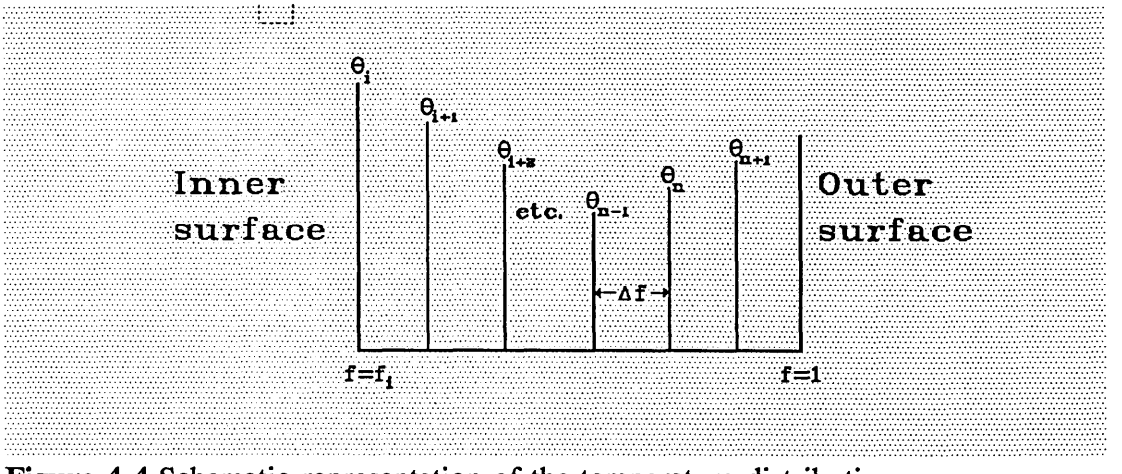

Figure 4.4 Schematic representation of the temperature distribution.

Figure 4.4 shows schematically a representation of the temperature distribution at a moment in time corresponding to $\tau = \tau$. Given this, a strategy is need to calculate the temperature distribution at a later time, corresponding to $\tau = \tau + \Delta\tau$. The process could the be applied repeatedly to deduce temperature on a whole series of time steps, $\Delta\tau$ apart.

Considering three adjacent temperature intervals:

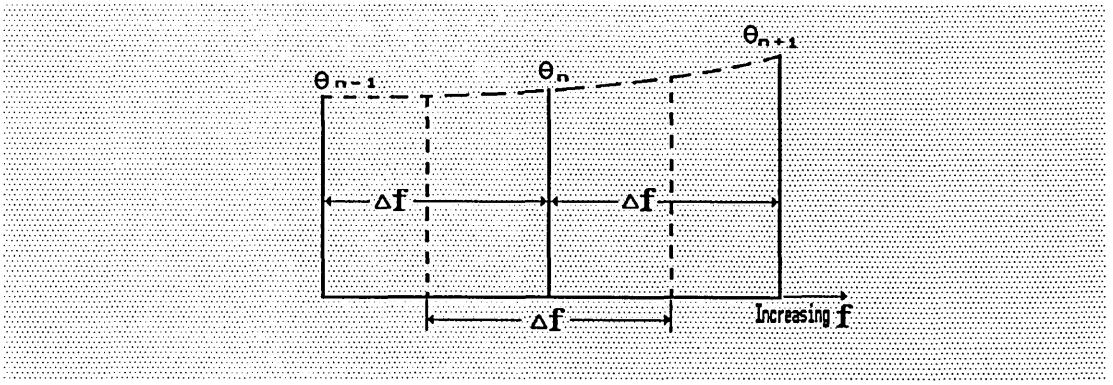

The gradients at the mid points 1 and 2 between temperature steps are given by:

$$G_1 = \left(\frac{\theta_n - \theta_{n-1}}{\Delta f}\right) \quad , \quad G_2 = \left(\frac{\theta_{n+1} - \theta_n}{\Delta f}\right)$$

The separation between mid points 1 and 2 is Δf, so the rate of change of gradient is:

$$\left(\frac{G_1 - G_2}{\Delta f}\right)$$

Thus:

$$\left(\frac{\partial^2\theta}{\partial f^2}\right) = \left(\frac{G_2 - G_1}{\Delta f}\right) \tag{4.58}$$

And substituting for G_1 and G_2 gives:

$$\begin{aligned}\left(\frac{\partial^2\theta}{\partial f^2}\right) &= \left\{\frac{\theta_{n+1} - \theta_n - (\theta_n - \theta_{n-1})}{(\Delta f)^2}\right\} \\ &\vdots \\ &= \left\{\frac{\theta_{n+1} - 2\theta_n + \theta_{n-1}}{(\Delta f)^2}\right\}\end{aligned} \tag{4.59}$$

The relationship between $(\partial\theta/\partial\tau)$ is obtained by letting $\theta"_n$ equal the value of θ_n on the next time step, later in time by an amount equivalent to $\Delta\tau$. Then

$$\left(\frac{\partial\theta}{\partial\tau}\right) = \left(\frac{\theta''_n - \theta_n}{\Delta\tau}\right) \tag{4.60}$$

This is a forward difference statement, and leads to an explicit statement of $\partial_{n+\Delta n}$, hence the term explicit net analysis which is applied to this technique.

To be consistent with the way in which the first time derivative is defined, $(\partial\theta/\partial f)$ must be written as:

$$\left(\frac{\theta_{n+1} - \theta_n}{\Delta f}\right)$$

whilst $1/f$ may be written as $1/n\Delta f$

The dimensionless form of difference equation.-

$$\left(\frac{\partial^2\theta}{\partial f^2} + \frac{1}{f}\frac{\partial\theta}{\partial f}\right) = \left(\frac{\partial\theta}{\partial\tau}\right) \qquad \textbf{(4.61)}$$

can now be written as a difference equation:

$$\left(\frac{\theta_{n+1} - 2\theta_n + \theta_{n-1}}{(\Delta f)^2}\right) + \left(\frac{1}{n}\cdot\frac{\theta_{n+1} - \theta_n}{(\Delta f)^2}\right) = \left(\frac{\theta''_n - \theta_n}{\Delta\tau}\right) \qquad \textbf{(4.62)}$$

or

$$\theta''_n = \theta_n + \left(\frac{\Delta\tau}{(\Delta f)^2}\right)\left\{\theta_{n+1} - 2\theta_n + \theta_{n+1} + \frac{1}{n}(\theta_{n+1} - \theta_n)\right\} \qquad \textbf{(4.63)}$$

Because this equation requires both θ_{n+1}, θ_{n-1} as well as θ_n to specify θ''_n, boundary conditions must be specified independently.

(i) Finite outer surface heat transfer theory

Suppose that the nozzle is divided into a net mesh as follows:

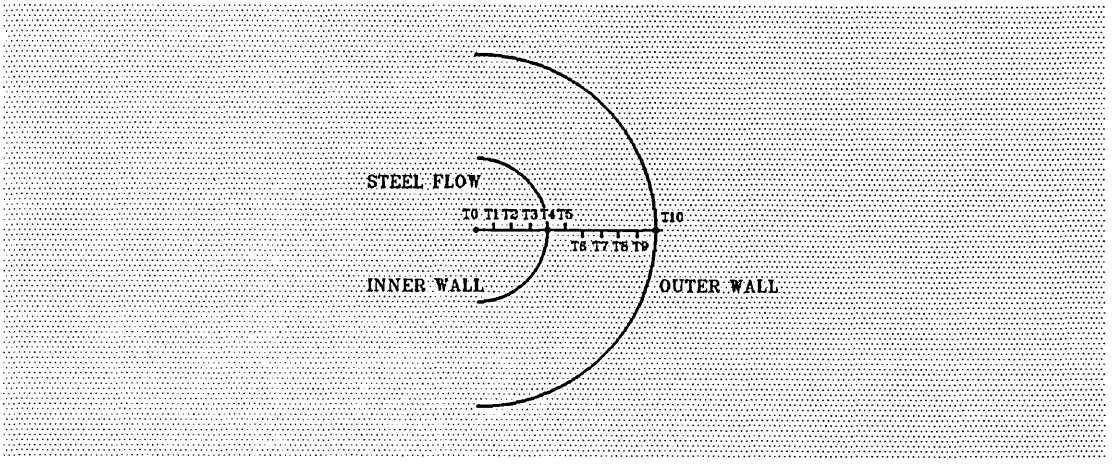

So that $\Delta f = 0.1$, θ_4 is the inner surface temperature, θ_{10} is the outer surface temperature.

The total number of intervals, including those that fall within the bore of the nozzle is m. In the illustration, m=10.

Consider the outer "half element" as a thin walled tube of thickness (Δr/2).

Then the outer radius = m Δr

and the inner radius = (m - ½)Δr

where: $\Delta r = a\,\Delta f$

and is effectively the net spacing for a real, dimensioned, nozzle.

For a unit length of nozzle, the outer area of the element is $= 2\pi m\Delta r$

and the inner area of the element is $= 2\pi(m-\frac{1}{2})\Delta r$

Because the inner surface is half way between θ_{m-1} and θ_m, the temperature gradient will be:

$$TEMPERATURE\ GRADIENT = \left(\frac{\theta_{m-1} - \theta_m}{\Delta r}\right)$$

Thus, for a thermal conductivity k, the rate of input of energy will be:

$$k \cdot 2\pi \left(m-\frac{1}{2}\right)\Delta r \cdot \left(\frac{\theta_{m-1} - \theta_m}{\Delta r}\right) = 2\pi k \left(m-\frac{1}{2}\right)(\theta_{m-1} - \theta_m) \qquad (4.64)$$

For the outer boundary, the surface heat transfer coefficient h is defined as the rate of energy transfer per unit area per unit temperature difference across the nozzle-air boundary. Thus, setting the air temperature at θ_a, the rate of output of energy becomes:

$$= 2\pi\ h\ m\ \Delta r(\theta_m - \theta_a) \qquad (4.65)$$

Now the volume of this element per unit length is:

$$= \left[\pi m^2 - \pi\left(m - \frac{1}{2}\right)^2\right](\Delta r)^2 \quad \rightarrow \quad = \pi\left(m - \frac{1}{4}\right)(\Delta r)^2 \qquad (4.66)$$

If the temperature gradient across the element is assumed to be linear, a reasonable assumption for a thin walled element, then:

$$\textit{Outer surface temperature} = \theta_m$$

$$\circ$$

$$\textit{inner surface temperature} = \frac{\theta_m - \theta_{m-1}}{2}$$

$$\circ$$

$$\textit{mean temperature} = \frac{1}{2}\left(\theta_m + \frac{\theta_m + \theta_{m-1}}{2}\right)$$

$$\circ$$

$$\textit{thus}$$

$$\textit{the mean temperature} = \frac{3}{4}\theta_m + \frac{1}{4}\theta_{m-1}$$

In general, θ_{m-1} and θ_m are known on a given time step, and θ_{m+1} on the next time step; from this a value of θ_m is seek.

The thermal capacity of the element per unit length is:

$$= \pi\left(m - \frac{1}{4}\right)(\Delta r)^2 \cdot \rho Cp \qquad \textbf{(4.67)}$$

and so the heat content on a given time step will be:

$$= \pi\left(m - \frac{1}{4}\right)(\Delta r)^2 \cdot \rho Cp \cdot \frac{1}{4}\{3\theta_m + \theta_{m-1}\} \qquad \textbf{(4.68)}$$

whilst on the next time step this will have become:

$$= \pi\left(m - \frac{1}{4}\right)(\Delta r)^2 \cdot \rho Cp \cdot \frac{1}{4}\{3\theta''_m + \theta''_{m-1}\} \qquad \textbf{(4.69)}$$

Thus the energy gain will be:

$$- \frac{\pi}{4}\left(m - \frac{1}{4}\right)(\Delta r)^2 \cdot \rho Cp \cdot \left\{ 3\theta''_m - 3\theta_m + \theta''_{m-1} - \theta_{m-1} \right\} \qquad (4.70)$$

and the rate of energy gain:

$$- \frac{\pi}{4}\left(m - \frac{1}{4}\right)\frac{(\Delta r)^2}{\Delta \tau} \cdot \rho Cp \left\{ 3\left(\theta''_m - \theta_m\right) + \theta''_{m-1} - \theta_{m-1} \right\} \qquad (4.71)$$

Where $\Delta\tau$ is the time interval between the two sets of measurements.

This rate of energy gain must be the difference between the rate of energy input and output:

$$- 2\pi k \left(m - \frac{1}{2}\right)\left(\theta_{m-1} - \theta_m\right) - 2\pi\ h\ m\ \Delta r\left(\theta_m - \theta_a\right) \qquad (4.72)$$

Relating thermal conductivity and the surface heat transfer coefficient in term of a dimensionless parameter,γ, such that:

$$\gamma = \frac{\Delta r\ h}{k} \qquad (4.73)$$

Then the expression for the difference between the rates of input and output of energy becomes:

$$- 2\pi k \left\{ \left(m - \frac{1}{2}\right)\left(\theta_{m-1} - \theta_m\right) - \gamma \cdot m\ \left(\theta_m - \theta_a\right) \right\} \qquad (4.74)$$

Which can now be equated to the rate of energy gain of the element:

$$2\pi k \left\{\left(m - \frac{1}{2}\right)(\theta_{m-1} - \theta_m) - \gamma \cdot m\,(\theta_m - \theta_a)\right\} \\ \vdots \\ - \frac{\pi}{4}\left(m - \frac{1}{4}\right)\frac{(\Delta r)^2}{\Delta \tau}\,\rho Cp\,\{3\theta''_m - 3\theta_m - \theta''_{m-1} - \theta_{m-1}\} \tag{4.75}$$

or

$$\frac{8k}{\rho Cp} \cdot \frac{\Delta t}{(\Delta r)^2}\left\{\left(m - \frac{1}{2}\right)(\theta_{m-1} - \theta_m) - \gamma \cdot m\,(\theta_m - \theta_a)\right\}\left(m-\frac{1}{4}\right)^{-1} \\ \vdots \\ = 3\theta''_m - 3\theta_m + \theta''_{m-1} - \theta_{m-1} \tag{4.76}$$

Solving for θ''_m gives:

$$\theta''_m = \theta_m - \frac{1}{3}(\theta''_{m-1} - \theta_m) + \\ \vdots \\ \frac{8}{3}\frac{k}{\rho Cp}\frac{\Delta t}{(\Delta r)^2}\left\{\frac{\left(m - \frac{1}{2}\right)}{\left(m - \frac{1}{4}\right)}(\theta_{m-1} - \theta_m) - \gamma \cdot \frac{m}{\left(m - \frac{1}{4}\right)}(\theta_m - \theta_a)\right\} \tag{4.77}$$

From the original expression for the heat conduction equation in dimensionless form:

$$\alpha = \frac{k}{\rho Cp} \qquad \frac{\alpha t}{r^2} = \frac{\tau}{f^2}$$

$$\therefore$$

$$\frac{\alpha \Delta t}{(\Delta r)^2} = \frac{\Delta \tau}{(\Delta f)^2}$$

and the equation becomes:

$$\theta''_m = \theta_m - \frac{1}{3}\left(\theta''_{m-1} - \theta_{m-1}\right) +$$

$$\vdots$$

$$\frac{8}{3}\frac{\Delta\tau}{(\Delta f)^2}\left\{\frac{\left(m - \frac{1}{2}\right)}{\left(m - \frac{1}{4}\right)}\left(\theta_{m-1} - \theta_m\right) - \gamma \cdot \frac{m}{\left(m - \frac{1}{4}\right)}\left(\theta_m - \theta_a\right)\right\} \qquad \textbf{(4.78)}$$

From which the outer surface temperature on the next time step may be calculated.

(ii) Finite inner surface heat transfer theory

For the inner boundary, the surface heat transfer coefficient, h, is defined as the rate of energy transfer per unit area per unit temperature difference across the water-nozzle boundary. Thus, setting the water temperature at θ_w, the rate of input of energy per unit length of nozzle is:

$$-h \cdot 2\pi n \, \Delta r \left(\theta_w - \theta_n\right) \qquad \textbf{(4.79)}$$

Where the inner boundary is assumed to be on the *mth* net point.

As with the outer surface heat transfer, a "half element" region was defined as a nozzle of wall thickness ($\Delta r/2$).

So that the outer area of the element is $= 2\pi(m+\frac{1}{2})\Delta r$

Whilst the temperature gradient at the outer "half element" point will be approximately:

$$TEMPERATURE\ GRADIENT = \left(\frac{\theta_m - \theta_{m+1}}{\Delta r} \right)$$

Therefore the rate of heat flow across the outer boundary is given by:

$$2\pi k \left(m + \frac{1}{2}\right)\Delta r \cdot \left(\frac{\theta_m - \theta_{m+1}}{\Delta r}\right) = 2\pi k \left(m + \frac{1}{2}\right)(\theta_m - \theta_{m+1}) \qquad \textbf{(4.80)}$$

For a linear temperature gradient, reasonable for a thin element.

$$Inner\ surface\ temperature = \theta_m$$

$$Outer\ surface\ temperature = \frac{\theta_m + \theta_{m+1}}{2}$$

$$Mean\ temperature = \frac{1}{2}\left(\theta_m + \frac{\theta_m + \theta_{m+1}}{2}\right)$$

Thus,

$$\textit{The mean temperature} = \frac{3}{4}\theta_m + \frac{1}{4}\theta_{m+1}$$

Now, the volume of element per unit length:

$$= \left[\pi\left(m + \frac{1}{2}\right)^2 - \pi\, m^2\right](\Delta r)^2 = \pi \left(m + \frac{1}{4}\right)(\Delta r)^2 \qquad \textbf{(4.81)}$$

And the thermal capacity will be:

$$= \pi \left(m + \frac{1}{4}\right)(\Delta r)^2\, \rho C_p \qquad \textbf{(4.82)}$$

Thus the heat content on a given time step will be:

$$\frac{\pi}{4}\left(m + \frac{1}{4}\right)(\Delta r)^2\, \rho\, C_p \{3\theta_m + \theta_{m+1}\} \qquad \textbf{(4.83)}$$

And on the next step:

$$\frac{\pi}{4}\left(m + \frac{1}{4}\right)(\Delta r)^2\, \rho\, C_p \{ 3\theta''_m + \theta''_{m+1}\} \qquad \textbf{(4.84)}$$

So the rate of rise of internal energy will be:

$$\frac{\pi}{4}\left(m + \frac{1}{4}\right)\frac{(\Delta r)^2}{\Delta \tau}\, \rho C_p \left[3\left(\theta''_m - \theta_m\right) + \theta''_{m+1} - \theta_{m+1}\right] \qquad \textbf{(4.85)}$$

Where, as before, $\Delta\tau$ is the time interval between the two measurements.

This must be equal to the difference between the rates of energy input and output:

$$2\pi h \cdot m\Delta r \,(\theta_w - \theta_m) - 2\pi k \left(m+\frac{1}{2}\right)(\theta_m - \theta_{m+1}) \qquad (4.86)$$

Relating thermal conductivity and the surface heat transfer coefficient in terms of a dimensionless parameter, Γ, such that:

$$\Gamma = \frac{\Delta r\, h}{k} \qquad (4.87)$$

Then the expresion now becomes:

$$2\pi k \left[\Gamma\, m\, (\theta_w - \theta_m)) - \left(m + \frac{1}{2}\right)(\theta_m - \theta_{m+1})\right] =$$

$$\frac{\pi}{4}\left(m + \frac{1}{4}\right)\frac{(\Delta r)^2}{\Delta\tau}\,\rho C_p \left[3\theta''_m - 3\theta_m + \theta''_{m+1} - \theta_{m+1}\right] \qquad (4.88)$$

Solving for $\theta"_m$ gives:

$$\theta''_m = \theta_m - \frac{1}{3}\left(\theta''_{m+1} - \theta_{m+1}\right) +$$

$$\cdot\frac{8}{3}\frac{k}{\rho C_p}\frac{\Delta\tau}{(\Delta r)^2}\left\{\frac{\Gamma \cdot m}{\left(m + \frac{1}{4}\right)}(\theta_w - \theta_m) - \left(\frac{m + \frac{1}{2}}{m + \frac{1}{4}}\right)(\theta_m - \theta_{m+1})\right\} \qquad (4.89)$$

Transforming into dimensionless form, using:

$$\alpha = \frac{k}{\rho C_p} \quad ; \quad \frac{\alpha\tau}{r^2} = \frac{\tau}{f^2}$$

$$\theta''_m = \theta_m - \frac{1}{3}\left(\theta''_{m+1} - \theta_{m+1}\right) +$$

$$\frac{8}{3}\frac{\Delta\tau}{(\Delta f)^2}\left\{\frac{\Gamma m}{\left(m + \frac{1}{4}\right)}\left(\theta_w - \theta_m\right) - \left(\frac{m + \frac{1}{2}}{m + \frac{1}{4}}\right)\left(\theta_m - \theta_{m+1}\right)\right\} \qquad \textbf{(4.90)}$$

From which the inner surface temperature can be calculated.

However, in order for this method to remain stable, it must always have to be arranged that:

$$\frac{\Delta\tau}{(\Delta f)^2} \leq \frac{1}{2}$$

(d) The use of numerical techniques to estimate the internal wall temperature.

The earlier work describes a numerical technique for calculating the temperature within the nozzle wall, as a function of radius, for given external boundary conditions. However, the use of the technique to measure the internal surface temperature is quite different. The inner surface temperature must be determined from transient temperature measurements at one or more internal radial locations. In effect, the use of the **finite difference analysis results** is needed to "work backwards" to deduce the surface temperature - the inverse problem.

(i) Theory of wall temperature estimation:

The first point to note is that the conduction equation is a linear differential equation. Therefore, only consideration of the deviations from a steady state temperature distribution is needed. Since, the variations in steel temperature are likely to be small in comparison with the actual temperature, a reduction of any cumulative errors which might arise can be expected by considering only these deviations from the steady state. Thus, all temperatures considered below are, in effect, partial or deviatory temperatures from the steady state.

Consider a unit temperature "pulse" of duration $\Delta\tau$, where $\Delta\tau$ is the time interval between consecutive measurements of temperature at a fixed point in the nozzle wall. The finite difference method may then be used to calculate the effect of this unit pulse

at all subsequent measurement time intervals (each separated by $\Delta\tau$). These may be designated as fractions "f" of the unit pulse.

Thus, generally, $f_{n\Delta\tau}$ is the fractional partial temperature at the domain point at the end of the *nth* pulse time interval. There will also be throughout the measurement, a corresponding initial "steady state" surface temperature Θ^S and a thermocouple measured temperature Θ^M.

The variation of the deviatory surface temperature is represented as a series of step-wise pulses all of duration $\Delta\tau$, but having heights given by Θ^i_S on the *ith* time interval. Thus, the actual surface temperature:

$$\theta^i_{Surf} = \theta^S + \theta^i_S \tag{4.91}$$

Likewise, the actual measured temperature:

$$\theta^i_{Meas} = \theta^M + \theta^i_M \tag{4.92}$$

Thus, the initial pulse has a height Θ_S^0, related to Θ^0_M, the deviatory measured temperature at the end of this initial pulse, by the equation:

$$\theta^0_M = f_{0\Delta\tau} \cdot \theta^0_S \qquad \rightarrow \qquad \theta^0 = \frac{\theta^0_M}{f_{0\Delta\tau}}$$

This approach is effectively the simple application of a scaling factor to the explicit net analysis results for a pulse of unit height.

Thereafter, the situation becomes more complicated because of the steadily increasing number of such pulses, since all prior pulses contributed to Θ_M^i, the deviatory temperature measured. Hence for the next step Θ^0_S, and Θ^1_S will contribute:

$$\theta^1_M = (f_{1\Delta\tau} \cdot \theta^0_S + f_{0\Delta\tau} \cdot \theta^1_S) \quad \rightarrow \quad \theta^1_S = \frac{\theta^1_M}{f_{0\Delta\tau}} - \frac{f_{1\Delta\tau} \cdot \theta^0_S}{f_{0\delta\tau}}$$

Applying the same logic to Θ^2_M gives:

$$\theta^2_M = f_{2\Delta\tau} \cdot \theta^0_S + f_{1\Delta\tau} \cdot \theta^1_S + f_{0\Delta\tau} \cdot \theta^2_S \quad \rightarrow$$

$$\vdots$$

$$\theta^2_S = \frac{\theta^2_M}{f_{0\Delta\tau}} - \frac{1}{f_{0\Delta\tau}} \left[f_{2\Delta\tau} \cdot \theta^0_S + f_{1\Delta\tau} \cdot \theta^1_S \right]$$

In general, the expression for Θ^n_S will of the form:

$$\theta^n_S = \frac{\Theta^n_M}{f_{0\Delta\tau}} - \frac{1}{f_{0\Delta\tau}} \left[f_{n\Delta\tau} \cdot \theta^0_S + f_{(n-1)\Delta\tau} \cdot \theta^1_S + \ldots\ldots + f_{\Delta\tau} \cdot \theta^{n-1}_S \right] \quad \textbf{(4.93)}$$

or in more compact notation:

$$\theta^n_S = \frac{\theta^n_M}{f_{0\Delta\tau}} - \frac{1}{f_{0\Delta\tau}} \cdot \sum_{i=0}^{n-1} f_{(n-i)\Delta\tau} \cdot \theta^i_S \quad \textbf{(4.94)}$$

And the **current estimate of the surface temperature** is:

$$\theta_{SURF} = \theta^{S} + \theta_{S}^{n} \tag{4.95}$$

In order to calculate Θ_S^n , all prior values of Θ_S up to Θ_S^{n-1} need to be known. In practice, these will all be estimates based upon earlier applications of the above equation. There is therefore a risk of cumulative errors, but fortunately, the fractional partial temperature at domain point, $f_{\Delta\tau}$, drops very rapidly as i increases, so that the summation is only effectively taken over a small number of terms. It is very important to realise that the time interval between measurements is not the same as the time step used in the finite difference analysis, when converted from dimensionless to true time. In order to secure accurate value for $f_{\Delta\tau}$, the finite difference time steps need to be very much smaller.

5

EXPERIMENTAL RESULTS

5.1 TREATMENT OF DATA.

The data for the residence time distribution in either the water model or the prototype system are in the form of pairs of values representing the concentration of the tracer and the sampling time. To generalize the response of the model system the results are plotted in dimensionless form.

The dimensionless time (τ) is calculated by dividing the elapsed time (t) by the mean residence time (t) of the fluid in the tundish:

$$\tau = \frac{Elapsed\ time}{Mean\ residence\ time} = \frac{t}{\bar{t}} \qquad (5.1)$$

The mean residence time for the tundish is obtained by dividing the volume of the fluid in the tundish by the volumetric flow rate as follows:

$$\bar{t} = \frac{V}{\dot{Q}''} \qquad (5.2)$$

Where: V is the total volume of the tundish and

$\dot{Q}$" is the total volumetric flow rate

The dimensionless concentration for the pulse input technique is determined by dividing the actual concentration of the tracer at the outlet by the average concentration of the tracer in the tundish as follows:

$$C_\theta = \frac{\textit{Concentration of tracer inothe exit stream}}{\textit{Calculated mean concentration of tracer inothe tundish}} \qquad (5.3)$$

The calculated mean concentration is obtained by dividing the injected amount of tracer by the volume of the fluid in the tundish:

$$C_{mean} = \frac{\textit{Amount of tracer injected}}{\textit{Total volume of the tundish}} \qquad (5.4)$$

The normalized temperature for the step method is simply the fraction of the change from the initial ladle temperature to the subsequent ladle temperature.

$$F_\theta = \frac{(\theta_m - \theta_o)}{(\theta_f - \theta_o)} \qquad (5.5)$$

Where: F_θ is the dimensionless fractional temperature

θ_m is the measured temperature

θ_o is the initial temperature

θ_f is the final temperature

The residence time distribution of water flowing in the tundish model is analyzed by the modified mixed model proposed by Sahai and Ahuja[13]. The tundish volume is divided into three parts: a dispersed plug volume V_{plug}, a completely mixed volume V_{mixed}, and a dead volume V_{dead}. These fractional volumes are calculated as follows:

$$V_{dead} = 1 - \tau_{mean} \tag{5.6}$$

$$V_{plug} = \frac{\left(\tau_{min} + \tau_{peak} \right)}{2} \tag{5.7}$$

$$V_{mixed} = 1 - V_{dead} - V_{plug} \tag{5.8}$$

Where: τ_{mean} is the mean residence time (dimensionless)

τ_{min} is the dimensionless time of first appearance of tracer

τ_{peak} is the dimensionless time of maximum concentration of tracer

The dimensionless mean residence time (τ_{mean}) is obtained by dividing actual dimensionless residence time by calculated residence time distribution.

This model was used to characterize the experimentally obtained residence time distribution curves.

5.2 DETERMINATION OF THE DISPERSION PARAMETER.

Typical dimensionless concentration-time curves obtained experimentally, in response to a pulse injection of tracer are shown in figures 5.1 and 5.6. These curves were obtained by using the tundish water model described in chapter 3, the experiments being carried out under isothermal conditions. Hydrochloric acid was used as tracer, and a variety of flow control devices were used.

In chapter 4, the tracer plot of the dimensionless concentration distribution against dimensionless time was demonstrated to be a unique function of the vessel dispersion number, known as the *dispersion parameter*. This parameter measures the extent of longitudinal or axial dispersion. Thus:

$$\left(\frac{D_i}{uL}\right) \rightarrow 0 \qquad \textit{negligible dispersion, hence plug flow}$$

$$\left(\frac{D_i}{uL}\right) \rightarrow \infty \qquad \textit{large dispersion, hence mixed flow}$$

A method suggested by Levenspiel and Smith[40], using the experimental dimensionless concentration-time curves to determine the value of the dispersion parameter for the different flow control arrangements in the tundish model was used. This method exploits the relation between the curve variance and the dispersion parameter, given by

the relationship:

$$\sigma^2 = 8\left(\frac{D_i}{uL}\right)^2 + 2\left(\frac{D_i}{uL}\right) \tag{5.9}$$

or, solving for the dispersion parameter,

$$\left(\frac{D_i}{uL}\right) = \frac{1}{8}\left(\sqrt{8\,\sigma^2 + 1} - 1\right) \tag{5.10}$$

To estimate the variance of the concentration-time curves, the method uses a series of concentration readings at uniformly spaced time intervals. The variance is defined as:

$$\sigma^2 = \frac{\int_0^\infty (t-\bar{t})^2\, C\, dt}{\int_0^\infty C\, dt} = \frac{\int_0^\infty t^2\, C\, dt}{\int_0^\infty C\, dt} - \bar{t}^2 \tag{5.11}$$

Replacing the integrals by finite sums, the variance can be written in discret form:

$$\sigma^2 = \frac{\sum t_i^2 C_i}{\sum C_i} - \bar{t}^2 = \frac{\sum t_i^2 C_i}{\sum C_i} - \left(\frac{\sum t_i C_i}{\sum C_i}\right)^2 \tag{5.12}$$

(a) Determination of the dispersion parameter for the tundish model using different flow control devices.

Table 5.1 shows the concentration analysis for a pulse input of tracer from the sub-ladle entry nozzle. Air bubbling was used as a flow control device at the centre of the tundish model. From this analysis the dispersion parameter was estimated to be 0.106 as shown in table 5.2. Substituting this value in equation (4.32), in chapter 4, the fractional temperature drop at Submerged Mould Entry Nozzle for a step change in temperature applied at the sub-lance tundish entry nozzle has been predicted, and the results for the measured and predicted fractional temperature change are shown in table 5.2 and plotted in figure 5.2.

The dispersion parameter estimated for a similar experiment with no flow control devices was found to be 0.114, similar to the predicted value when air bubbling was used as flow control. This is shown graphically in figure 5.4. It can be seen that air bubbling does not have any considerable effect in the longitudinal mixing of the tracer, however, figure 5.5 shows that air bubbling produced a small reduction of the dead volume.

The analysis of this experiment is given in tables 5.3 and 5.4. Figure 5.3 shows the measured and predicted fractional temperature drop at the model SEN for a step change in water temperature applied at the sub-lance tundish entry nozzle.

Similar sets of experiments were carried out using three different flow control arrangements, as shown schematically in diagrams 5.1, 5.2 and 5.3:

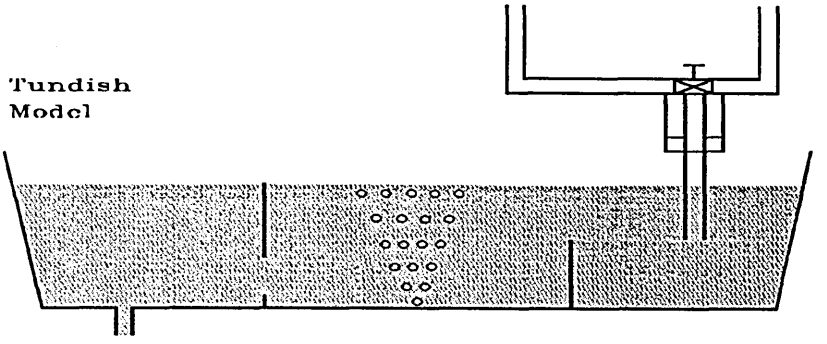

Diagram 5.1 Schematic flow control arrengement using a weir, a dam and bubbling air in the centre of the tundish model.

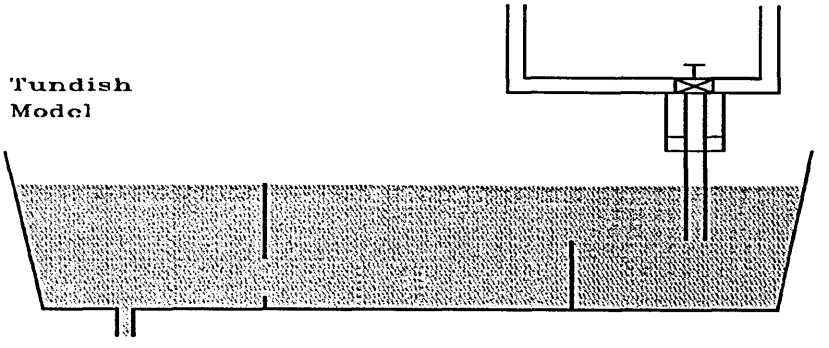

Diagram 5.2 Schematic flow control arrengement using a weir and a dam.

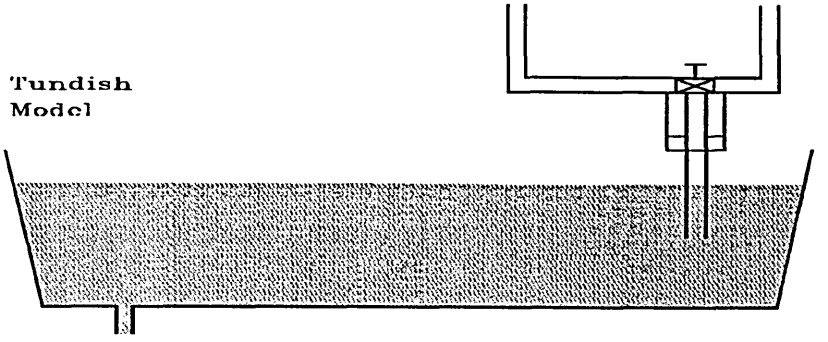

Diagram 5.3 Not flow control divices

The experimental dimensionless concentration-time curves obtained in response to a pulse injection of tracer at the sub-ladle entry nozzle are given in figure 5.6. The analysis of these curves are given in tables 5.5, 5.7, and 5.9. Dispersion parameters estimated from these results, using the method described by Levenspiel and Smith[40], are given in tables 5.6, 5.8 and 5.10. The dispersion parameter values are very close for three different flow control arrangements; thereafter, the predicted fractional temperature drop predicted using the dispersion model for this set of experiments are similar. One important difference is the first appearance of the tracer for the experimental readings in both the pulse and the step input. For the pulse input when no flow control devices are present the tracer takes longer to reach the Submerged Mould Entry Nozzle.

Figures 5.7, 5.8, and 5.9 show the predicted and measured fluid temperature at the outlet nozzle after a step change in fluid temperature introduced at the tundish entry nozzle.

Figure 5.10 shows the determined dispersion parameter and the dispersed plug volume for the three different flow control arrangements, where it can be seen that these flow control devices did not have much effect on the longitudinal dispersion parameter, however they decreased the dispersed plug volume. Air bubbling did not have any considerable effect on the dispersion parameter but it increased the plug volume.

Using a simple mixed model suggested by Sahai and Ahuja[13] the tundish volume fractions were determined. This volume fractions are the dispersed plug volume, the mixed volume and the dead volume. This results are shown in figure 5.11, where it can be seen that when no flow control devices are present in the tundish the plug volume fraction and the mixed volume fraction are very similar. However, by the application of flow control devices the mixed volume fraction increased considerably decreasing the plug volume fraction. Air bubbling in conjunction with the flow control devices did not change the completely mixed volume fraction, however, the dead volume fraction decreased. The completely mixed volume fraction varied from approximately 0.46 to 0.57 for various configurations studied.

(b) Determination of the dispersion parameter for the tundish model using the heat compensation system.

In order to obtain a more precise control of the steel temperature entering the mould of the continuous casting machine the residence times from the sub-ladle tundish entry nozzle and from the "dog-house" have to be known to match heat supply to input temperature, for this the pulse input analysis has to be carried out twice.

The dispersion parameter can be determined from the concentration-time response to the pulse injection of tracer, first for the fluid path A - this is from the entry nozzle to the outlet and then for the fluid path B - this is from the steam nozzle to the outlet. Path A and Path B are shown schematically in diagram 5.4

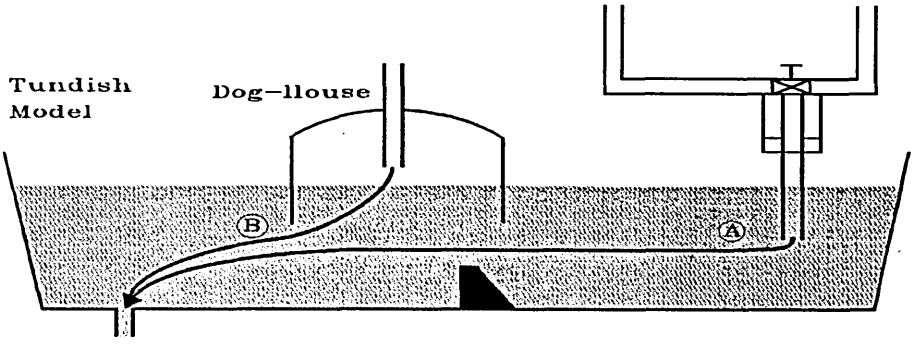

Diagram 5.4 Schematic representation of tracer paths A and B.

A set of experiments were carried out placing the "dog house" at different distances away from the sub-ladle entry nozzle, as shown schematically in diagrams 5.5 and 5.6.

Figure 5.12 shows the experimental dimensionless concentration-time curves obtained in response of a pulse injection of tracer at the sub-ladle entry nozzle and at the steam entry nozzle in the "dog house". The tundish arrengement is shown schematically in diagram 5.5. Table 5.11 shows the concentration analysis for the pulse imposed at the entry nozzle, and table 5.12 shows the concentration analysis for the pulse imposed at the steam entry nozzle.

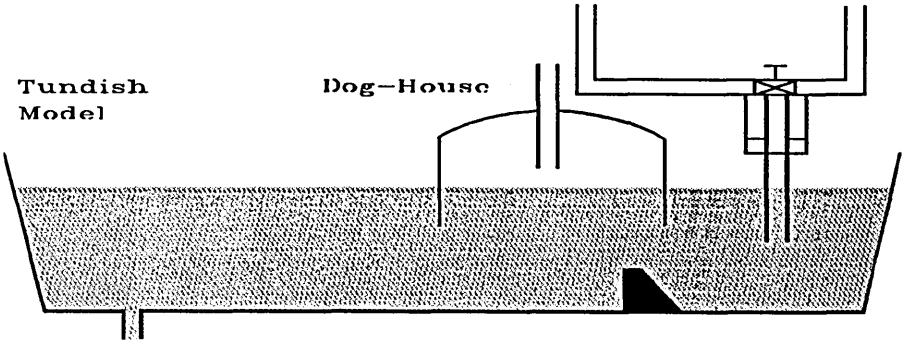

Diagram 5.5 Schematic arrengement for tundish heating

From this analysis the dispersion parameter has been determined using the method described above, and it is shown in table 5.13. Figure 5.13 shows the comparison between the measured temperature change and that predicted theoretically using the equations developed in chapter 4. This temperature change was generated from the step change in the water temperature at the entry nozzle after 1.14 units of dimensionless time the steam heating system was started, raising the temperature of water flowing down stream towards the measuring point in the outer nozzle.

The volume fractions for the tundish arrangement was estimated using the mixing model and the results are plotted in figure 5.14. Figure 5.15 shows the comparison between the dispersion parameter and the dispersed plug volume.

Similar experiment was carried out for the arrangement shown schematically in diagram 5.6. The "dog-house" was moved to the centre of the tundish model, closer to the exit

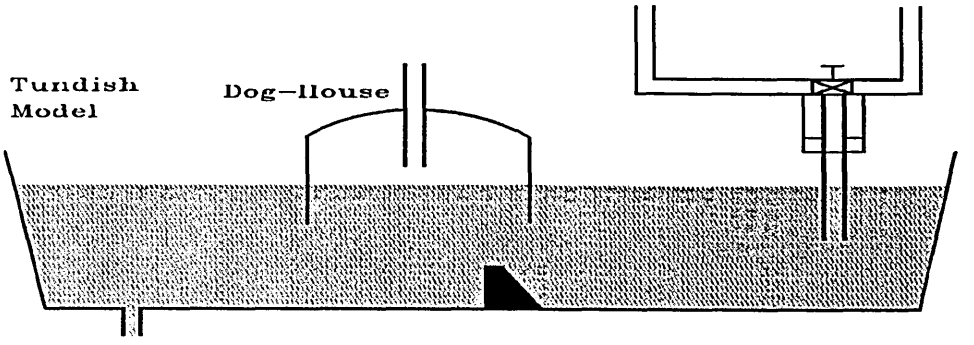

Diagram 5.6 Schematic arrengement for tundish heating

nozzle. Figure 5.16 shows the experimental dimensionless concentration-time curve obtained in response of a pulse injection of tracer at the sub-ladle entry nozzle and at the steam entry nozzle in the "dog-house". Table 5.14 shows the concentration analysis for the pulse imposed at the entry nozzle, and table 5.15 shows the concentration analysis for the pulse imposed at the steam entry nozzle.

Using the method described above the dispersion parameter was estimated from these analyses the estimates are shown in table 5.16. Figure 5.17 shows the theoretically predicted and measured fractional temperature response to a step input at the sub-ladle entry nozzle, and application of steam heating 1.5 units of time later, to compensate the temperature drop.

Using the mixed model the volume fractions of the tundish model were determined for both paths - from the entry nozzle and from the steam nozzle to the exit, and they are

plotted in figure 5.18. Figure 5.19 shows a comparison between dispersion parameter and the dispersed plug volume.

5.3 ESTIMATION OF INTERNAL SURFACE TEMPERATURE

The estimation of internal surface temperature was investigated using a remote sensing method, the method involves the incorporation of three thermocouples into the walls of the ladle and tundish nozzles tubes, which sense the liquid steel temperatures in the inlet stream to the tundish and in the submerged entry nozzle. As the temperature of liquid steel in either tube changes, the temperature indicated by the thermocouple will also change, but a later time and to a later extent. The liquid steel temperatures must be deduced from the measured changes - a classic inverse problem since the liquid steel temperatures are the boundary conditions for the solution to the heat conduction in the tube wall.

Chapter 4 described the development of an inverse heat conduction algorithm to estimate the temperature of a fluid flowing throughout a nozzle. Two sets of experiments were carried out in order to validate this algorithm, a theoretical simulation experiment and experimental measurements using the water model described in chapter 3.

(a) Theoretical simulation experiments

The theoretical simulation experiment consisted of using the numerical technique to calculate the internal fractional partial temperature of the nozzle, creating look-up tables for $f_{\Delta\tau}$, $f_{2\Delta\tau}$, $f_{3\Delta\tau}$, etc. for the thermocouple positions r_1, r_2 and r_3. Infinite heat tranfer conditions are assumed, for this experiments. The thermal properties of the refractory nozzle used are given in table 5.17.

Table 5.17 Properties of the material used in the experimental tests.

Properties	Refractory nozzle	Perspex nozzle
Thermal conductivity (W $°K^{-1}$ m^{-1})	1.39	0.21
Density (Kg m^{-3})	2.09	1.19
Specific heat (J $°K^{-1}$ Kg^{-1})	1.21	1.52
Thermal diffusivity (m^2 sec^{-1})	5.49 X 10^{-6}	1.16 X 10^{-7}

The numerical method was used to predict temperatures at thermocouple interior domain positions for:

(i) A sudden jump in the interior surface temperature - Simulating the submerged entry nozzle preheating at 1200 °C and steel entering at 1600 °C.

(ii) A ramp up in temperature from 1550 °C to 1600 °C - Simulating a ladle change operation.

(iii) A slow fall in temperature at 0.5 °C min^{-1} - Simulating the ladle cooling.

The predicted temperatures were used in the inverse heat conduction algorithm to estimate the internal surface temperature of the nozzle.

The corresponding initial "steady state" temperatures for the initial pulse and for the domain are estimated from straight line fit at the start. Then the deviatory temperatures are estimated by applying the algorithm to predict the domain temperatures. The computer code written in Power Basic used for this simulation is listed in appendix 1.

Figure 5.21 shows the results for the simulation experiment where the temperature was left to reach a steady state at 1200 °C and then subject to a sudden increase to 1600 °C, followed by ladle cooling at a rate of 0.5 °C min^{-1}. Figures 5.22 and 5.23 shows the same results plotted in a finer scale.

Figure 5.24 shows the results for the ladle change simulation, the temperature is left to reach a steady state at 1550 °C and ramp up over three times the tundish residence time to 1600 °C followed by a steady temperature fall at a rate of 0.5 °C min^{-1}.

(b) Experimental measurements

In order to verify the inverse heat conduction algorithm a set of experimental measurements were carried out using the tundish water model. Inverse problems are extremely sensitive to measurements errors. The thermal properties of the wall material have to be accurately known, as well as thermocouple position and thickness of the wall.

The thermal conductivity of the perspex material used in the tundish nozzles of the water model was measured using the "Lee's disk conductivity apparatus" (electrical method). A 3 mm sample was taken from the perspex block in the form of a disc the same diameter as the copper discs constituting the apparatus. The value estimated was 0.21 $W K^{-1} m^{-1}$ and is given in table 5.17, together with density, and specific heat used in these validation experiments.

Three needle thermocouples were embedded inside the sub-ladle entry nozzle wall with a tickness of 18 mm, the thermocouples were placed radially at two, four and six millimetres away from the internal surface of the nozzle. Two more thermocouples were installed, one in the inlet and the other in the outlet water streams. The five thermocouples were connected to a 386 SX personal computer and the temperatures were registered by the data acquisition package "WorkBench™" and logged to a disk.

The first experiment involved a severe test placing a sudden change in the inlet water temperature, registering three transient interior nozzle temperatures, and logging at 40 seconds intervals. Then, the inverse heat transfer algorithm and the three internal wall temperatures were used to estimate the inlet water temperature. Finally, the estimated and the measured input water temperatures were compared and the results are plotted in figure 5.27.

A second set of experiments were carried out using five thermocouples; three embedded inside the wall, one in the inlet water stream and the other one in the outlet stream. A

step change in the inlet water temperature was introduced, and the output of the thermocouples was registered and logged to a disk at forty seconds intervals. One hundred seconds after the step input, the steam jet was switched to blow the steam on to the water surface.

The temperatures logged for the three thermocouples embedded inside the wall were used to estimate the inlet water temperature using the inverse heat transfer algorithm and the dispersion model was used to predict the outlet water temperature. The estimated inlet water temperature and the predicted outlet temperatures were compared to the measured at the inlet and outlet temperatures respectively. The estimated and measured results are plotted in figures 5.28 and 5.29.

Table 5.1.
Concentration readings representing the continuous response to a pulse input of a tracer

Time (Sec)	Conductivity (mmho/cm)	Concentration (g-Mol/l)	Time [-]	Concentration [-]	Concentration Time [-]	Concentration Time ^ 2 [-]
0.00	1.064	0.0033	0.00	0.2261	0.0000	0.0000
15.71	1.064	0.0033	0.24	0.2261	0.0532	0.0125
20.00	3.546	0.0110	0.30	0.7538	0.2256	0.0675
40.00	28.014	0.0869	0.60	5.9548	3.5647	2.1339
47.85	28.901	0.0897	0.72	6.1432	4.3992	3.1503
60.00	24.113	0.0748	0.90	5.1256	4.6025	4.1327
80.00	15.248	0.0473	1.20	3.2412	3.8805	4.6460
100.00	7.801	0.0242	1.50	1.6583	2.4817	3.7141
120.00	3.900	0.0121	1.80	0.8290	1.4888	2.6736
140.00	2.128	0.0066	2.10	0.4523	0.9476	1.9853
160.00	1.241	0.0039	2.39	0.2638	0.6317	1.5126
180.00	1.064	0.0033	2.69	0.2261	0.6091	1.6409
200.00	1.064	0.0033	2.99	0.2261	0.6768	2.0258

Tundish volume: 13.7 L
Water flow rate: 12.4 L/min
Air bubbling in the centre of the tundish model

Table 5.2
Temperature readings representing the continuous response to a step input of the tracer

Concentration curve variance	*Dispersion Parameter*	*Time (Sec)*	*Temperature (C)*	*Time [-]*	*Experimental frac. temperature change*	*Calculated frac. temperature change*
0.3025	*0.1062*	*0.00*	*20.000*	*0.00*	*1.0000*	*1.0000*
		17.14	*19.900*	*0.26*	*0.9890*	*0.9996*
		20.00	*19.750*	*0.30*	*0.9720*	*0.9973*
		40.00	*17.729*	*0.60*	*0.7480*	*0.8711*
		60.00	*15.416*	*0.90*	*0.4910*	*0.5950*
		80.00	*13.692*	*1.20*	*0.2990*	*0.3411*
		100.00	*12.598*	*1.50*	*0.1780*	*0.1903*
		120.00	*12.009*	*1.81*	*0.1120*	*0.0991*
		140.00	*11.757*	*2.11*	*0.0840*	*0.0505*
		160.00	*11.505*	*2.41*	*0.0560*	*0.0255*
		180.00	*11.379*	*2.71*	*0.0420*	*0.0127*
		200.00	*11.294*	*3.01*	*0.0327*	*0.0062*

Tundish volume: 13.7 L
Water flow rate: 12.4 L/min
Air bubbling in the centre of the tundish model

Table 5.3
Concentration readings representing the continuous response to a pulse input of a tracer

Time (Sec)	Conductivity (mmhoms/cm)	Concentration (g-Mol/L)	Time [-]	Concentration [-]	Concentration * time [-]	Concentration * time ^ 2 [-]
0.00	1.0563	0.0033	0.00	0.2245	0.0000	0.0000
15.42	1.0563	0.0033	0.23	0.2245	0.0518	0.0120
20.00	8.4507	0.0262	0.30	1.7963	0.5377	0.1609
40.00	26.4084	0.0819	0.60	5.6135	3.3604	2.0116
44.14	27.2887	0.0847	0.66	5.8006	3.8318	2.5312
60.00	21.1268	0.0656	0.90	4.4908	4.0324	3.6209
80.00	12.5000	0.0388	1.20	2.6570	3.1811	3.8086
100.00	6.6901	0.0208	1.50	1.4221	2.1282	3.1850
120.00	3.8732	0.0120	1.80	0.8233	1.4786	2.6553
140.00	1.9366	0.0060	2.10	0.4117	0.8625	1.8071
160.00	1.4085	0.0044	2.39	0.2994	0.7169	1.7166
180.00	1.0563	0.0033	2.69	0.2245	0.6049	1.6294
200.00	1.0563	0.0033	2.99	0.2245	0.6721	2.0116

Tundish volume: 13.7 L
Water flow rate: 12.4 L/min
No flow control devices

Table 5.4.
Temperature readings representing the continuous response to a step input of the tracer

Concentration curve variance	Dispersion parameter	Time (Sec)	Temperature (C)	Time [-]	Experimental frac. temperature change	Calculated frac. temperature change
0.3315	0.1139	200.0	22.00	0.000	1.0000	1.0000
		19.9	21.95	0.299	0.9944	0.9965
		20.0	21.90	0.301	0.9889	0.9900
		40.0	19.48	0.602	0.7200	0.8620
		60.0	17.14	0.903	0.4600	0.5845
		80.0	14.71	1.204	0.1900	0.3516
		100.0	13.99	1.505	0.1100	0.1980
		120.0	13.72	1.806	0.0800	0.1065
		140.0	13.36	2.107	0.0400	0.0565
		160.0	13.18	2.408	0.0200	0.2900
		180.0	13.17	2.709	0.0189	0.1500
		200.0	13.15	3.010	0.0167	0.0080

Tundish volume: 13.7 L
Water flow rate: 12.4 L
Not flow control devices

Table 5.5
Concentration readings representing the continuous response to a pulse input of tracer

Time (Sec)	Conductivity (mmhoms/cm)	Concentration (g-Mol/L)	Time [-]	Concentration [-]	Concentration * time [-]	Concentration * time ^ 2 [-]
0.00	1.020	0.0032	0.00	0.2169	0.0000	0.0000
11.52	1.020	0.0032	0.17	0.2169	0.0377	0.0066
20.00	13.265	0.0412	0.30	2.8197	0.8507	0.2567
40.00	23.469	0.0728	0.60	4.9887	3.0102	1.8164
60.00	18.027	0.0559	0.91	3.8319	3.4683	3.1392
80.00	11.905	0.0369	1.21	2.5305	3.0539	3.6855
100.00	6.803	0.0211	1.51	1.4460	2.1813	3.2906
120.00	3.741	0.0116	1.81	0.7953	1.4397	2.6062
140.00	2.381	0.0074	2.11	0.5061	1.0689	2.2574
160.00	1.701	0.0053	2.41	0.3615	0.8725	2.1060
180.00	1.190	0.0037	2.72	0.2530	0.6871	1.8657
200.00	1.020	0.0032	3.02	0.2169	0.6544	1.9744

Tundish volume: 13.7 L
Water flow rate: 12.4 L/min
Air bubbling in the centre of the tundish

Table 5.6
Temperature readings representing the continuous response to a step input of the tracer

Concentration curve variance	Dispersion parameter	Time (Sec)	Temperature (C)	Time [-]	Experimental frac. temperature change	Calculated frac. temperature change
0.3543	0.1198	0	20.000	0.00	1.000	1.000
		20	20.000	0.30	1.000	1.000
		40	19.700	0.60	0.967	0.995
		60	17.680	0.91	0.742	0.852
		80	15.620	1.21	0.513	0.578
		100	13.762	1.51	0.307	0.351
		120	12.871	1.81	0.208	0.198
		140	12.114	2.11	0.124	0.109
		160	11.802	2.41	0.089	0.058
		180	11.535	2.72	0.059	0.032
		200	11.446	3.02	0.050	0.017

Water flow rate: 12.4 L/min
Air bubbling in the centre of the tundish model

Table 5.7
Concentration readings representing the continuous response to a pulse input of tracer

Time (Sec)	Concentration (mmhoms/cm)	Concentration (g-Mol/cm)	Time [-]	Concentration [-]	Concentration * time [-]	Concentration * time ^ 2 [-]
0.00	1.040	0.003	0.000	0.221	0.0000	0.0000
11.43	1.040	0.003	0.172	0.221	0.0381	0.0066
20.00	20.830	0.065	0.302	4.428	1.3359	0.4030
31.43	25.694	0.080	0.474	5.462	2.5894	1.2277
40.00	23.264	0.072	0.603	4.945	2.9839	1.8005
60.00	15.972	0.050	0.905	3.395	3.0730	2.7814
80.00	10.764	0.033	1.207	2.288	2.7612	3.3323
100.00	6.250	0.019	1.509	1.329	2.0041	3.0232
120.00	3.646	0.011	1.810	0.775	1.4029	2.5395
140.00	2.778	0.009	2.112	0.590	1.2470	2.6335
160.00	1.736	0.005	2.414	0.369	0.8907	2.1499
180.00	1.389	0.004	2.715	0.295	0.8016	2.1766
200.00	1.040	0.003	3.017	0.221	0.6670	2.0123

Tundish volume: 13.7 L
Water flow rate: 12.4 L/min
Using a weir and a dam

Table 5.8
Temperature readings representing the continuous response to a step input of the tracer

Concentration curve variance	Dispersion parameter	Time (Sec)	Temperature (C)	Time [-]	Experimental frac. temperature change	Calculated Frac. temperature change
0.3848	0.1274	0.00	19.000	0.00	1.0000	1.0000
		12.86	19.000	0.19	1.0000	0.9999
		20.00	18.554	0.30	0.9505	0.9941
		40.00	16.149	0.60	0.6832	0.8457
		60.00	13.921	0.91	0.4356	0.5785
		80.00	12.430	1.21	0.2700	0.3565
		100.00	11.604	1.51	0.1782	0.2060
		120.00	10.980	1.81	0.1089	0.1175
		140.00	10.624	2.11	0.0693	0.0651
		160.00	10.446	2.41	0.0495	0.0363
		180.00	10.178	2.72	0.0198	0.0194
		200.00	10.089	3.02	0.0099	0.0106

Tundish volume: 13.7 L
Water flow rate: 12.4 L/min
Using a weir and a dam

Table 5.9
Concentration readings representing the continuous response to a pulse input of tracer

Time (Sec)	Conductivity (mmhoms/cm)	Concentration (g-Mol/L)	Time [-]	Concentration [-]	Concentration * time [-]	Concentration * time [-]
0.00	1.0270	0.0032	0.00	0.2183	0.0000	0.0000
18.57	1.0270	0.0032	0.28	0.2183	0.0612	0.0171
20.00	1.7123	0.0053	0.30	0.3640	0.1098	0.0331
40.00	23.9726	0.0744	0.60	5.0957	3.0748	1.8554
45.71	25.0000	0.0776	0.69	5.3141	3.6646	2.5271
60.00	19.1780	0.0595	0.91	4.0765	3.6897	3.3396
80.00	11.3014	0.0351	1.21	2.4023	2.8991	3.4987
100.00	7.5342	0.0234	1.51	1.6015	2.4159	3.6445
120.00	3.7671	0.0117	1.81	0.8008	1.4495	2.6240
140.00	2.0548	0.0064	2.11	0.4368	0.9224	1.9481
160.00	1.5411	0.0048	2.41	0.3276	0.7907	1.9084
180.00	1.1986	0.0037	2.72	0.2548	0.6918	1.8785
200.00	1.0270	0.0032	3.02	0.2183	0.6586	1.9871

Tundish volume: 13.7 L
Water flow rate: 12.4 L/min
No flow control devices

Table 5.10
Temperature readings representing the continuous response to a step input of the tracer

Concentration Curve variance	Dispersion parameter	Time (Sec)	Temperature (C)	Time [-]	Experimental fractional temperature change	Calculated fractional temperature change
0.3597	0.1212	0	19.00	0.00	1.00	1.000
		20	18.82	0.30	0.98	0.995
		40	16.30	0.60	0.70	0.849
		60	13.87	0.91	0.43	0.578
		80	12.07	1.21	0.23	0.351
		100	11.26	1.51	0.14	0.202
		120	10.72	1.81	0.08	0.109
		140	10.54	2.11	0.06	0.060
		160	10.36	2.41	0.04	0.032
		180	10.27	2.72	0.03	0.017
		200	10.18	3.02	0.02	0.009

Tundish volume: 13.7L
Water flow rate: 12.4L/min
No flow control devices

Table 5.11
Concentration readings representing the response to a pulse input of a tracer at the entry nozzle

Time (Sec)	Conductivity (mmhoms/cm)	Concentration (g-mol/L)	Time [-]	Concentration [-]	Concentration * time [-]	Concentration * time ^ 2 [-]
0.00	1.0600	0.0033	0.00	0.2756	0.0000	0.0000
14.29	1.0600	0.0033	0.20	0.2756	0.0559	0.0113
20.00	10.0694	0.0312	0.28	2.6179	0.7432	0.2110
34.29	23.2629	0.0722	0.49	6.0482	2.9434	1.4325
40.00	22.2222	0.0690	0.57	5.7773	3.2802	1.8624
60.00	17.0139	0.0528	0.85	4.4233	3.7672	3.2084
80.00	12.5000	0.0388	1.14	3.2498	3.6903	4.1905
100.00	9.3750	0.0291	1.42	2.4373	3.4597	4.9108
120.00	4.8611	0.0151	1.70	1.2638	2.1527	3.6667
140.00	2.7777	0.0086	1.99	0.7221	1.4351	2.8518
160.00	2.0833	0.0065	2.27	0.5416	1.2301	2.7937
180.00	1.3288	0.0041	2.56	0.3455	0.8827	2.2552
200.00	1.1000	0.0034	2.84	0.2860	0.8119	2.3048

Tundish volume: 15.5 L
Water flow rate: 13.2 L/min

Table 5.12
Concentration readings representing the response to a pulse input of a tracer at the steam nozzle

Time (Sec)	Conductivity (mmhoms/cm)	Concentration (g_Mol/L)	Time [-]	Concentration [-]	Concentration * time [-]	Concentration * time ^ 2 [-]
0.00	1.0270	0.0032	0.00	0.2670	0.0000	0.0000
17.14	1.0270	0.0032	0.24	0.2670	0.0650	0.0158
20.00	7.3630	0.0228	0.28	1.9142	0.5434	0.1543
28.57	32.1918	0.0999	0.41	8.3693	3.3942	1.3765
40.00	23.9726	0.0744	0.57	6.2324	3.5386	2.0092
60.00	15.7534	0.0489	0.85	4.0956	3.4881	2.9707
80.00	9.5890	0.0298	1.14	2.4930	2.8309	3.2146
100.00	5.4794	0.0170	1.42	1.4245	2.0221	2.8702
120.00	3.0822	0.0096	1.70	0.8013	1.3649	2.3249
140.00	2.0547	0.0064	1.99	0.5342	1.0615	2.1095
160.00	1.3698	0.0043	2.27	0.3561	0.8088	1.8369
180.00	1.1986	0.0037	2.56	0.3116	0.7962	2.0343
200.00	1.0270	0.0032	2.84	0.2670	0.7580	2.1518

Tundish volume: 15.5 L
Water flow rate: 13.2 L/min

Table 5.13: Temperature readings representing the response to a step inpu at the entry nozzle and heat loss compensation at the steam nozzle

Concentration curve variance	Dispersion parameter	Time (Sec)	Temperature (C)	Time [-]	Calculated frac. temperature change	Experimental frac. temperature change
Entry	Entry	0	20.0000	0.00	1.0000	1.0000
nozzle	Nozzle	20	19.9019	0.28	0.9976	0.9891
0.332	0.114	40	16.4783	0.57	0.8738	0.6087
		60	14.2283	0.85	0.6328	0.3587
Steam	Steam	80	12.9566	1.14	0.3943	0.2174
Nozzle	Nozzle	100	12.6641	1.42	0.2398	0.1849
0.312	0.109	120	15.1085	1.70	0.3431	0.4565
		140	18.5321	1.99	0.5932	0.8369
		160	19.7066	2.27	0.7855	0.9674
		180	20.0000	2.56	0.8948	1.0000
		200	20.3915	2.84	0.9494	1.0435

Tundish volume: 15.5 L
Water flow rate: 13.2 L

Table 5.14
Concentration readings representing the response to a pulse input of a tracer at the entry nozzle

Time (Sec)	Conductivity (mmhoms/cm)	Concentration (g-Mol/L)	Time [-]	Concentration [-]	Concentration * time [-]	Concentration * time ^ 2 [-]
0.00	1.04	0.0032	0.00	0.2214	0.0000	0.0000
7.14	1.04	0.0032	0.11	0.2214	0.0237	0.0025
20.00	20.14	0.0625	0.30	4.2808	1.2813	0.3835
27.85	21.18	0.0657	0.42	4.5021	1.8764	0.7821
40.00	19.09	0.0592	0.60	4.0578	2.4291	1.4541
60.00	14.55	0.0451	0.90	3.0928	2.7771	2.4937
80.00	10.41	0.0323	1.20	2.2128	2.6492	3.1718
100.00	7.81	0.0242	1.50	1.6607	2.4853	3.7193
120.00	4.86	0.0151	1.80	1.0333	1.8557	3.3325
140.00	3.03	0.0094	2.10	0.6441	1.3494	2.8273
160.00	3.47	0.0108	2.39	0.7381	1.7673	4.2318
180.00	2.43	0.0075	2.69	0.5165	1.3914	3.7482
200.00	1.56	0.0048	2.99	0.3321	0.9941	2.9755

Tundish volume: 13.7 L
Water flow rate: 12.3 L/min

Table 5.15
Concentration readings representing the response to a pulse input of a tracer at the steam nozzle

Time (Sec)	Conductivity (mmhoms/cm)	Concentration (g-Mol/L)	Time [-]	Concentration [-]	Concentration * time [-]	Concentration * time ^ 2 [-]
0.00	1.0638	0.0033	0.00	0.2261	0.0000	0.0000
4.28	1.0638	0.0033	0.06	0.2261	0.0145	0.0009
10.00	4.6099	0.0143	0.15	0.9799	0.1466	0.0219
20.00	38.2978	0.1188	0.30	8.1407	2.4366	0.7293
30.00	31.2056	0.0968	0.45	6.6332	2.9781	1.3371
40.00	26.5957	0.0825	0.60	5.6533	3.3842	2.0258
50.00	17.3758	0.0539	0.75	3.6935	2.7637	2.0680
60.00	12.4113	0.0385	0.90	2.6382	2.3689	2.1271
70.00	8.5106	0.0264	1.05	1.8090	1.8951	1.9853
80.00	6.7375	0.0209	1.20	1.4321	1.7146	2.0528
100.00	4.9645	0.0154	1.50	1.0553	1.5793	2.3635
120.00	2.8368	0.0088	1.80	0.6030	1.0829	1.9448
140.00	1.7730	0.0055	2.10	0.3769	0.7896	1.6544
160.00	1.4245	0.0044	2.39	0.3028	0.7250	1.7361
180.00	1.0638	0.0033	2.69	0.2261	0.6091	1.6409
200.00	1.0638	0.0033	2.99	0.2261	0.6768	2.0258

Tundish volume: 13.7 L
Water flow rate: 12.3 L

Table 5.16: Temperature readings representing the response to a step in/out at the entry nozzle and heat losse compensation at the steam nozzle

Concentration curve variance	Dispersion parameter	Time (Sec)	Temperature (C)	Time [-]	Experimental frac. temperature change	Calculated Frac. temperature change
Entry	Entry	0	21.067	0.00	0.9984	1.0000
Nozzle	Nozzle	20	21.033	0.30	0.9944	0.9916
0.450	0.143	40	19.058	0.60	0.7587	0.8354
		60	17.106	0.90	0.5258	0.5785
Steam	Steam	80	15.948	1.20	0.3876	0.3672
Nozzle	Nozzle	100	14.888	1.50	0.2611	0.2225
0.235	0.087	120	15.556	1.80	0.3408	0.1967
		140	18.426	2.10	0.6833	0.6349
		160	19.933	2.39	0.8631	0.9173
		180	20.087	2.69	0.8815	0.9952
		200	21.468	2.99	1.0463	1.0083

Tundish volume: 13.7 L
Water flow rate: 12.3 L/min

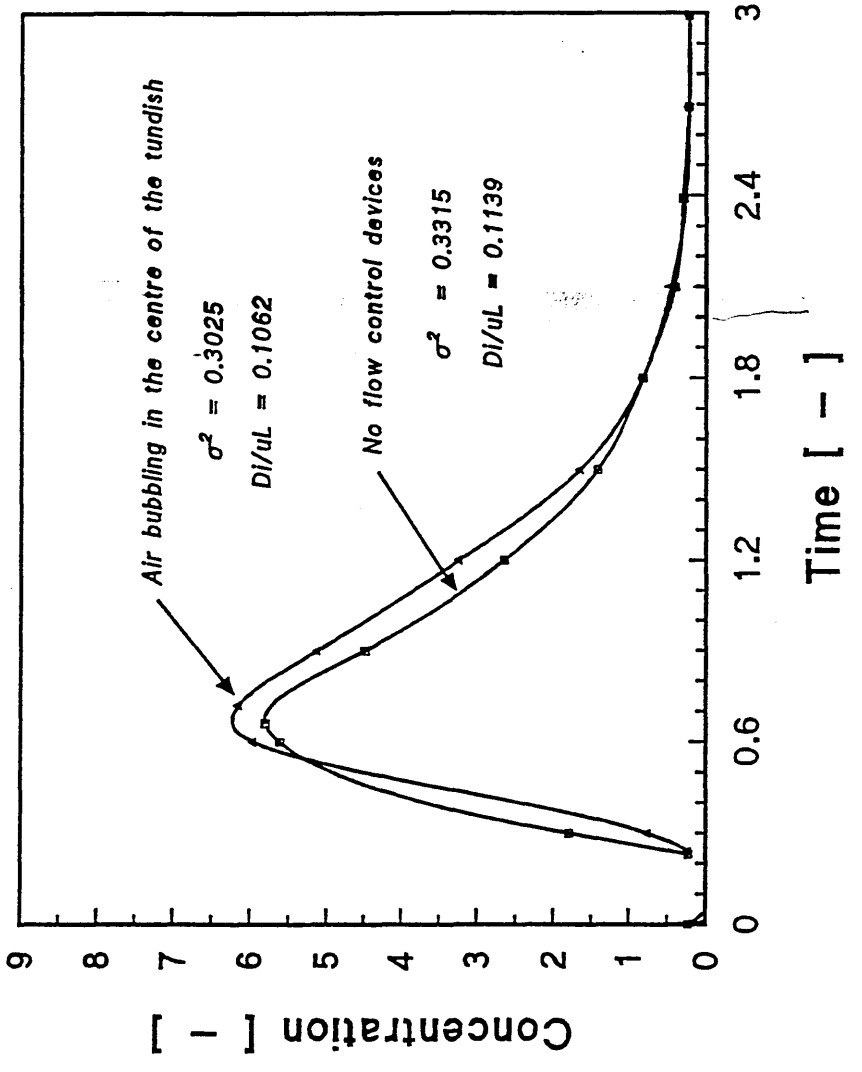

FIGURE 5.1 Concentration readings representing the continuous response to a pulse input of a tracer injected to the fluid entering the tundish.

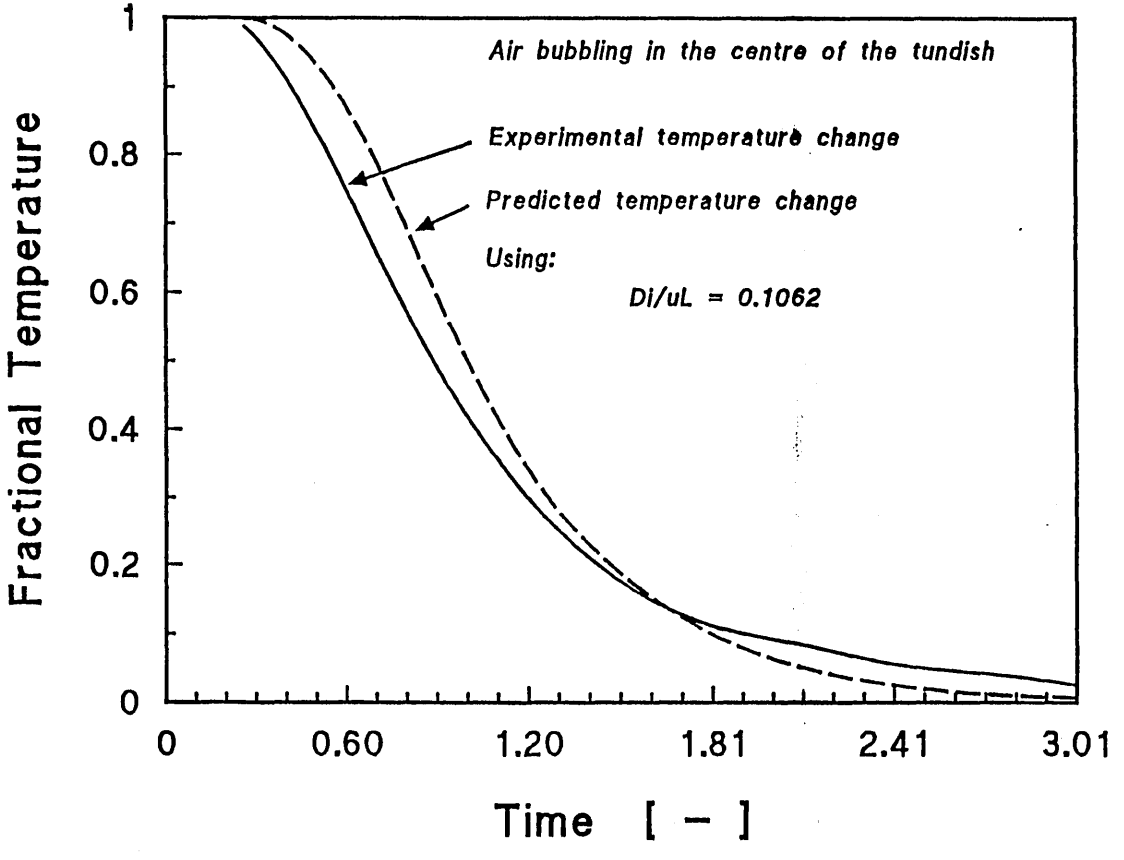

FIGURE 5.2 Temperature readings representing the continuous response to a step input of a tracer at the tundish entry nozzle

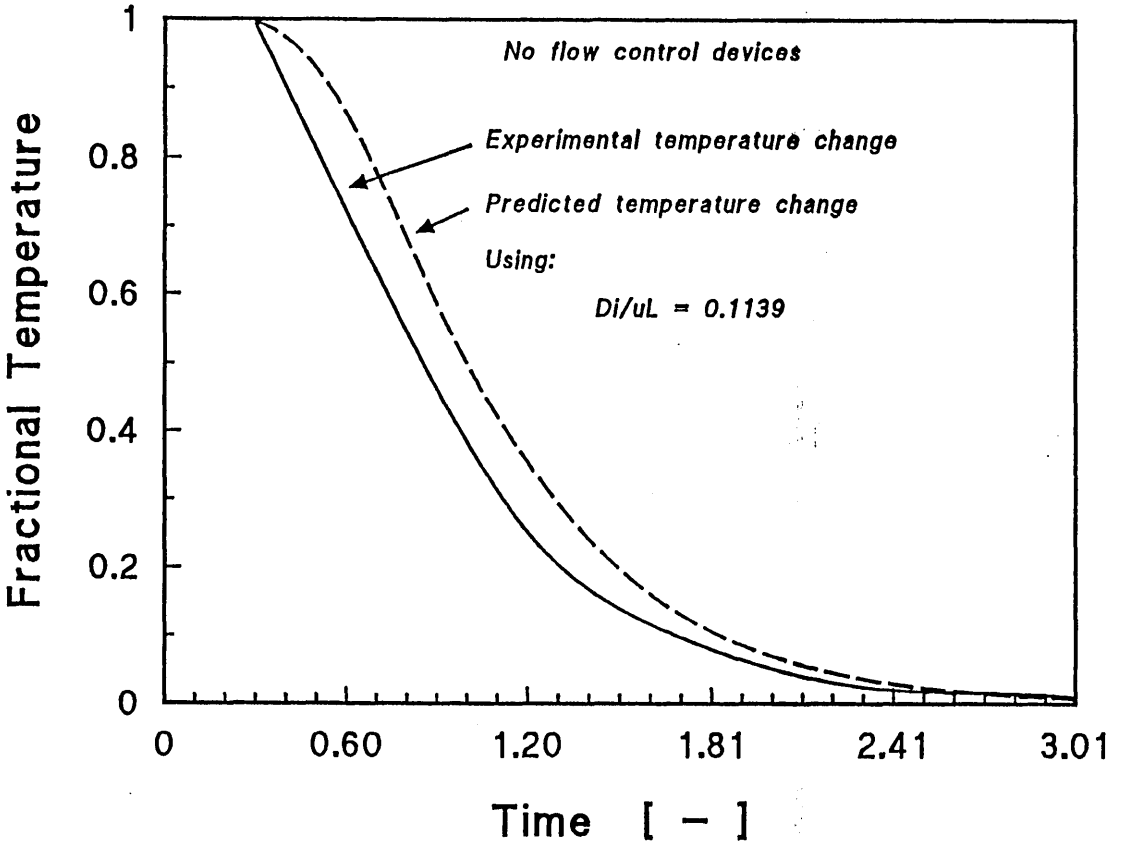

FIGURE 5.3 Temperature readings representing the continuous response to a step input of a tracer at the tundish entry nozzle.

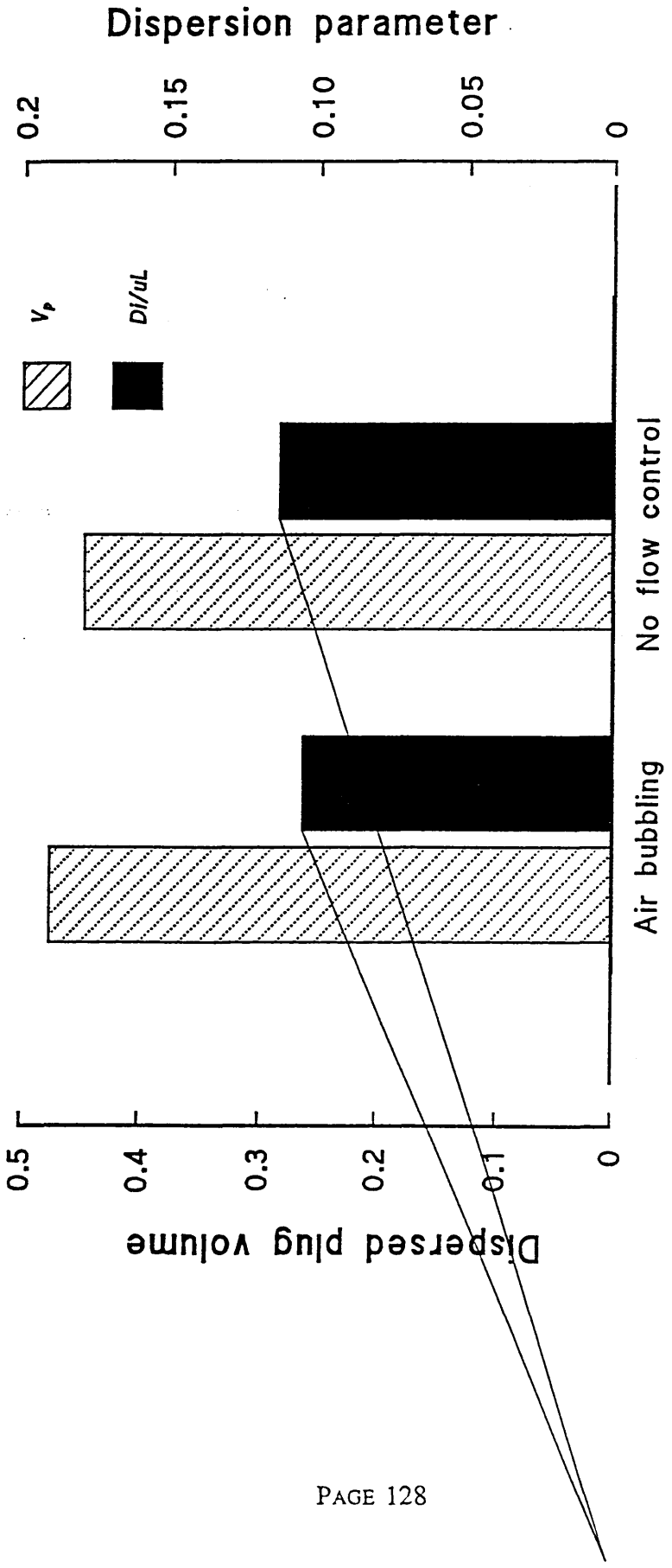

FIGURE 5.4 Effect of air bubbling on the dispersed plug volume fraction and the dispersion parameter.

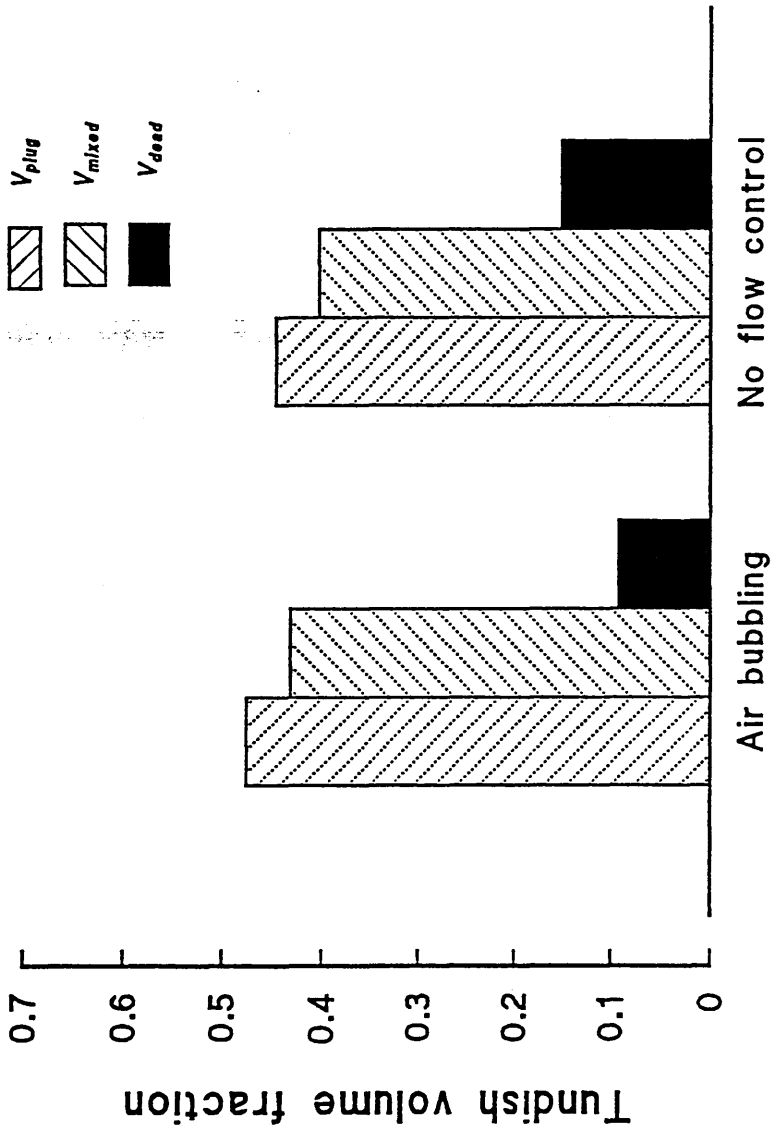

FIGURE 5.5 Effect of air bubbling on the dispersed plug volume fraction, mixed volume fraction and dead volume fraction.

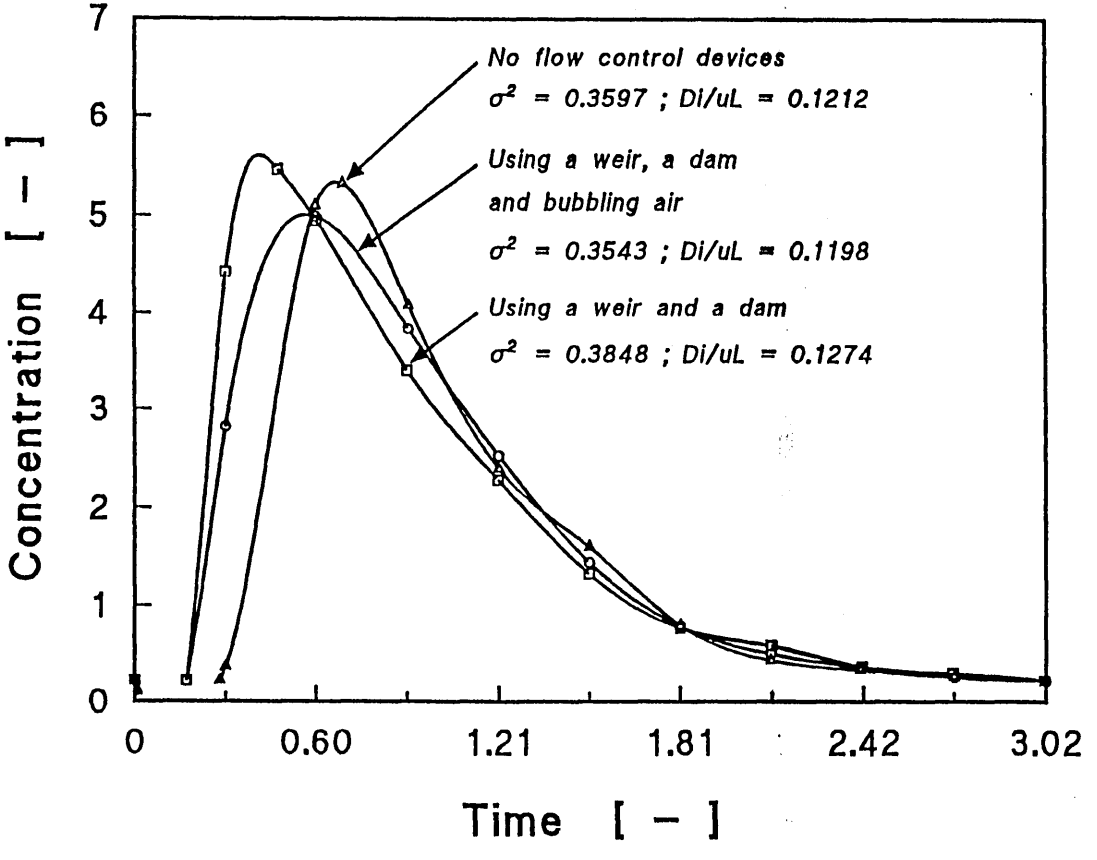

FIGURE 5.6 Concentration readings representing the continuous response to a pulse input of a tracer injected to the fluid entering the tundish.

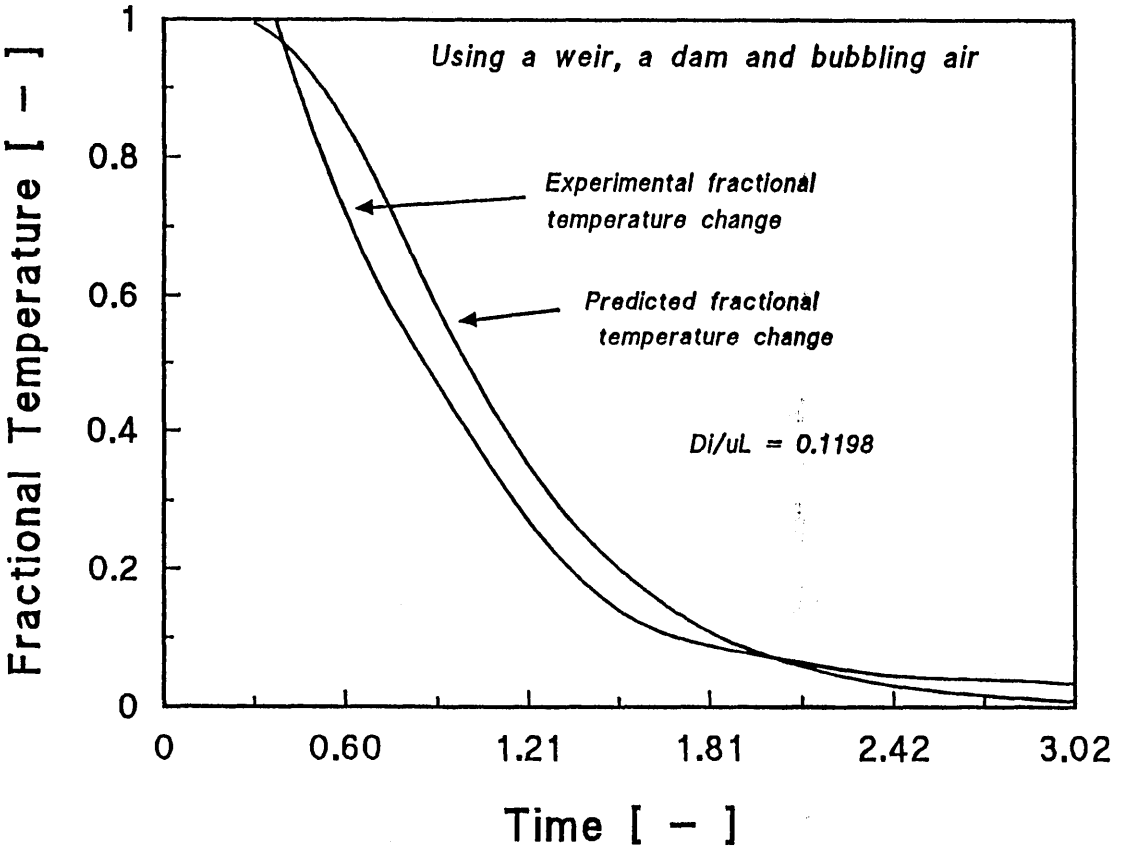

FIGURE 5.7 Temperature reading the representing the continuous response to a pulse input of a tracer at the entry nozzle.

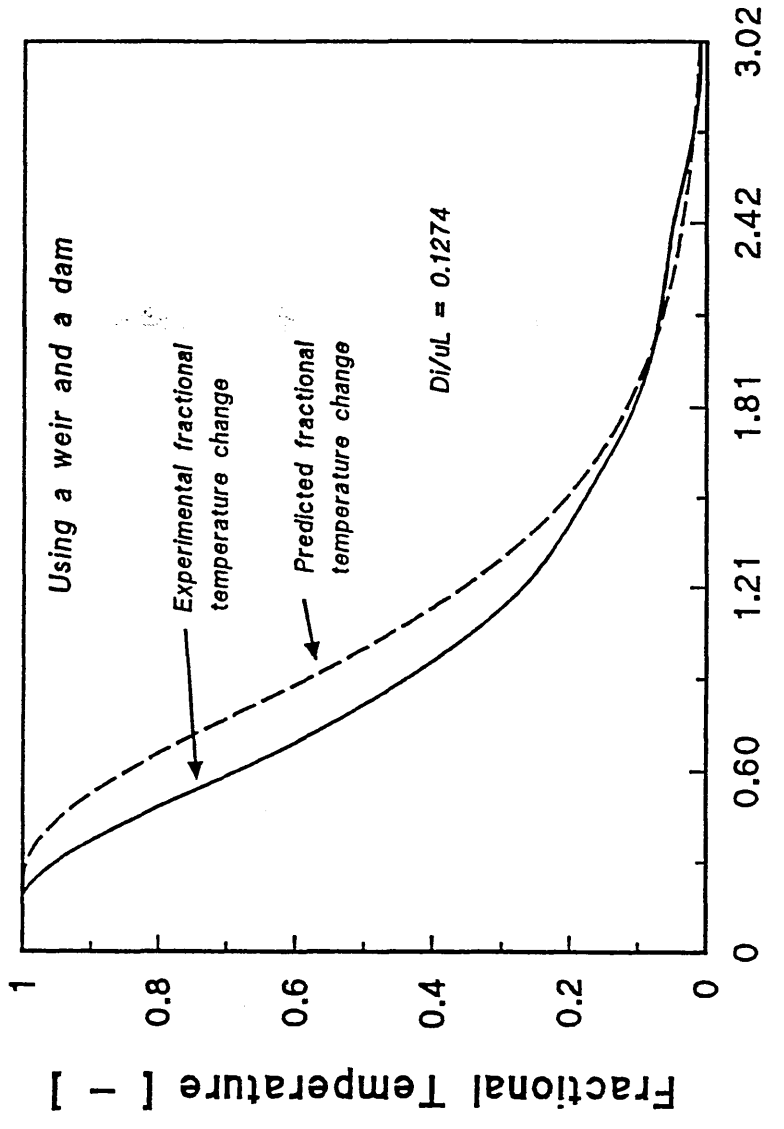

FIGURE 5.8 Temperature reading the representing the continuous response to a step input of a tracer at the tundish entry nozzle.

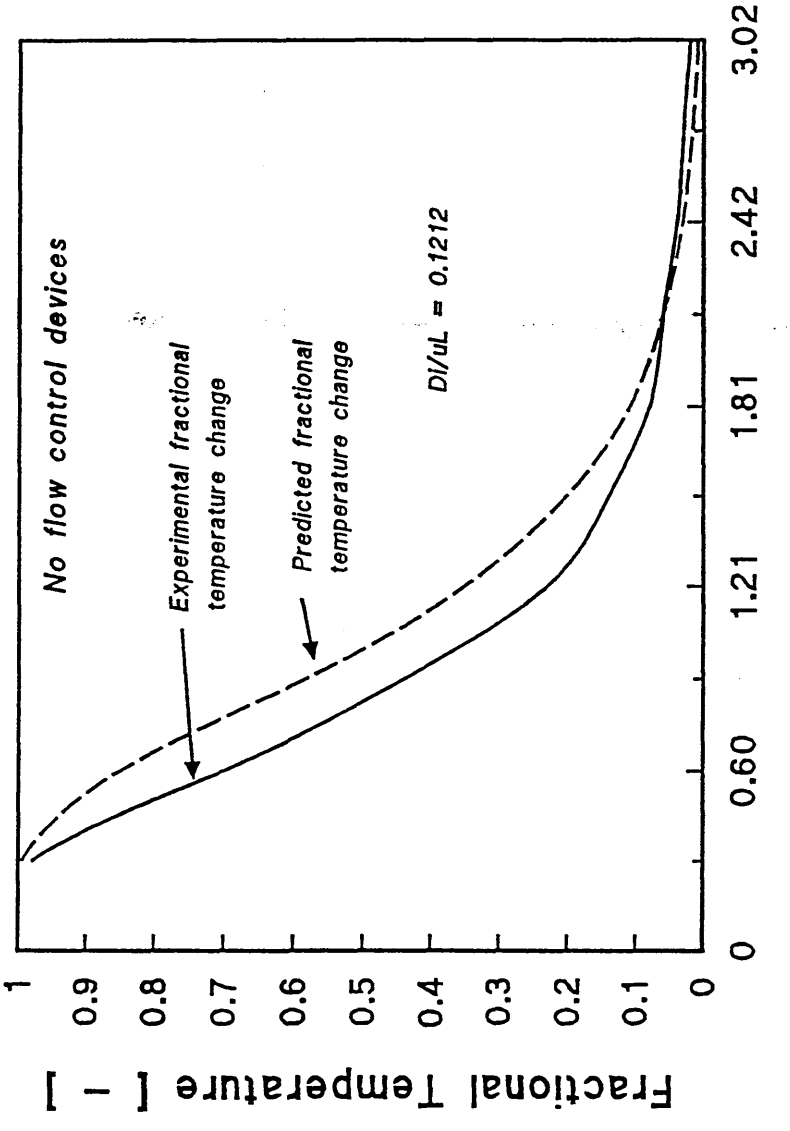

FIGURE 5.9 Temperature reading the representing the continuous response to a step input of a tracer at the tundish entry nozzle.

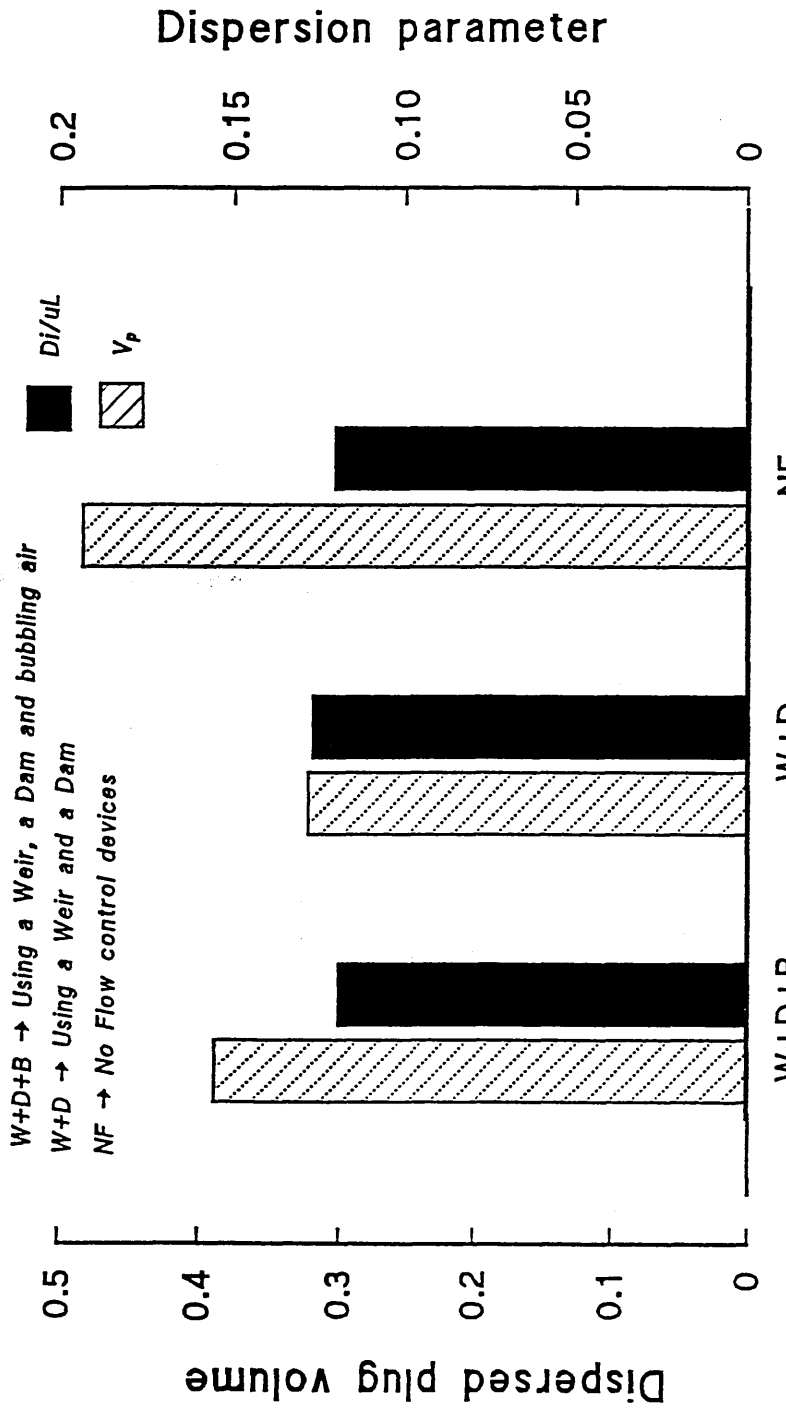

FIGURE 5.10 Dispersed plug volume fraction and dispersion parameter for different flow control configurations

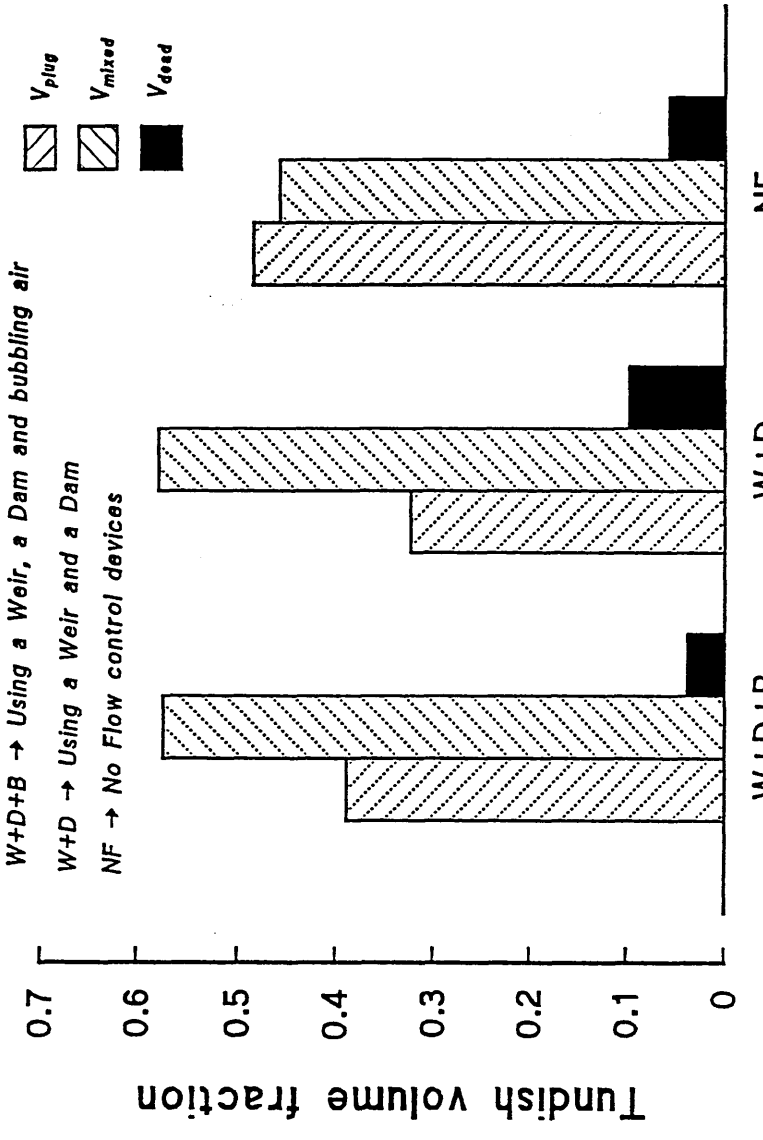

FIGURE 5.11 Dispersed plug volume fraction, mixed volume fraction and dead volume fraction for different flow control configurations

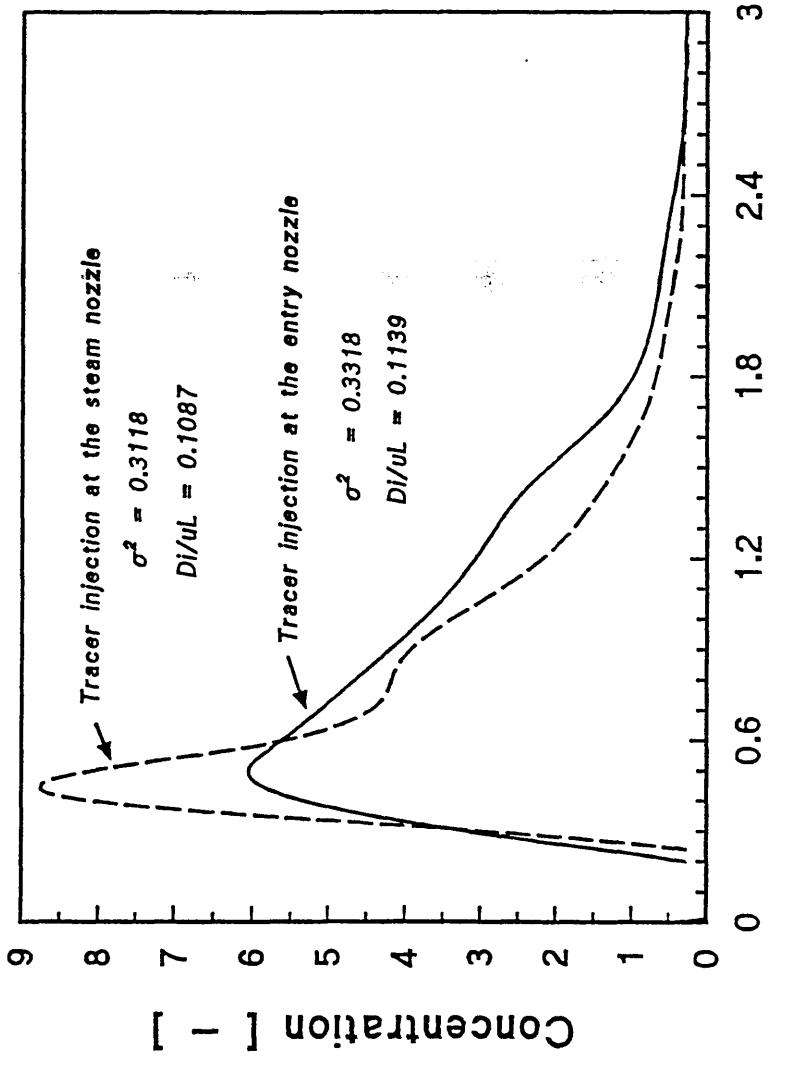

FIGURE 5.12 Concentration readings representing the continuous response to a pulse input of a tracer injected to the fluid entering the tundish

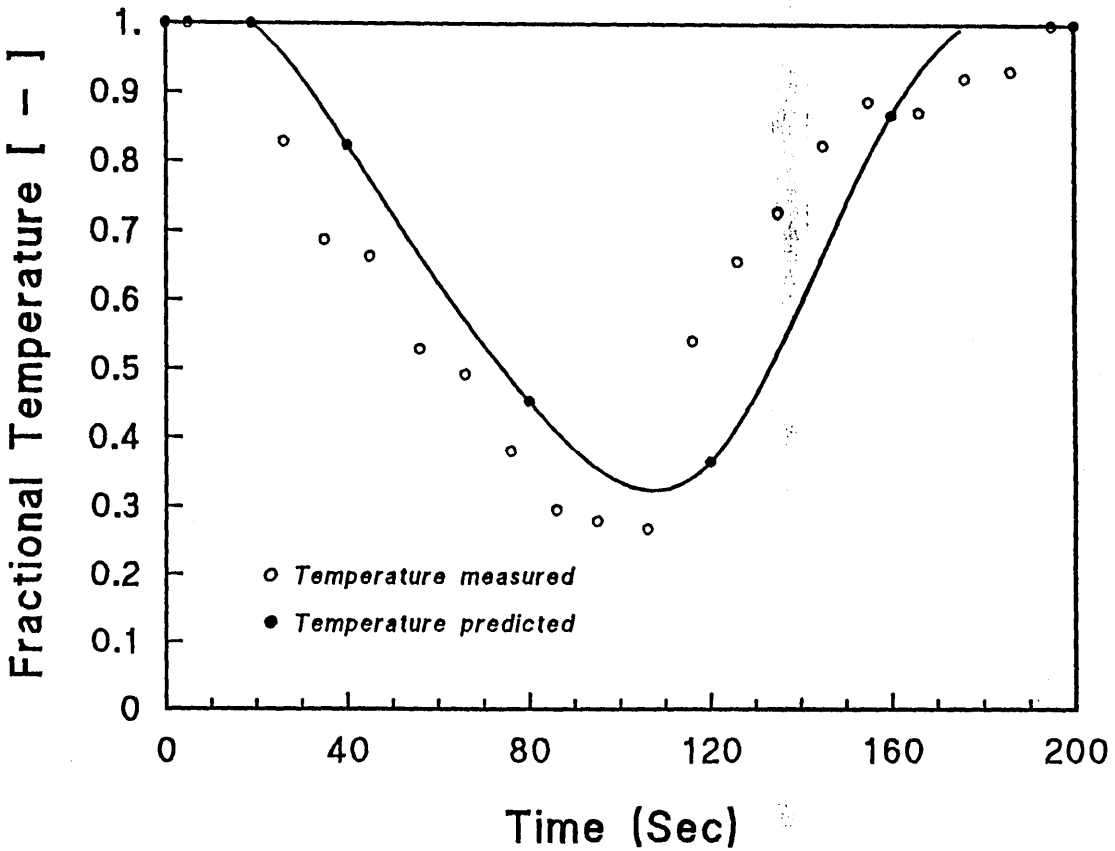

FIGURE 5.13 Temperature readings representing the continuous measurement and temperature prediction after a step change at at the entry nozzle and blowing steam on the water surface 80 Sec later.

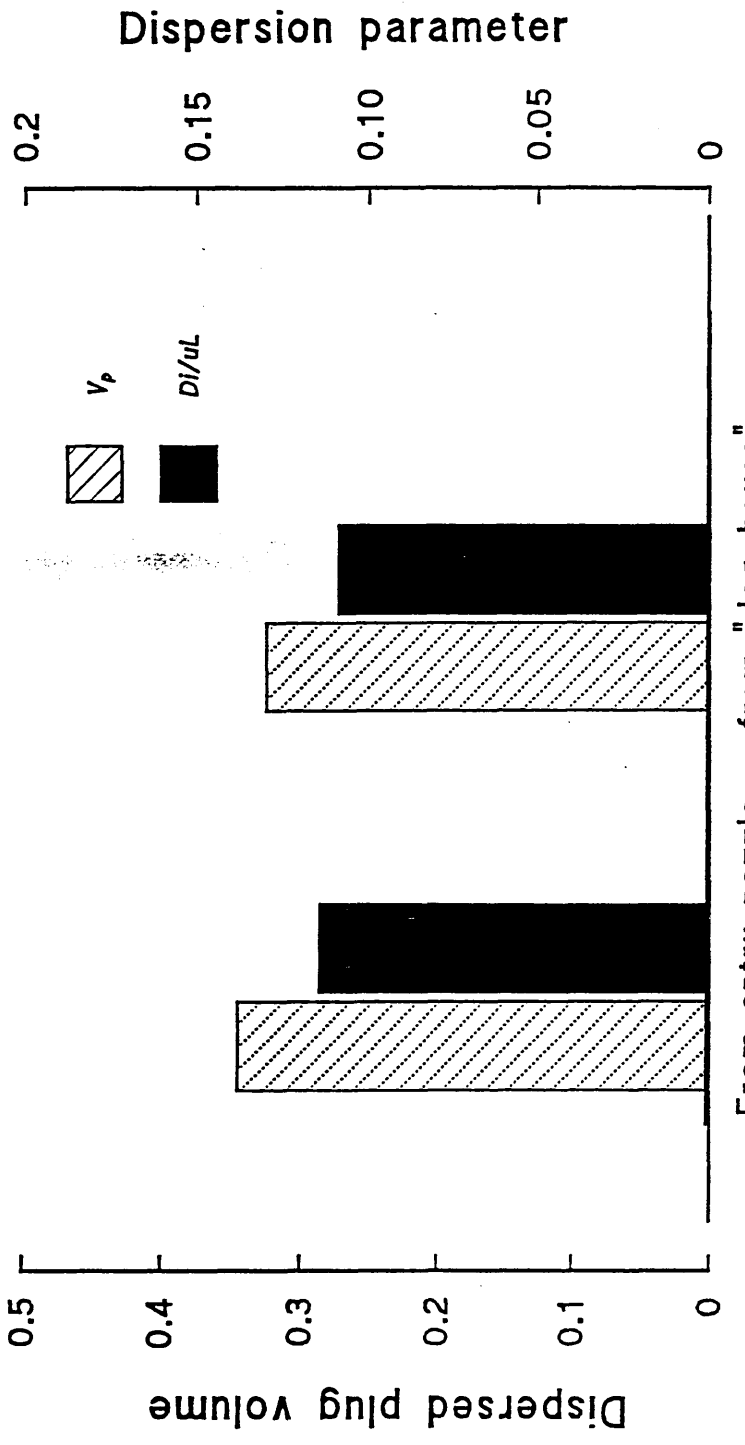

FIGURE 5.14 Dispersed plug volume fraction and dispersion parameter from the entry nozzle and from the "dog-house", which is only 12 cm closer to the mould SEN.

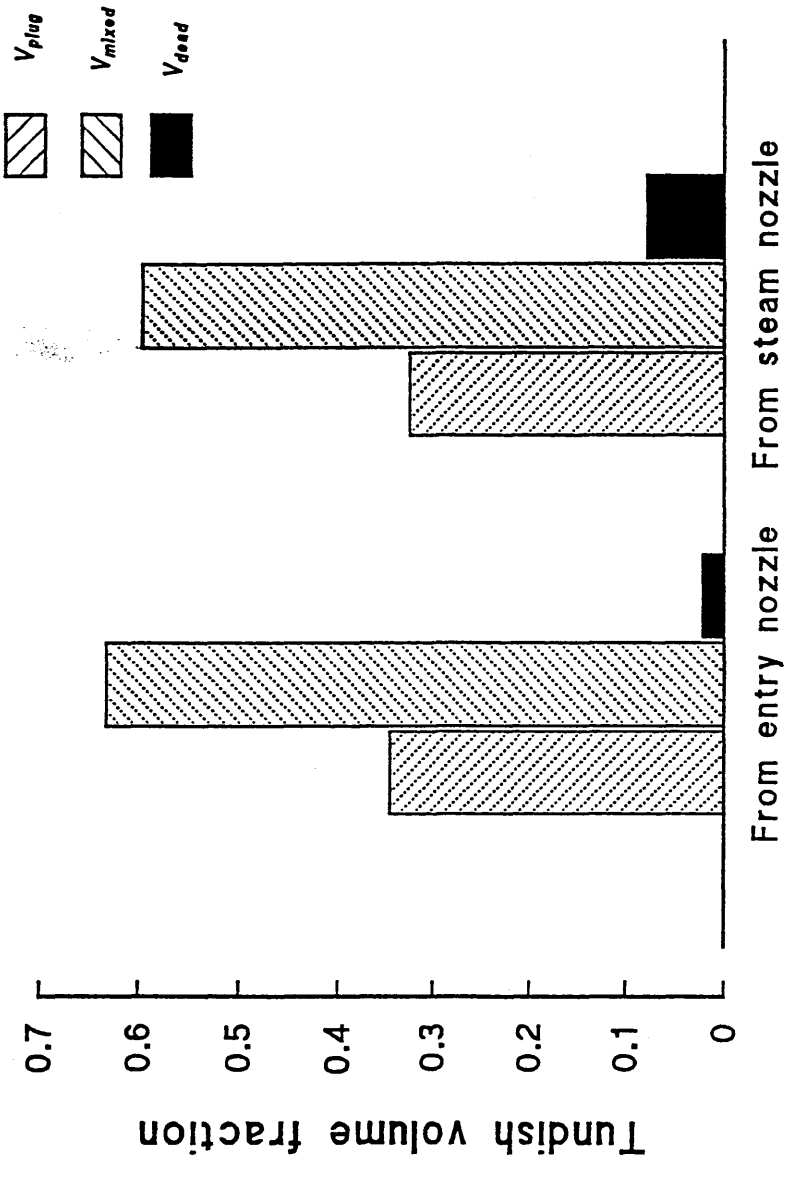

FIGURE 5.15 Dispersed plug volume fraction, mixed volume fraction and dead volume fraction for the the path from the entry nozzle and for the path from the steam nozzle.

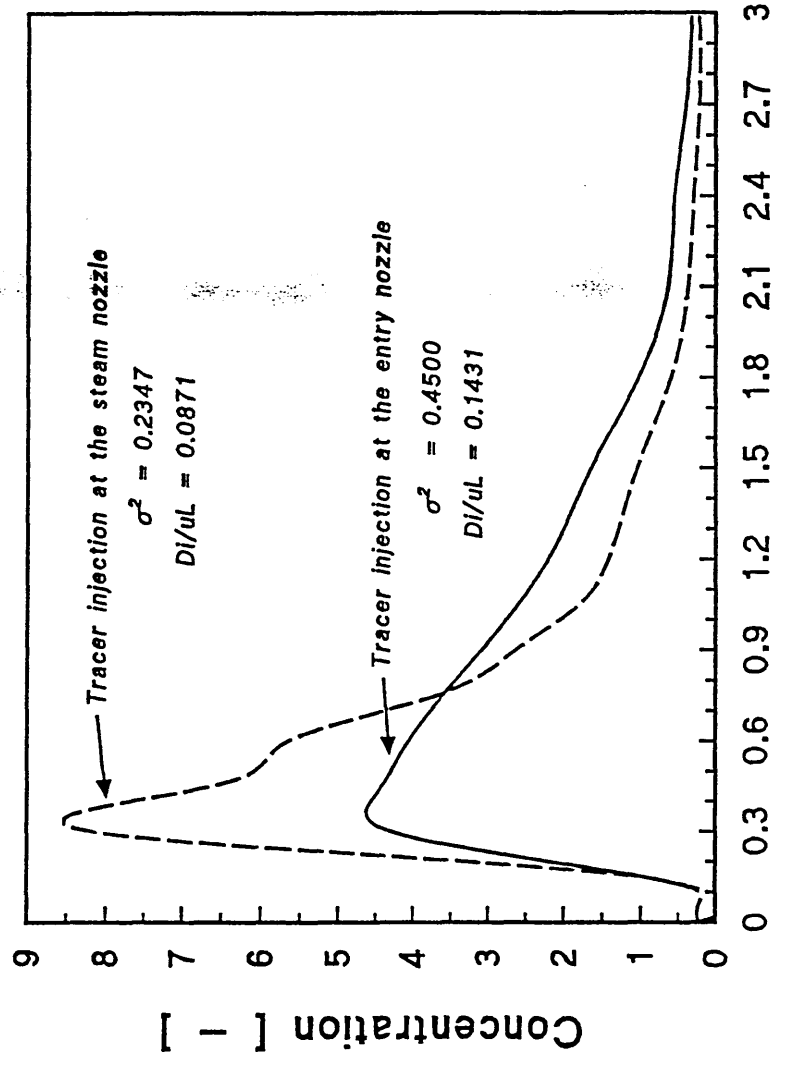

FIGURE 5.16 Concentration readings representing the continuous response to a pulse input of a tracer injected to the fluid entering the tundish

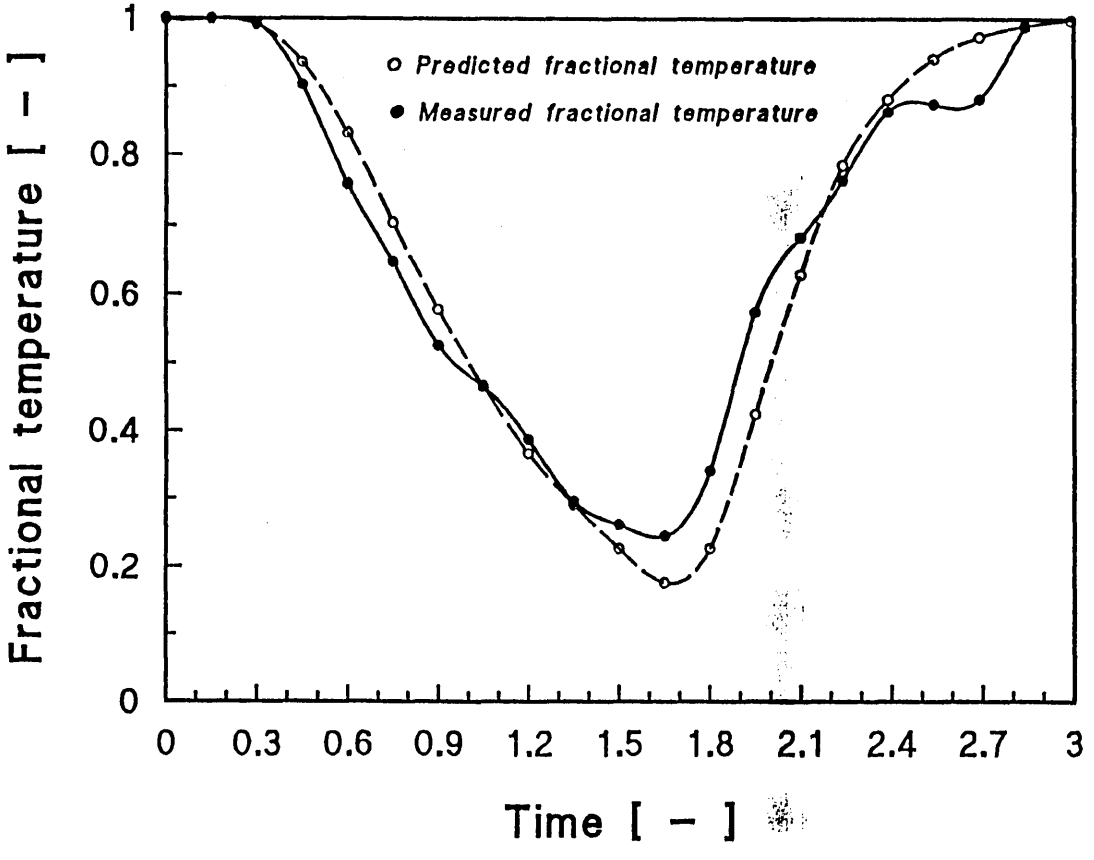

FIGURE 5.17 Temperature response to a step input at the sub-ladle entry nozzle, and application of steam heating 1.5 time units later to compensate heat loss.

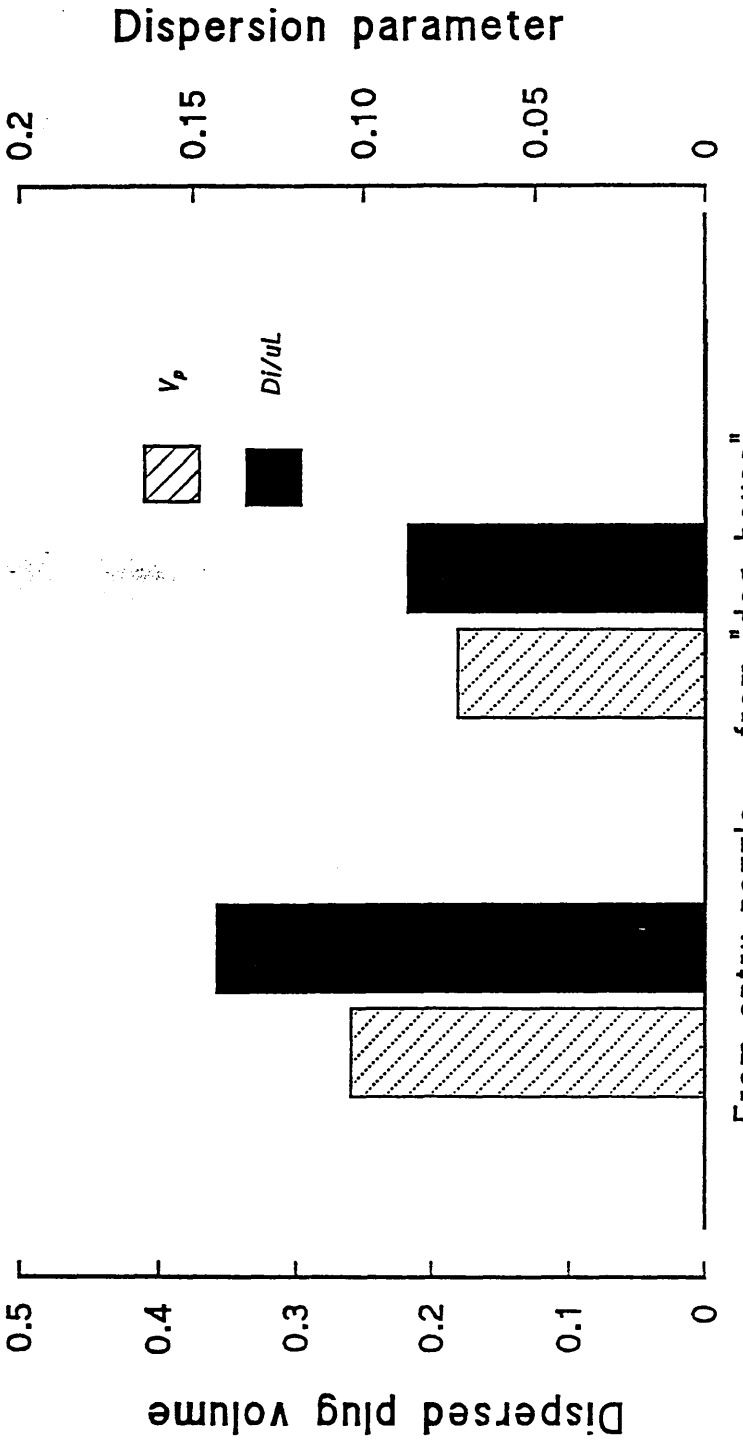

FIGURE 5.18 Dispersed plug volume fraction and dispersion parameter from the entry nozzle and from the "dog-house".

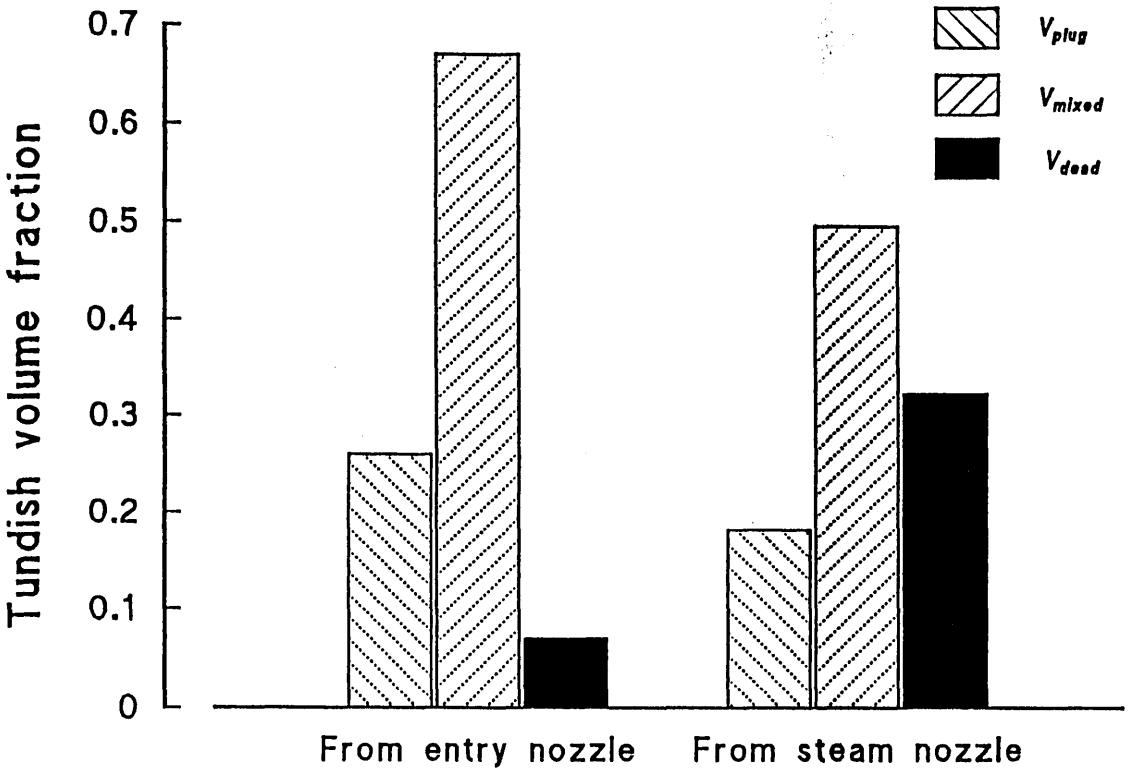

FIGURE 5.19 Dispersed plug volume fraction, mixed volume fraction and dead volume fraction for the path from the entry nozzle and for the path from the steam nozzle.

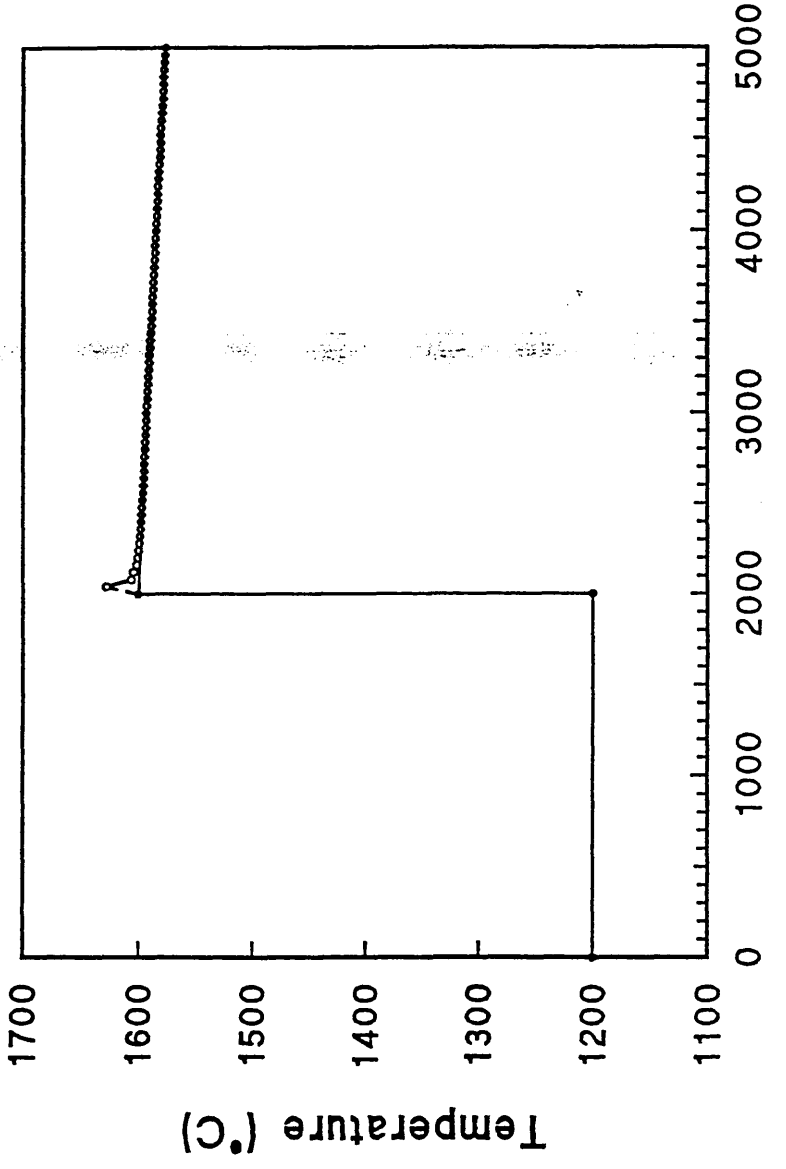

Figure 5.20:- Steady state established at 1200 °C, Step change to 1600 °C ; Subsequently temperature decay at 0.5 °C Min^{-1}

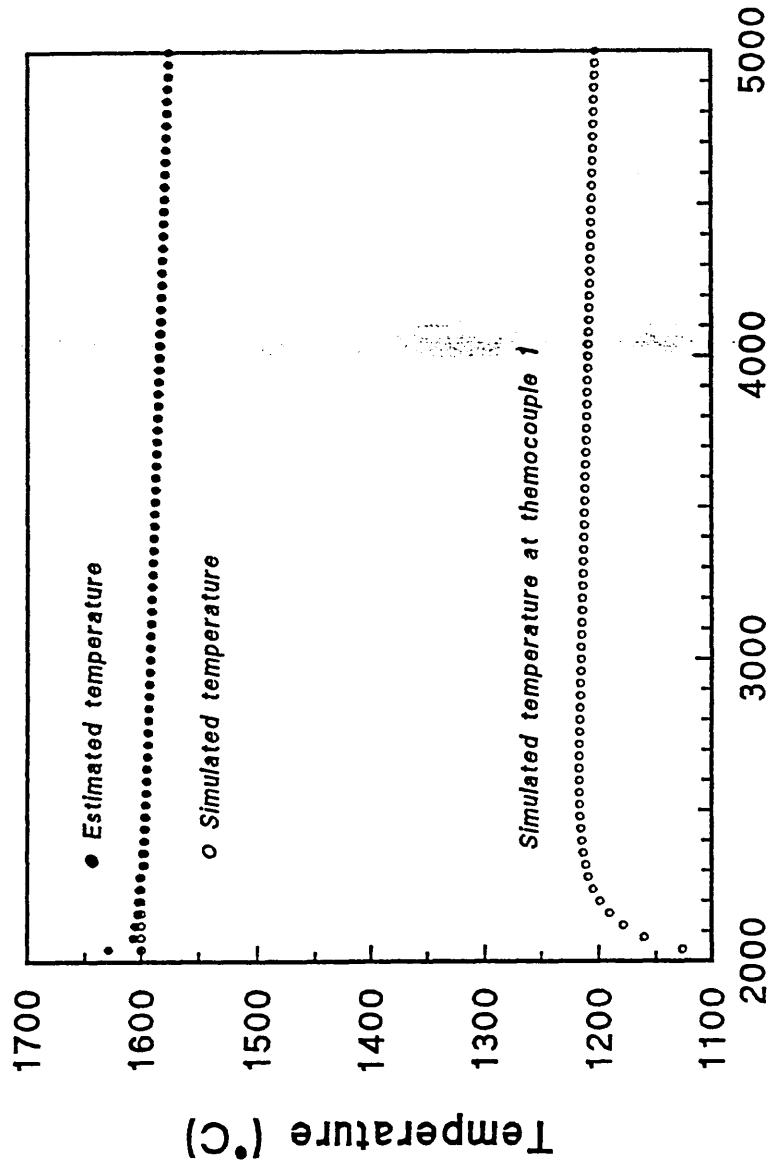

Figure 5.21:- Steady state established at 1200 °C, Step change to 1600 °C; Temperature decay rate at 0.5 °C/min

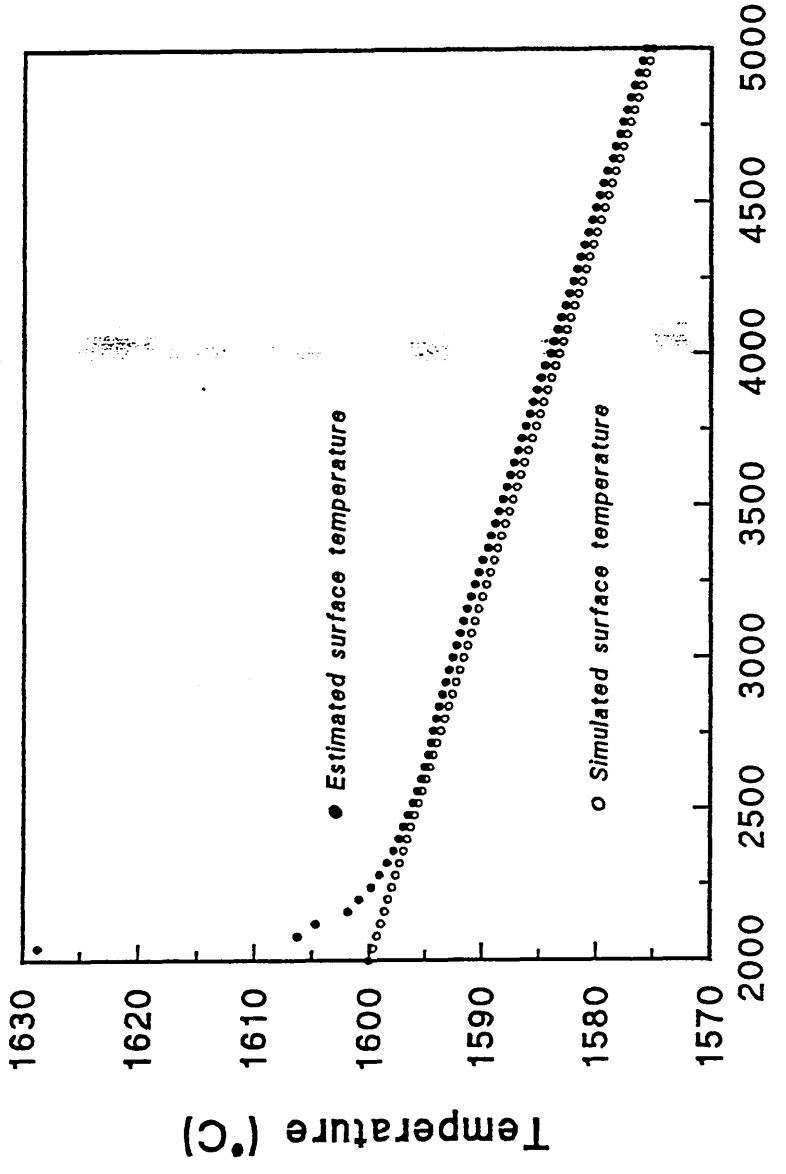

Figure 5.22 Simulated and estimated surface temperatures plotted on a finer temperature scale. (average dicrepancy is 0.6°C)

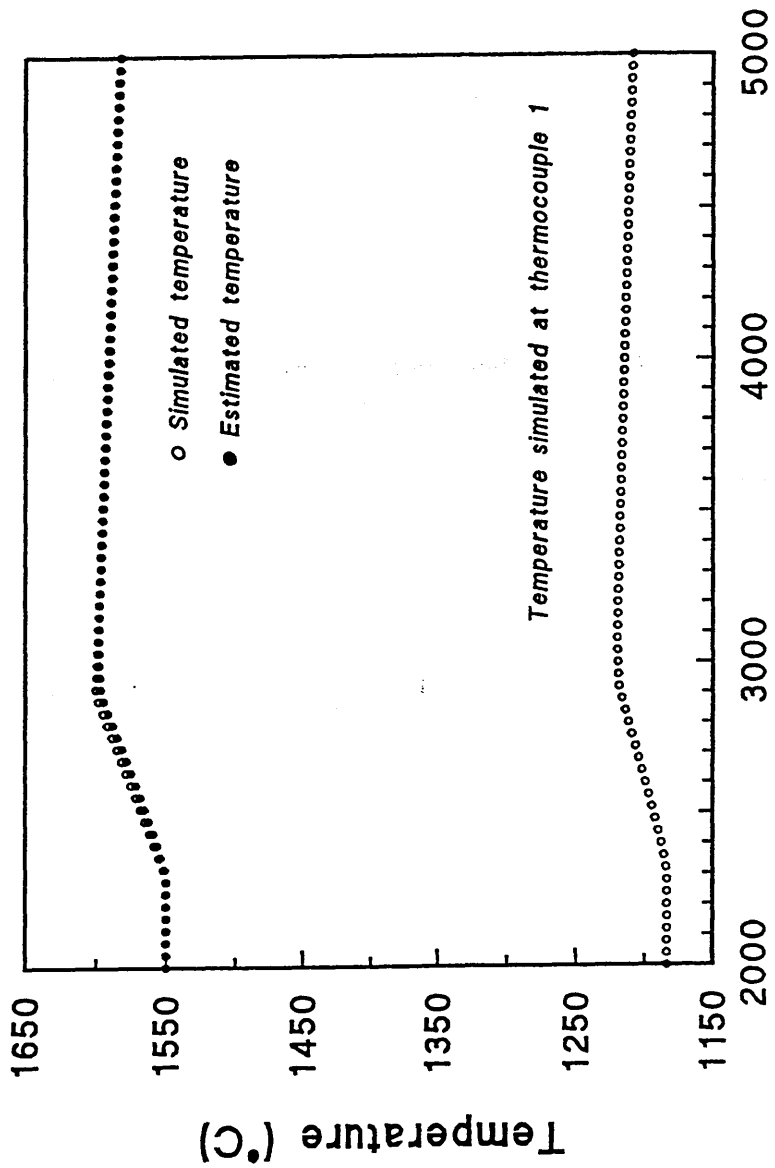

Figure 5.23: Temperature simulated and estimated in the SEN below the tundish. Ladle change simulated by temperature ramp over three times the tundish residence time followed by a steady temperature fall at 0.5 °C Min^{-1}

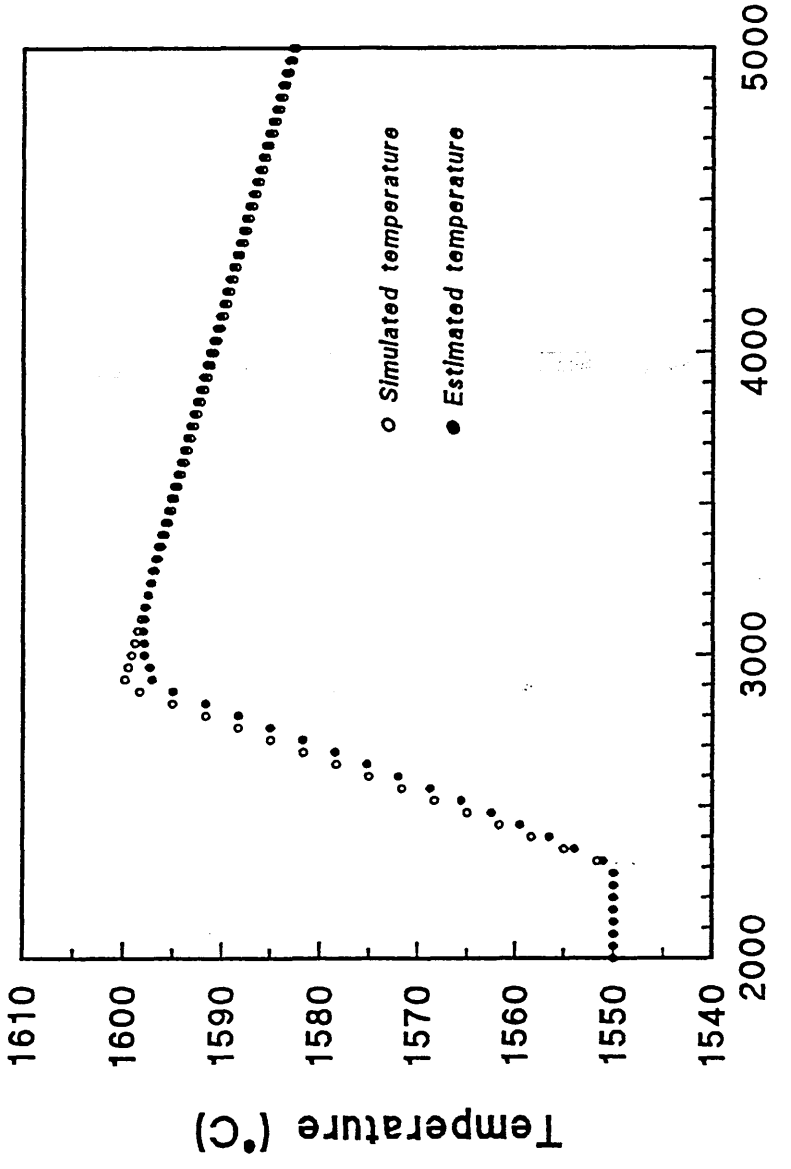

Figure 5.24 Simulated and estimated internal surface temperature at SEN during and after simulated ladle change, plotted on a finer temperature scale.

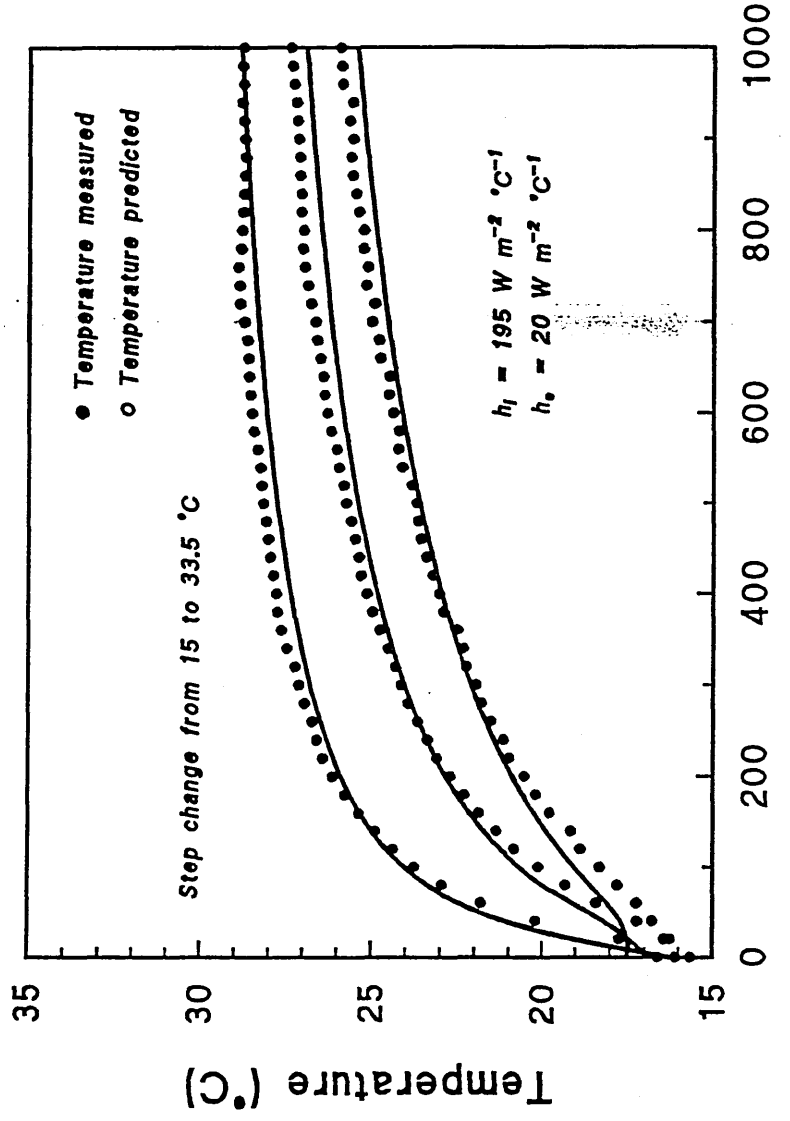

Figure 5.25 Temperature gradient representing the continuous temperature measurement and temperature prediction (using finite difference analysis) inside the sub-ladle entry nozzle, after a step change in water temperature.

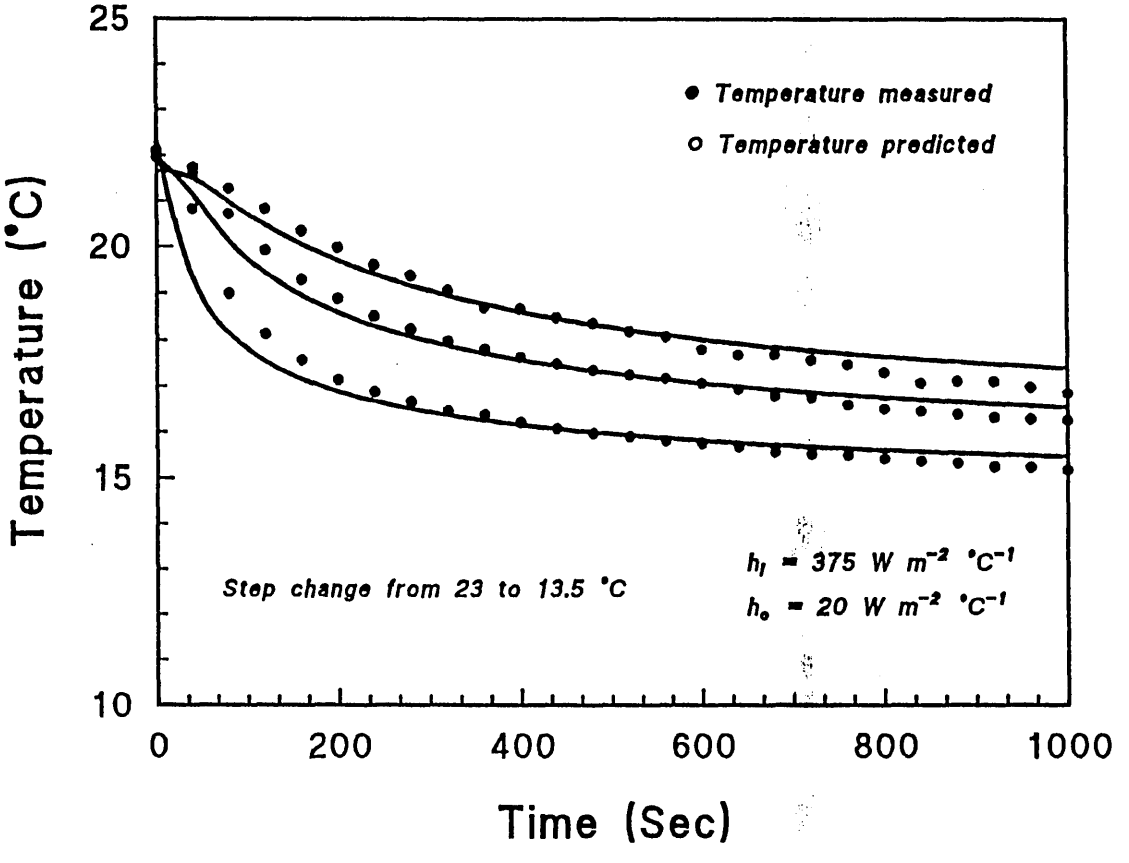

Figure 5.26 Temperature gradient representing the continuous temperature measurement and temperature prediction (using finite difference analisys) inside the sub-ladle entry nozzle wall, after a step change in water temperature.

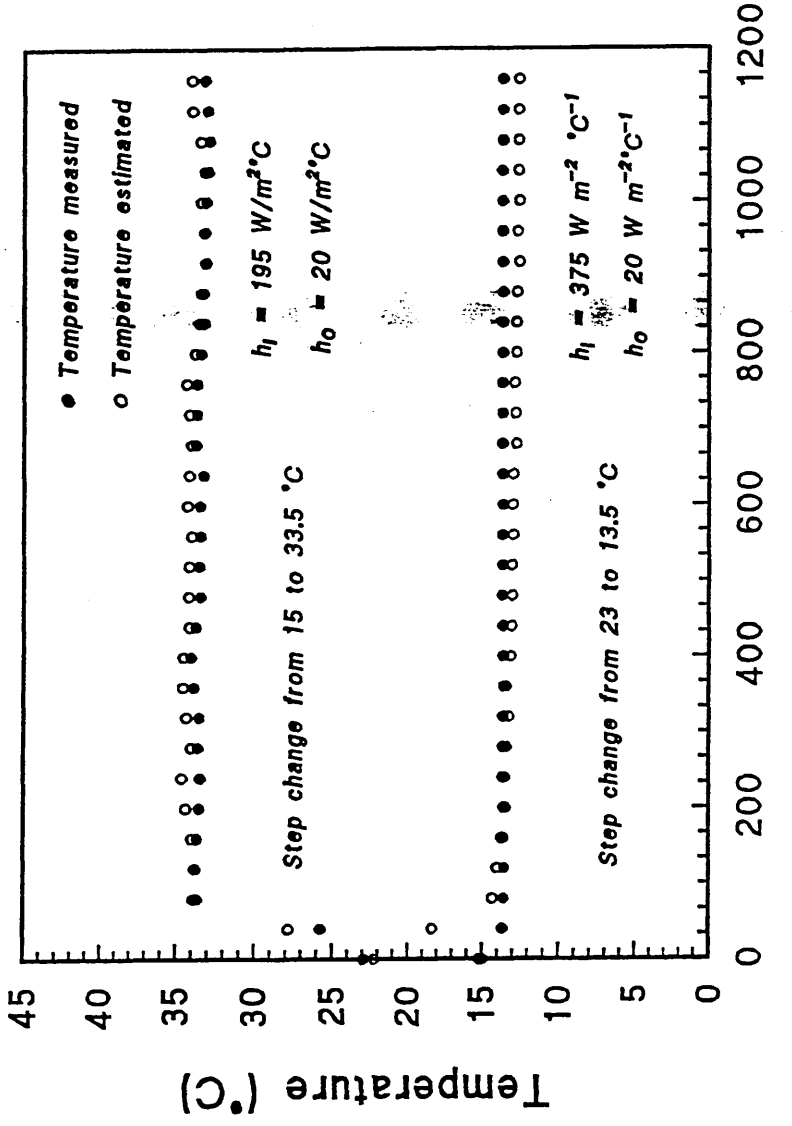

Figure 5.27 Temperature readings representing the continuous measurement and temperature estimation of water temperature after a step input at the entry nozzle.

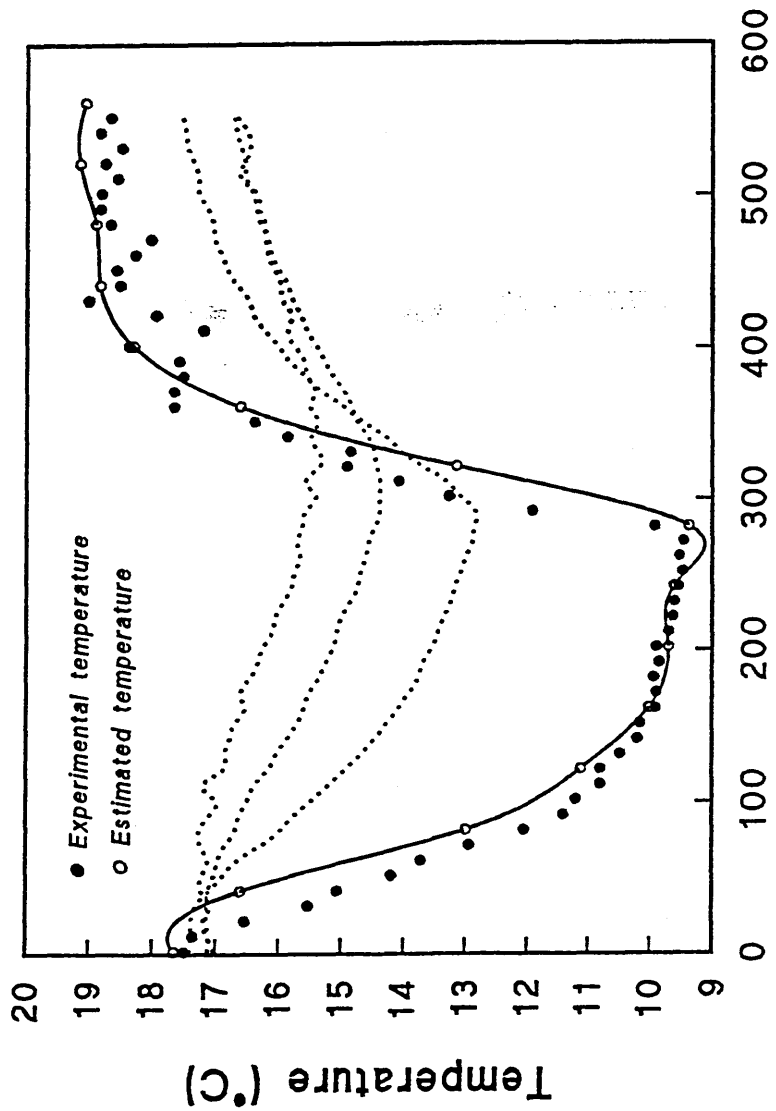

Figure 5.28: Temperature gradient inside the submerged mould entry nozzle wall, the measured water temperature and the estimated temperature (using the inverse heat conduction algorithm) after a step change at the sub-ladle entry nozzle; 260 Sec later steam was blown onto the water surface.

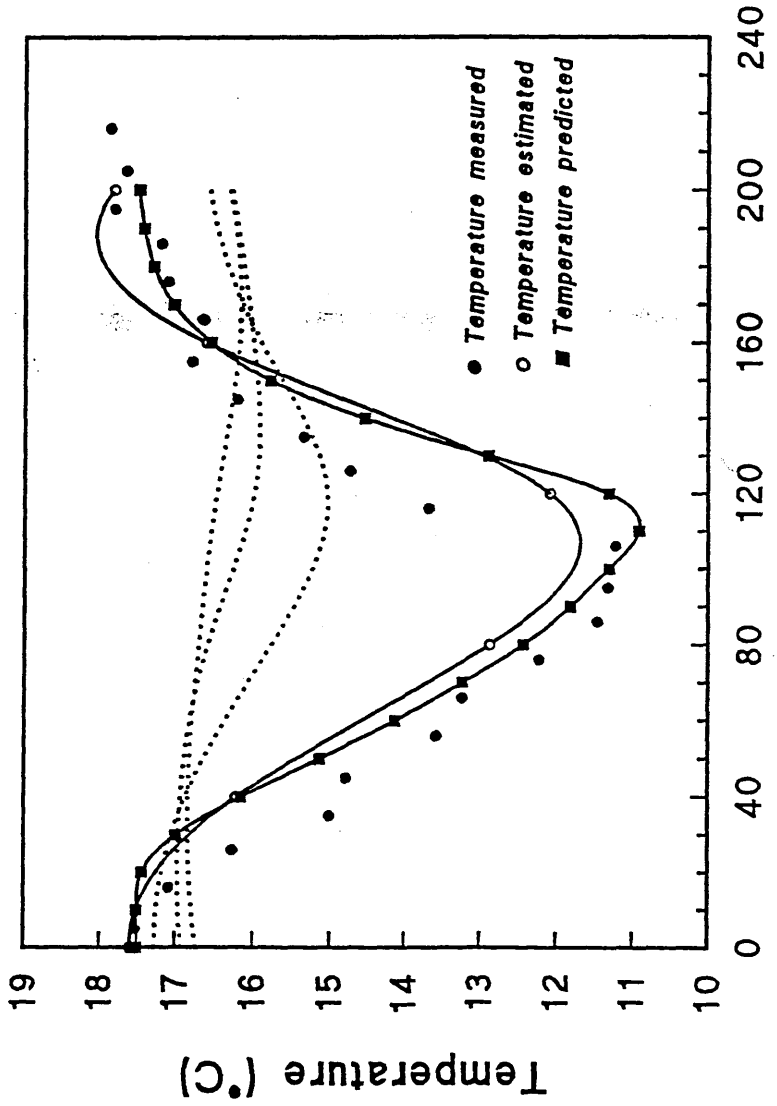

Figure 5.29 Temperature readings representing the continuous measurement, the temperature estimated by the IHCA and the temperature predicted using the dispersion model – after a step change in water temperature at the tundish entry nozzle and blowing steam 100 sec later

6

DISCUSSION

6.1. ACCURACY AND ERRORS OF THE EXPERIMENTAL METHOD

Before deducing any conclusion from the work reported here, it is necessary to assess the accuracy and errors of the experimental method. For this assessment the following terminology will be used:

- *Absolute errors:*

The absolute error of a variable **C** is defined as the result of its true value **C** minus its approximation **c**, this is:

$$\Delta = C - c \tag{6.1}$$

The true value **C** is unknown, therefore Δ can not be establish. However, its magnitude can usually be estimated as follows:

$$| \Delta | = | C - c | < \epsilon \tag{6.2}$$

Where: ϵ is the limit of the absolute error of approximation

Consequently

$$C = c \pm \epsilon \tag{6.3}$$

or

$$c - \epsilon \leq C \leq c + \epsilon \tag{6.4}$$

- *Relative errors:*

The ratio of the absolute errors and the true value of a approximation:

$$\delta C = \frac{\Delta}{C} \tag{6.5}$$

is defined as the relative error of the approximation **c**.

Because the true value **C** is unknown, in practice the approximation **c** is used instead of the true value **C**. Thus:

$$\delta C = \frac{\Delta}{c} \tag{6.6}$$

And the upper limit ψ of the absolute value of the relative error:

$$| \delta C | = \left| \frac{\Delta}{c} \right| \leq \psi \tag{6.7}$$

is defined as the limit of the relative error of an approximation.

- *Reliability of measurements:*

(a) Flow rate Measurement

The volumetric flow rate of water in the tundish was determined by measuring the flow rate for the nozzle. To establish the margin of error a test was carried out, the test consisted in measuring a volume of water and weighing it on the balance, then adding 50 cm^3 of water, and reading its increase in weight. Once 1000 cm^3 had been added a regressive test was carried out removing 50 cm^3 and the graph is plotted in figure (6.1).

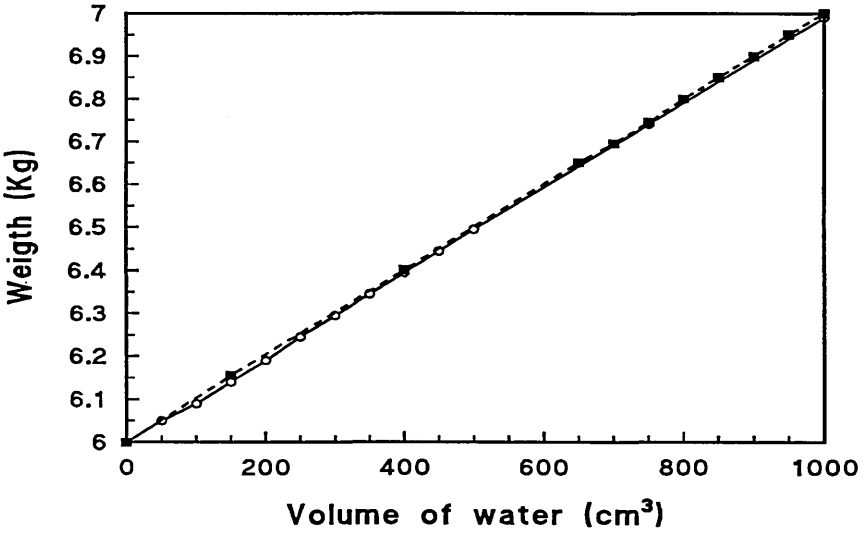

Figure 6.1. Calibration curve for volumetric flow rate

According to figure 6.1 the error range was of ± 5 cm^3 in 1000 cm^3, for the increase and decrease in volume. This gives a ½% error in the volumetric flow rate.

(b) Conductivity Measurements

The conductivity measurements were made using a digital conductivity meter, with a specified accuracy for the range between 0 to 199.99 mS of $\pm$ 0.5%. The calibration curve for conductivity measurements shown in figure (6.2) gives a maximum error for the concentration 0.006867 g-mol/l.

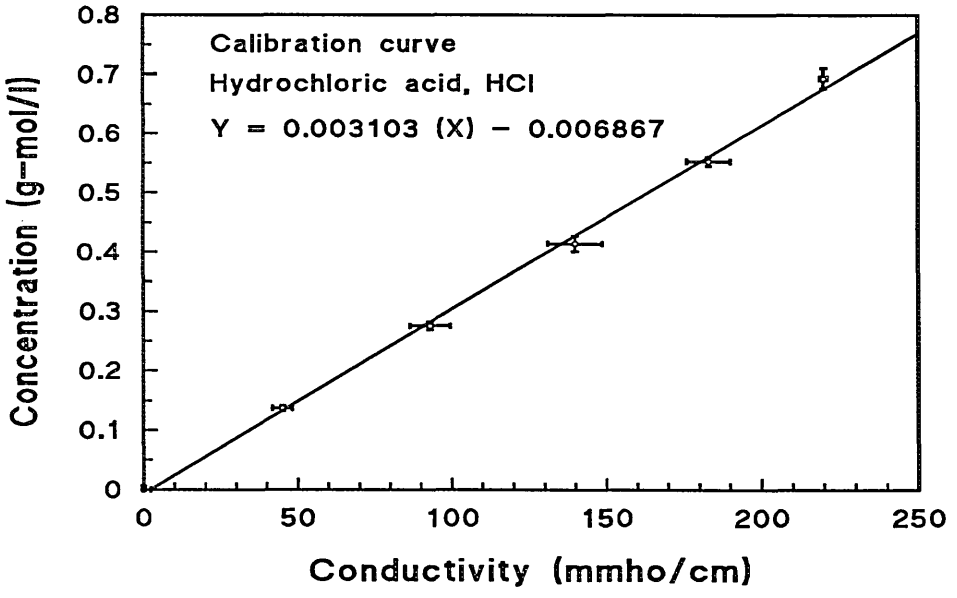

Figure 6.2. Calibration plot for conductivity measurements

(c) Temperature Measurements

An analog connection card was used for the thermocouple temperature measurement, the card provide cold junction compensation and linearization for different thermocouple types, including type "T". The accuracy of the analog card is $\pm$ 0.3% of the reading, and the thermocouple is the $\pm$ 1 °C in the temperature range of 0 to 100 °C and $\pm$ 1% in the temperature range of 100 to 350 °C.

6.2. MODELLING OF PLASMA HEATING

Although geometric and kinematic similarity may be maintained between the actual steel system and an appropriately designed water model, simultaneous thermal similarity is difficult to obtain. It is also difficult to simulate the actual rates of heat loss through the tundish walls and the top surface in a water model.

(a) Plasma heating similarity criteria.

Plasma heating was simulated using a steam jet blown onto the surface of the water flowing through the tundish model system. In order to establish similarity between steam heating in the water model and plasma heating in a tundish a further dimensionless criteria has to be considered. A parameter is required to indicate the extent of the interaction between the flow field within the tundish, and the "thermal

wave" penetration into the flow field from the heated steel surface within the "dog-house".

Similarity can be achieved when the fraction of the flow field affected by this thermal wave is the same in the model and the prototype. Provided that fluid flow similarity between the model and the prototype is attained, the fraction of the fluid flow affected by the heat applied within the confines of the "dog-house" can be characterised by the depth to which the thermal wave in the "dog-house" penetrates into the tundish fluid in the time (τ_p), that the fluid takes to flow beneath the "dog-house", this is shown schematically in figure 6.3. The average fluid velocity can be used to characterise this time:

$$\tau_p = \frac{L_D}{V_{Av}}$$

Where: τ_p is the characteristic dwell time by the fluid beneath the "dog-house"

L_D is the "Dog-house" length for the model and the prototype

V_{Av} is the average velocity of water and steel

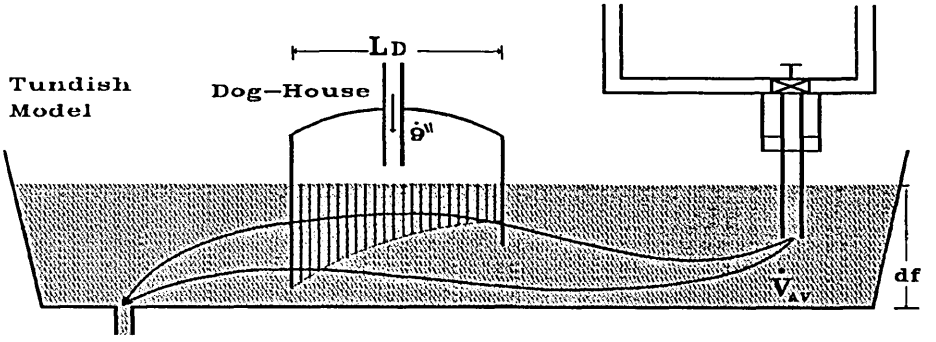

Figure 6.3 Schematic representation of plasma heating modelling criteria.

The depth of penetration of the heat wave can then, in turn, be characterised using the thermal diffusivity in the tundish fluid, as:

$$d_p = \sqrt{\alpha \, \tau_p} = \sqrt{\frac{\alpha \cdot L_D}{V_{Av}}}$$

Where: d_p is the depth of penetration of the heat wave

α is the thermal diffusivity of water and steel respectively

The fractional penetration of the thermal wave into the tundish flow field can thus be characterised by dividing this penetration depth by the depth of the tundish.

Thus, **the dimensionless plasma heating number** can be expressed as:

$$\textit{Plasma heating No.} \propto \left(\frac{\sqrt{\frac{\alpha \cdot L_D}{V_{Av}}}}{d_f} \right)$$

Where: d_f is the depth of water and steel in the tundish

Hence, the criteria for surface heating similarity between the model and the prototype can be expressed as:

$$\left(\frac{\sqrt{\frac{\alpha_{steel} \cdot L_D}{V_{Av}}}}{d_{steel}} \right)_{Prototype} = \left(\frac{\sqrt{\frac{\alpha_{water} \cdot L_D}{V_{Av}}}}{d_{water}} \right)_{model}$$

TABLE 6.1. Values for Model and Prototype

PARAMETER	PROTOTYPE	MODEL
Thermal diffusivity	14.50 X 10^{-6} m^2 sec^{-1}	14.70 X 10^{-8} m^2 sec^{-1}
Coef. of vol. expansion	3.90 X 10^{-4} $°C^{-1}$	2.93 X 10^{-4} $°C^{-1}$
Mean velocity	0.030 m sec^{-1}	0.012 m sec^{-1}
"Dog-house" length	0.79 m	0.30 m
Fluid depth	0.79 m	0.13 m
Plasma heating No.	0.025	0.015

Table 6.1 shows that, although perfect similarity for surface heating has not been achieved between the model and the prototype tundish, the similarity is quite close.

(b) Thermal striation similarity criteria.

Thermal striation effects can occur during plasma heating with the heated steel tending to flow along the surface. The flow patterns will then be modified by the relative buoyancy of this heated steel. In order to establish thermal striation similarity between plasma heating of steel in the tundish and steam heating of water in the tundish model, the ratio of the inertial to buoyancy forces in the model and prototype have to be the same. Thus:

$$\frac{(Re)^2}{Gr} = \frac{V_{Av}^2}{\beta_\theta g \Delta\theta L} = \frac{inertial\ force}{buoyancy\ force}$$

Where: Re is Reynolds number

Gr is Grashof number

β_θ is the temperature coefficient of thermal expansion for water or steel respectively

L is characteristic length

g is acceleration due to gravity

$\Delta\theta$ is average rise in fluid temperature resulting from the heat input

$$\left(\Delta\theta = \frac{\dot{q}}{\rho C_p \dot{V}}\right)$$

Hence, the criteria for thermal striation similarity between the model and the prototype can be expressed as:

$$\left(\frac{V^2}{\beta g \Delta\theta L} \right)_{prototype} = \left(\frac{V^2}{\beta g \Delta\theta L} \right)_{model}$$

This means that, for any given required temperature rise in the tundish there will be a fixed temperature rise in the water model for which thermal striation similarity can be given by the above equatity.

It is interesting to note from the above discussion that the flow patterns within an operating tundish with a plasma heater will change as the rate of heat input is changed. At high heat input rates, the flow of the heated steel along the surface will be intensified. This could delay the entry of heated steel into the continuous casting strand. In a multiple strand tundish, moreover, this effect could result in a persistent maldistribution of the hotter steel between different moulds. Thus modelling studies should be carried out at a range of different heat input rates in order to fully characterise the flow characteristics of a tundish with a plasma heater. It might be that different input rates would require different flow control systems - a facility that could only really be provided through the use of variable gas bubble curtains.

Substituting in the criteria for thermal straition similarity the Froude velocity and length scale factors formulated in chapter 3, for convenience re-written here:

$$V_{model} = X^{\frac{1}{2}} V_{prototype}$$

and

$$L_{model} = X\, L_{prototype}$$

The temperature difference similarity between steam heating of water in the model and plasma heating of steel in the prototype tundish can be expressed as:

$$(\theta_i - \theta_f)_{prototype} = \left(\frac{\beta_{water}}{\beta_{steel}}\right)(\theta_i - \theta_f)_{model}$$

Where: β_θ is the temperature coefficient of thermal expansion for water or steel respectively.

θ_i is the temperature of water or steel before heating starts.

θ_f is the temperature of water or steel after heating.

Therefore, substituting the values for the temperature coefficient of volume expansion given in table 6.1, the similarity equation will yield:

$$(\theta_i - \theta_f)_{steel\ prototype} = 0.75\,(\theta_i - \theta_f)_{water\ model}$$

Thus it is relatively straight forward to arrange for thermal striation similarity between the water model and the prototype tundish.

6.3. CHARACTERISTICS OF FLOW CONTROL CONFIGURATIONS

Unsurprisingly the fluid flow characteristics developed from the model investigation were similar to those described by Sahai and Ahuja. A tundish without any flow control device is perhaps the most used configuration. In this case, the plug and mixed volumes occupied the largest fraction of the total volume, as shown in figure 5.11. Adding a weir and a dam created a slow secondary recirculation in the downstream region behind them, enlarging the dead volume fraction and reducing the plug volume, leaving the largest fraction to the mixed volume. The use of air bubbling in the centre of the tundish in combination with these control devices helped to increase the plug volume fraction and to decrease the dead volume by activating the slow recirculation zones created by the weir and the dam. However, air bubbling did not have any noticeable effect on the mixed volume fraction. This fraction varied from 0.46 to 0.57 for the configurations studied,as shown in figure 5.11.

The longitudinal dispersion parameters estimated from the conductivity measurements were in the range between 0.119 to 0.127, for the various tundish configurations studied as shown in figure 5.10. For a tundish without any flow control devices the amount of dispersion predicted was 0.121, the use of a weir and a dam increased the dispersion parameter to 0.127. The addition of flow control devices increased the mixed fraction,

enlarging the longitudinal dispersion. However, air bubbling in conjunction with the weir and the dam did not show any effect on the dispersion parameter calculated as 0.119. The air bubbling from the bottom of the tundish acts as a barrier for longitudinal dispersion but encourages mixing in the vertical direction.

6.4. PREDICTION OF FLUID TEMPERATURE CHANGE

The estimated values for the longitudinal dispersion parameter were used to predict the water temperature change at the outlet nozzle after a step change is introduced at the entry tundish nozzle, and were compared to the experimental temperature step change results. The temperature drop from 1 to 0 and the theoretical equation employed to predict it is reproduced here:

$$T_\Theta = \frac{1}{2}\left\{1 + erf\left(\frac{1-\Theta}{\sqrt{4\,\Theta\left(\frac{D_i}{uL}\right)}}\right)\right\} \qquad \textbf{(4.32)}$$

Where: T_θ is the fractional fluid temperature change

Θ is the sampling time

(D_i/uL) is the dispersion parameter

The experimental fractional temperature drop rate measured at the outlet, is faster than the predicted rate for all the tundish configuration studied, as shown in figures 5.7, 5.8, 5.9. A possible explanation of this mismatch is that the estimate for the longitudinal

dispersion parameter was obtained under isothermal conditions, whereas the experimental fractional changes were measured after the step change in water temperature. Non-isothermal conditions prevailed after the step input and it takes about 2.4 multiples of time to re-establish steady state conditions. This indicates that the relatively colder water entering the tundish will alter the flow pattern in the tundish.

The physical property responsible for this alteration in flow is the change in density as a function of temperature. The densities of both water and steel increase with decreasing temperature. This density difference effect in the flow pattern due to temperature may be counterbalanced by the higher density of both the tracer used in the isothermal water model and the colder water entering the tundish after the step change in the non-isothermal model. This neutralization is because both the tracer and the colder water will tend to flow closer to the bottom of the tundish. However, the water temperature difference provides a buoyancy force component to the flow velocity, and the faster temperature decay rate obtained experimentally may be due to the higher flow velocities gain under non-isothermal conditions.

6.5 TEMPERATURE COMPENSATION BY USING THE STEAM HEATING SYSTEM

The compensation temperature in the tundish model was predicted by estimating the longitudinal dispersion parameter, first for the fluid path A - this is from the entry

nozzle to the outlet and then for the fluid path B - this is from the steam nozzle to the outlet. Paths A and B were shown schematically in diagram 5.4, in chapter 5. These estimated values were used to predict the temperature compensation as a function of the thermal dispersion and sampling time.

The fluid temperature change at the outer nozzle was predicted as a fraction, which starts at steady state and then a step input in temperature is applied at the tundish entry nozzle. At later time the heat compensating system is started and the fluid temperature will begin to raise until it attains its initial fractional value.

The estimated dispersion parameter values for both fluid paths A and B is given in tables 5.13 and 5.16, these are for two different flow control arrangements. These values were employed in the theoretical equation to predict the outlet temperature response to the heat input, for convenience the equation is reproduced here:

$$T_\theta = \frac{1}{2}\left\{1 + erf\left(\frac{1-\theta_A}{\sqrt{4\,\theta_A\left(\frac{D_i}{ul}\right)_A}}\right)\right\} + \frac{1}{2}\left\{1 - erf\left(\frac{1-\theta_B}{\sqrt{4\,\theta_B\left(\frac{D_i}{ul}\right)_B}}\right)\right\} \qquad \textbf{(4.33)}$$

Where: T_θ is the fractional temperature

Θ_A is the sampling time after the step input

Θ_B is the sampling time after the torch is started

(Di/uL) is the dispersion parameter for the fluid paths A and B respectively

The dispersion parameter for the arrangement schematized in diagram 5.5 were very similar for both fluid paths. For the fluid path A, from the entry to the outlet nozzle, the dispersion parameter was 0.114. For the fluid path B, from the steam nozzle to the outlet, the dispersion parameter was 0.109. This is simply because the entry nozzle and the steam nozzle are close together and the distance to the outlet is about the same. However, this experiment shows that the steam acts as a good tracer carrier, and that the tracer is injected to the water stream under the "dog-house".

For a different arrangement schematized in diagram 5.6, the dispersion parameter values were considerably different, for the fluid path A the dispersion parameter estimated was 0.143, and for the fluid path B was 0.087 as shown in table 5.16. The fluid path B is significantly shorter than the path A.

The results obtained from substituting this estimated values for the dispersion parameters in the equation (4.33), were compared to experimental temperature measurements at the outlet nozzle and the temperature response curves are plotted in figures 5.30 and 5.31. Both the experimental fractional temperature decay rate and the experimental fractional temperature rise rate are faster than the predicted ones. However, this is due to the combination of effects in the water model, as discussed in the previous section.

The dispersion parameter for the fluid path A was estimated under isothermal conditions. Before steam heating starts, the effects of the step input of temperature on

the flow pattern due to non-isothermal conditions will be the same as discussed in the temperature decay situation. The cold water tend to flow closer to the tundish floor, displacing the hot water already present to move upwards to the surface, creating a stratification of temperatures. This stratification produces a slow back flow at the very top of the water moving towards the "dog-house", creating a dead zone, the deeper the "dog-house" the bigger the dead zone, and the thicker the upper stratum. The mismatch between the fractional temperature measured and predicted may be due to the density difference and to the higher flow velocities gain under non-isothermal conditions.

The dispersion parameter for the fluid path B was estimated under non-isothermal conditions, the steam blown onto the surface of the water acts as a tracer carrier, so the temperature of the fluid increased. The tracer spend some time in the "dog-house" due to the turbulence created by the steam jet in there. The hotter water tends to rise and flow across the top, over the relatively colder water. The turbulence and the fact that the heated water rises and mixes with the hotter water present at the upper stratum produces that the first appearance of the tracer for the fluid path B takes longer time than for the fluid path A, delaying the entry of heated fluid into the continuous casting strand, as shown in figure 5.12 and 5.16. However, the peak time is about the same, and the maximum concentration is considerably higher for the fluid path B indicating less total amount of mixing.

When heat is supplied to the colder water passing beneath the "dog-house", this is at a time θ_B, a second completely mixed zone is created beneath the "dog-house" due to

the steam penetration, the fluid spends some time in this zone because of the turbulence created in there. The heated flow tend to rise to the upper stratum over the relative colder water already present in the tundish moving towards the outer nozzle at a higher velocity, mixing better with the flow present at the upper stratum homogenizing the water temperature, and activating the dead zones behind the "dog-house". Because of this homogenisation of temperature driven by thermal convection, the use of any other flow control devices after the "dog-house" will create stagnant zones which will not participate in the heat transfer process, decreasing the effectiveness of the heating system.

The flow pattern in the water model is modified by the steam heating due to the temperature effect on the density of the fluid and the mixing phenomena under the "dog-house". Non-isothermal conditions prevails during the whole casting process, after the step input the temperature of the incoming water is about 9 °C lower than the water already present, under isothermal conditions, in the tundish. This develops a fairly significant degree of temperature stratification. Once the steam heating system has started a second mixed volume is created by the steam penetration, and the heat transfer process begins. This mixing phenomena under the "dog-house" and the convective heat transfer process are the main contributors to the modification of the flow pattern and the residence time distribution in the tundish.

6.6 ESTIMATION OF INTERNAL SURFACE TEMPERATURE AT THE ENTRY AND OUTER NOZZLES.

The estimation of internal surface temperature was investigated using a remote sensing method. The liquid steel temperature is estimated from the changes registered by the thermocouples embedded in the nozzle wall. As the temperature of liquid steel in either nozzle changes the temperature indicated by the thermocouples will also change, but at later time and to a lesser extent. The liquid steel temperatures must be deduced from the measured changes - a classic inverse problem since these temperatures are the boundary conditions for the solution of the heat conduction equation in the nozzle wall.

Inverse methods are frequently unstable since inaccuracies in the estimated surface temperatures can accumulate and multiply rapidly. The method developed involves forcing the errors from the estimated boundary conditions to decay, because the measured and estimated temperatures are analyzed in terms of a steady component with small deviatory components of short duration.

(a) Theoretical simulation experiments

In order to test the stability and reliability of the method developed a set of theoretical simulation experiments were carried out. The finite difference method, developed in chapter 4, was used to create look-up tables for $\mathbf{f}_{\Delta\tau}$, $\mathbf{f}_{2\Delta\tau}$, $\mathbf{f}_{3\Delta\tau}$ etc. for the thermocouple positions; this finite difference method was also used to predict temperatures at wall

interior domain positions, infinite heat transfer conditions were assumed. The predicted temperatures were used in the algorithm to estimate surface temperature.

Figure 5.21 and 5.22 show the estimated and predicted temperatures originated from a sudden jump in the interior surface temperature, this is simulating steel entering the submerged entry nozzle after it has been preheated at a 1200 °C and it is at steady state. Figure 5.23 shows that the inverse heat transfer algorithm takes about four minutes to estimate a more accurate temperature value, subsequently it follows the temperature decay with an average discrepancy of about 0.6 °C. For this severe test, the algorithm beyond the four minutes that it took to stabilise the precision, can be considered reliable.

Figure 5.24 shows a less severe test, the simulation of a ladle change with the interior surface temperature increasing is from 1550 °C to 1600 °C followed by a slow fall in temperature, simulating the ladle cooling. Figure 5.25 reveals that the method produces a two minutes lag before the simulated temperature reaches its maximum value.

Using the temperatures predicted by the numerical method, the calculated temperature values for both tests are in very good agreement with the exact temperature. The only periods with discernible errors are those intervals in which the surface temperature changes abruptly. The lags observed in the above tests results from the very nature of heat conduction as a diffusive process; this is, the effect at an interior location of a surface heat input at a time zero lags behind the effect at the surface.

(b) Experimental measurements

In the inverse heat conduction problem there are a number of measured quantities in addition to temperature; such as time, sensor location, and specimen thickness. Each is assumed to be accurately known except temperature. The thermal conductivity, k, density, ρ, and specific heat, C_p, are postulated to be known functions of temperature. If any of these thermal properties varies with temperature, the inverse problem becomes nonlinear. The location of the thermocouples is measured, and the thickness of the plate is also known.

The inverse problem is difficult because it is extremely sensitive to measurement errors. The difficulties are particulary pronounced as one tries to obtain the maximum amount of information from the data for the internal surface temperature estimation - maximizing the amount of information implies the use of small times steps. However, the use of small time steps introduces instability in the solution. The use of small time steps in the inverse algorithm has the opposite effect in the inverse problem compared to that in the numerical solution of the heat conduction equation.

A set of experimental measurements were carried out using three temperature sensors embedded radially in the tundish entry nozzle wall. The first experiment was for a step increase in the internal surface temperature, this is one of the most stringent tests of an inverse heat conduction problem algorithm. Then, a step decrease in the internal surface temperature was applied, the tests were compared and after examination it was detected

that the results were asymmetrical. Thus, it became necessary to investigate the convective heat transfer coefficient for the internal surface of the perspex tube in the presence of the water flow.

(i) Heat transfer coefficient estimation

The heat transfer coefficient estimation was performed by matching the measured internal temperature gradients with the calculated temperature gradient by the finite difference method. The value for the best fitted curve was taken as the heat transfer coefficient for the experimental test, this shown in figure 5.25, and 5.26. It is also shown that the value for the heat transfer coefficient is smaller when the step change in the internal surface temperature is increased; this is flowing cold water to reach steady state and performing the sudden change to hot water, as shown in figure 6.4.

This is considered to be due to a phenomena occurring at the "T" junction at entry nozzle to the tundish model used for this experimental measurements, since cold water and hot water enter the flow tube from different directions.

Cold water flows from the left hand side ladle, when it gets to the entry nozzle the flow is directed towards the opposite side of the internal wall, where the nearest sensor to the surface is situated, as shown schematically in figure 6.4. This thermocouple has the dominant effect because its registered temperature is the one used in the inverse heat transfer algorithm. Figure 6.5 show a comparison of the temperature gradient measured

by the three thermocouples embedded in the nozzle wall and the temperature predicted by the finite difference method considering infinite heat transfer conditions at the inner surface. In order to improve the matching of these curves a convective heat transfer resistance has to be included in the finite difference method. The heat transfer coefficient which gives a better matching is in the laminar region and is equal to 195 W m^{-2} $°C^{-1}$, and figure 5.26 shows a much better matching. However, as expected, the prediction for the outer thermocouple deteriorated.

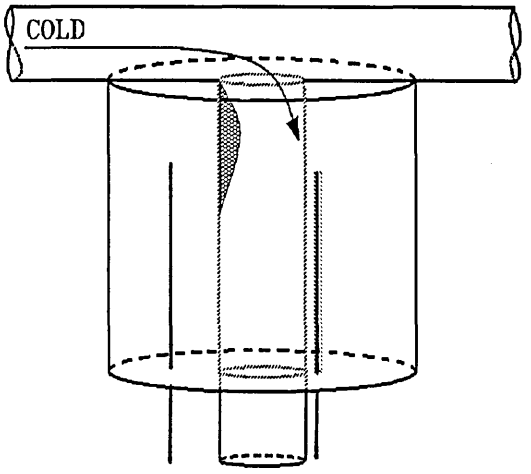

Figure 6.4. Schematic diagram of the flow tube entry effect, when cold water enter the tundish.

Hot water flows from the right hand side ladle, when the flow reaches the entry nozzle the water will impact the opposite side, creating an thicker boundary layer between the water and the internal surface nearest to the first sensor this is shown schematically in figure 6.6. For infinite heat transfer conditions in the inside boundary, the measured and the predicted temperature gradient in the nozzle wall are in poor agreement for the

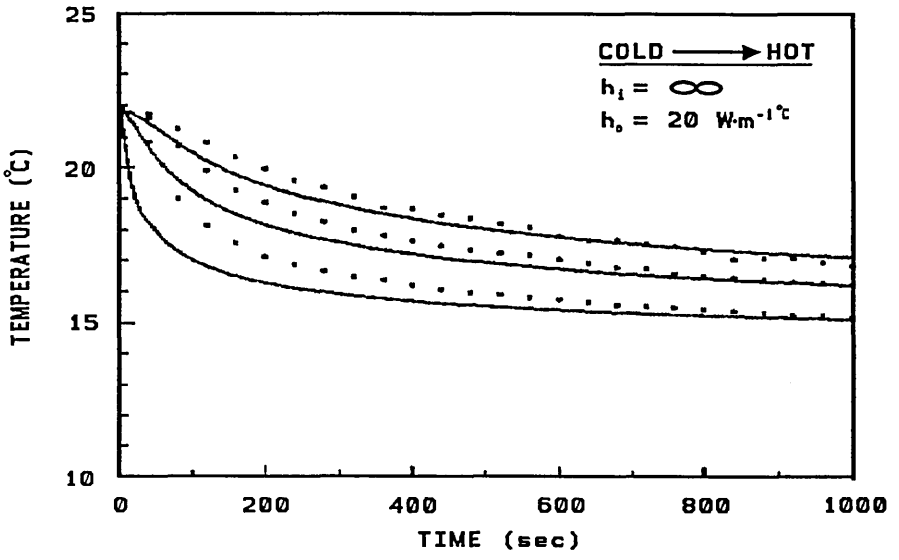

Figure 6.5 Temperature gradient measured and predicted by the finite difference method considering infinite heat transfer conditions in the inner surface.

inner thermocouple reading, as shown in figure 6.7, a better agreement is shown for the outer surface. Figure 5.28 shows that the agreement is improved by using a higher laminar heat transfer coefficient equal to 375 W m^{-2} °C^{-1}.

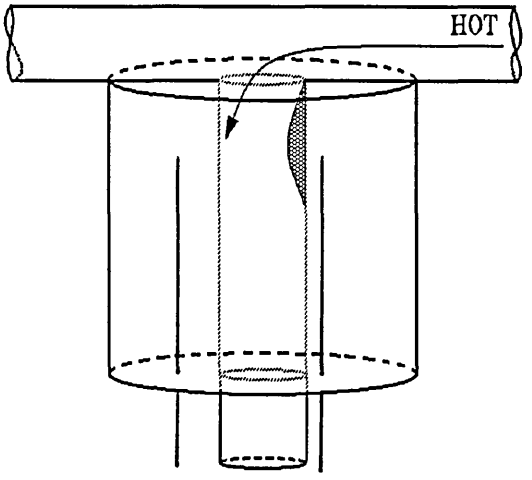

Figure 6.6 Schematic diagram of the flow tube effect when hot water is entering the tundish model

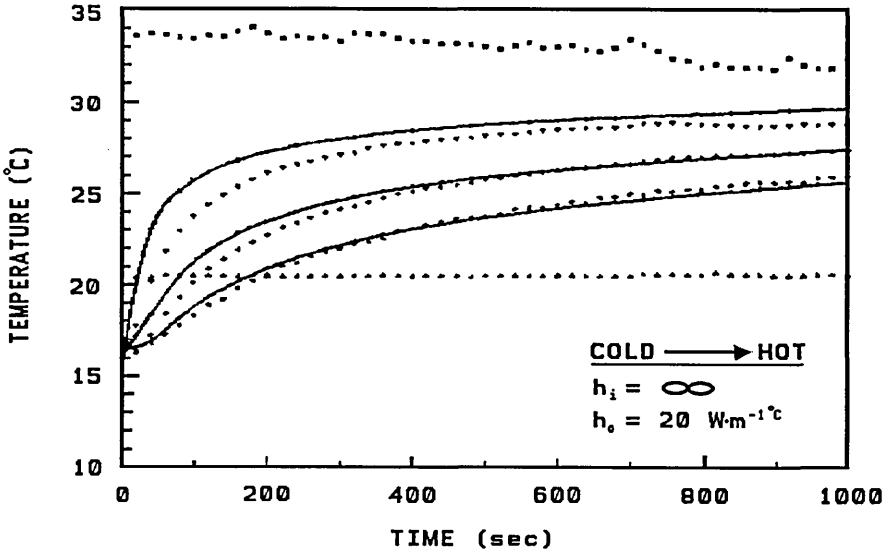

Figure 6.7 Temperature gradient measured and predicted by the finite difference method considering infinite heat transfer conditions in the inner surface.

Figure 5.27 shows the results of the step input changes in water temperature, it can be seen that the method on the water analogue model is able to detect temperature changes in the liquid flowing into the tundish to an accuracy better than 5%. This accuracy was obtained after the incorporation into the finite difference analysis the resistance for the convective heat transfer at the inner surface of the flow tube.

6.7 APPLICATION OF THE INVERSE HEAT TRANSFER METHOD IN THE CONTINUOUS CASTING TUNDISH.

The occurrence of alumina build-up on the inner wall of the sub-ladle tundish entry nozzle and on the submerged mould entry nozzle and the erosion of the internal wall of the nozzles will affect the location distance for the first sensor, this is the sensor closer to the internal surface. Therefore, in order to apply the inverse heat conduction method in real nozzles it should be extended to estimate the location of the first sensor from measurements at the second sensor behind, since the distance from the second to the first is known.

Where slides gates are used to control the ladle to tundish or tundish to mould flow, at the moment the gate opens the flow is directed to the internal wall opposite to the opening direction, creating break away in the flow pattern. The flow problems encountered at the model entry nozzle, as discussed in the previous section, also suggest that the thermocouples should be positioned one behind the other and not radially.

CONCLUSIONS

A physical model of a conventional tundish and a tundish heater system have been design, constructed and used to simulate the plasma heating systems operated by some of the most modern continuous casting plants. Similarity between steam heating in the water model and plasma heating in a tundish has been establish. A dimensionless criteria was developed to validate the simulation experiments and it is represented by a plasma heating number. Using this similarity criteria plasma heating can be simulated by a steam heater in an appropriately design water tundish model.

A theoretical dispersion model has been formulated for the flow through the tundish and the dispersion parameter in this model was determined from the results obtained using the conductivity method. In order to validate this model, measurements were also made of the changes in temperature at the exit resulting both from changes in the temperature of the inlet stream and from the use of the steam heater system. The dispersion model was then used to predict these temperature changes, using the dispersion parameter based on the conductivity measurements.

This temperature changes indicated that the relative colder water entering the tundish will alter the flow pattern in the tundish, the steam heater also modified the flow pattern due to the temperature effect on density and the mixing volume created beneath the "dog-house". However, sufficiently good agreement has been obtained to suggest that

the model could be incorporated into a control algorithm that can maintain the exit temperature constant in the facing of changing inlet temperatures.

A stable inverse heat conduction method has been developed in which the measured and estimated temperatures are analyzed in terms of a steady component with small deviatory components of short duration. A finite difference method has been used to predict the effect on a thermocouple temperature of the deviatory component of the liquid steel temperature. Distinction is made between effects during the period for which the deviatory temperatures operate and their subsequent decaying effects. The incorporation of these predictions into look-up tables has allowed an algorithm to be developed that can deduce the current deviatory component of the steel temperature from the thermocouple response.

The method was tested by theoretical simulation experiments using temperatures predicted by the numerical method, the estimated values using this algorithm are in very good agreement with the exact simulated temperature. The only periods with discernible errors are those intervals in which the surface temperature changes abruptly.

The algorithm was also tested practically in the water tundish model, and was able to detect temperatures changes in the liquid flowing into the tundish to an accuracy of better than 5%. In order to achieve this accuracy, however, it was necessary to incorporate into the finite difference analyses a resistance for the convective heat transfer at the inner surface of the flow tube. The flow tube is short, and the

thermocouples are mounted into the wall close to the entry into the tube so that entry effects were found to be important. Since the hot water and cold water enter the flow tube from different directions, the entry effects are not the same when the water temperature is increased as when the water temperature decreased. This resulted in a lack of symmetry between heating and cooling experiments, consequently it became necessary to investigate the convective heat transfer coefficient for the internal surface of the perspex tube in the presence of the water flow.

8

FURTHER WORK

(i) Using the plasma heating similarity criteria and the dispersion model, modelling work should be carried to study the optimum "dog-house" location for adding thermal energy to multi-strand tundishes.

(ii) Modelling studies should be carried out at a range of different heat input rates in order to fully characterise the flow characteristics of a tundish with a plasma heater.

(iii) The inverse heat conduction algorithm should be extended to simultaneously estimate sensor location and surface temperature.

(iv) High temperature experiments should be further carried out using crucibles from castable refractories to contain wall thermocouples. The reading of these thermocouples should be monitored and used to estimate the varying temperature of liquid metals held in the crucibles.

(v) An evaluation should be undertaken to estimate the operating life of the thermocouples embedded in castable refractories walls.

(vi) Plant trial should be venture making and testing prototype nozzles.

REFERENCES

1.- Debroy T., J.A. Sychterz: "Numerical calculation of fluid flow in a continuous casting tundish". *Metallurgical Transaction B*, Vol. 16B 1985, pp. 497-504.

2.- Tanaka S., M. Lye, M. Salcudean, R.I.L. Guthrie: "Physical and mathematical modelling of tundish systems". *Conf. Proc. 24th Annual Conference of Metallurgist*, Aug. 18-21, Vancouver, B.C. Canada. C I M . 1985, pp. 142-161.

3.- Jones W.P., B.E. Launder: "The prediction of laminarization with a Two-Equation model of turbulence". *Int. J. Heat and Mass Transfer*, Vol. 15 1972, pp. 301-314.

4.- Launder B.E., D.B. Spalding: *"Mathematical models of turbulence"*, Academic Press, New York, 1972.

5.- Lai K.Y.M., M. Salcudean, S. Tanaka, R.I.L. Guthrie: "Mathematical modelling of flows in large tundish systems in steelmaking". *Metallurgical Transaction B*, Vol. 17B 1986 pp. 449-459.

6.- Szekely, J., O.J. Ilegbusi, N. El-Kaddah: "The mathematical modelling of complex fluid flow phenomena in tundishes". *PhysicoChemical Hydrodynamics*. Vol.9, 3/4 1987 pp.453-472.

7.- Ilegbusi O.J., J. Szekely: "Fluid flow and tracer dispersion in shallow tundishes". *Steel Research*, 59 No.9 1988 pp. 399-405.

8.- He Y., Y. Sahai: "The effect of tundish wall inclination on the fluid flow and mixing: a modelling study". *Metallurgical Transaction B*, Vol.18B 1987, pp. 81-92.

9.- He Y., Y. Sahai: "Fluid dynamics of continuous casting tundishes". *Acta Metallurgica Sinica*, series B, Vol.1 No.2, 1988, pp.93-102.

10.- Chakraborty S., Y. Sahai: "Role of Near-Wall location on the prediction of the melt flow and residence time distribution in tundishes by mathematical modelling". *Metallurgical Transaction B*, Vol. 22B 1991 pp. 429-437.

11.- Heaslip, L.J., A. McLean, I.D. Sommerville: "Fluid Flow", *In Continuous Casting*, Chapter 2. A Publication of ISS of AIME. Vol. I 1983 pp. 67-71.

12.- Kemeny F., D.J. Harris, A. McLean, T.R. Meadowcroft, J.D. Young: "Fluid flow studies in the tundish of a slab caster". *Proc. 2nd Process Technology Conference* Vol. II, 1981, pp. 232-246.

13.- Sahai Y., R. Ahuaja: "Fluid flow and mixing of melts in steelmaking tundishes". *Ironmaking and Steelmaking*, Vol.13 1986 pp.241-247.

14.- Hashio, M., M. Toduka, M. Kawasaki, T. Watanabe: *Proc. 2nd Process Technology Conference*, Chicago, ISS of AIME Vol. II 1981 pp. 65-74.

15.- Dobson, C.J., R. Serje, K. Gregory: "Physical and mathematical modelling of fluid flow in BHP'S continuous casting Tundishes". *4th International Conference on Continuous Casting*, The Institute of Metals, Brussels, May 17-19, 1988 - pp.682-693.

16.- Martinez E., M. Maeda, L.J. Heaslip, G. Rodrigez, A. Mclean: "Effects of fluid flow on the inclusion separation in continuous casting tundish". *Transaction ISIJ*, Vol. 26 1986 pp. 724-731.

17.- Van der Heiden A., P.W. Van Hasselt, W.A. de Jong, F. Blaas: "Inclusion control for continuously cast products". *Procs. of the 5th International Iron and Steel Conference*, Washington D.C., ISS-USA 1986 pp. 755-760.

18.- Ilegbusi O.J., J. Szekely, R. Boom, A. van der Heiden, J. Klootwijk: "Physical and mathematical modelling of fluid flow and trace dispersion in a large tundish and a comparison with measurements in Hoogovens' system". *Procs. Conf. W.O. Philbrook Memorial Symposium*, ISS - USA. 1988 pp. 185-191.

19.- Lowry M.L., Y. Sahai: "Investigation of Steel Flow in a Continuous Casting Tundish with Multiple-Hole Baffles Using Mathematical Models and Tracer Studies". *Iron and Steelmaker*, Vol.18 - 8 1991 pp. 53-60.

20.- Ilegbusi, O.J., J. Szekely: "Transport phenomena in tundishes: Heat transfer and the role of auxiliary heating." *Steel Research*, 62 No.5 1991, pp.193-200.

21.- Szekely J., O.J. Ilegbusi: "*The Physical and Mathematical Modelling of Tundish Operations*". Spriger-Verlang, 1989

22.- Joo S., R.I.L. Guthrie: "Scientific flow visualization of heat flow and inclusion behaviour in a Tundish for slab casting". *Procs. of the Int. Symposium on Developments in Ladle Steelmaking and Continuous Casting*, (CIM), Canada. 1990 pp. 264-289.

23.- Joo S., R.L.I. Guthrie: "Heat flow and inclusion behaviour in a tundish for slab casting". *Canadian Metallurgical Quarterly*, Vol.30 - 4 1991 pp. 261-269.

24.- Chakraborty S., Y. Sahai: "Effect of varying ladle stream temperature on the melt flow and heat transfer in continuous casting tundishes". *ISIJ International*, Vol.31 - 9 1991 pp.960-967.

25.- Chakraborty, S., Y. Sahai: "Mathematical modelling of transport phenomena in continuous casting tundishes. Part 1 Transient effects during ladle transfer operations", *Ironmaking and Steelmaking*, Vol.19 - 6 1992 pp. 479-504.

26.- Chakraborty, S., Y. Sahai: "Mathematical modelling of transport phenomena in continuous casting tundishes. Part 2 Transient effects owing to varying ladle stream temperature". *Ironmaking and Steelmaking* Vol.19 - 6 1992 pp. 488-494.

27.- Lowry, M. L., Y. Sahai: "Modelling of thermal effects in liquid steel flow in tundishes". *Steelmaking Conference Proc.*, Washington DC, USA. Vol. 74 1991 pp. 505-511.

28.- Mori, M., M. Oosaki, M. Iwasaki, N. Tsutsumi, I. Sawada.: "Analysis of heat transfer and fluid flow in continuous caster tundish". *Nippon Steel Technical Report*, No.4 1991 pp. 34-40.

29.- Kuwabara T., K. Umezawa, T. Nuibe, M. Fukuyama: "Development of Tundish plasma heater". *Proc. of the 8th Int. Symposium on Plasma Chemistry*, IUPAC. 1987 pp.2247-2252.

30.- Matsumoto K., Y. Hoshijima, K. Ishikura, K. Umezawa, Y. Nuri, Y. Ohori: "The implementation of Tundish plasma heater and its application for improvement of steel qualities". *Proc. of The Sixth Int. Iron and Steel Congress*, Nagoya,(ISIJ). Vol. 3 1990 pp. 222-229.

31.- Mizushina, M., Y. Kitano, Y. Suga, M. Saiki, Y. Seguro: "Development of tundish plasma heating system". *Proc. Conf. on Plasma for Industry and Environment*, British National Committee for Electroheat, Wadham College,

Oxford, Sept. 1990.

32.- Moore C., C.P. Heanley, P.M. Cowx: "Plasma tundish heating as an integral part of continuous casting". *Steel Times International*, May 1989 pp. 44-46.

33.- Moore C., C.P. Heanley, P.M. Cowx: "Plasma heating in hot metal processing". *Proc. Conf. on Plasma for Industry and Environment*, British National Committee for Electroheat, Wadham College, Oxford, England, 1990.

34.- Moore C., C.P. Heanley, C.D. Chapman, Y. Seguro: "The practical use of plasma tundish heating to control mould entry temperature". *Proc. of the 1st European Conf. on Continuous Casting*, Florence - A.I.M., Sept. Vol. 2 1991 pp. 185-192.

35.- Choi H., F. Mucciardi: "Modelling technique for the continuous measurement of steel temperature". *Conf. Procs. International Symposium on Ladle Steelmaking and Furnaces*. 27th Annual conference of metallurgists, August 28-31, Montreal, Quebec, Canada, CIM. 1988 pp. 59-79.

36.- Russo T.J., R.M. Phillippi.: "Continuous temperature measurement of liquid steel in the tundish: Three years of operating history at Bethlehem steel, sparrows point". *Steelmaking Conference Proceedings*, ISS-USA. 1990 pp. 237-246.

37.- Mori H., M. Sawa, Y. Shai, M. kabe, K. Kuwahara, K. Sakai.: "Continuous measurement of molten steel temperature". *Proc. of the Sixth Int. Iron and Steel Congress*, Nagoya, Japan. ISIJ. 1990.

38.- Nyssen P., C. Marique, F. Thill, C. Schoumacher: "Continuous temperature measurement of liquid steel". *Proc. of the Sixth International Iron and Steel Congress*, Nagoya, Japan. ISIJ. Vol. 5 1990 pp. 84-91.

39.- Cornelissen, M.C.M., W.A. de Jong, J.M. Rabenberg: "Instrumentation to monitor the caster condition and casting process at Hoogovens BOS No.2". *9th PTD Conference Proceedings*, ISS-USA. 1990 pp. 95-99.

40.- Levenspiel O., W.K. Smith:"Notes on the diffusion-type model for the longitudinal mixing of fluids in flow", *Chemical Engineering Science*, Vol. 6, 1957, pp. 227-233.

41.- Levenspiel O."*Chemical reaction engineering*", Second edition, Wiley International, 1972.

APPENDIX 1

PROGRAM LIST

```
'PROGRAM TO CALCULATE THE TEMPERATURE DISTRIBUTION IN AN
'INFINITE NOZZLE WALL

COLOR 7,9
CLS
DIM S(400),T(400),TK(600),TL(600),TM(600),TN(600)
Z = 0.37556  'TIME RELATED STEP SIZE (MAX VALUE O.5)"; Z
X = 0        'MINIMUM VALUE OF TORR"; X
V = 10000    'MAXIMUM VALUE OF TORR"; V
T(13) = 14.9 'STEEL TEMPERATURE ";T(4)
Y = 20.3     'INITIAL WALL TEMPERATURE"; Y
TA = 20.3    'ROOM TEMPERATURE"; TA
K=0
PRINT " HEAT CONDUCTION IN A NOZZLE"

PRINT "   RTIME   TORR    T(4)    T(5)    T(6)    T(7)    T(8)    T(9)   T(10) "

TORR = 0
JREAD = 0
FOR I = 14 TO 49
'FOR I = 13 TO 50
   T(I) = Y
NEXT I

STEPTIME:
TORR = TORR + Z
RTIMEX% =  ( TORR * (0.002/4)^2 / (0.9398E-7))

'IF RTIMEX% = 40 THEN
'   TW = 14.939
'END IF
IF RTIMEX% = 20 THEN
  T(13) = 15
END IF

'IF RTIMEX% = 6000 THEN
'   TW = 33.2
'END IF

IF RTIMEX% = 3000 THEN
  T(13) = 33
END IF
JREAD = JREAD + 1
'
```

```
'Eq. for heat tranfer coeff = 195 W/m^2 C for step input from cold to hot

S(13)=T(13)-((1/3)*(S(14)-T(14)))+(((8/3)*Z)*(((0.575*13)/13.25)*(TW-T(13))-((1
3.5/13.25)*(T(13)-T(14)))))

'Eq. for heat tranfer coeff = 375 W/M^2 C for step input from hot to cold

'S(13)=T(13)-((1/3)*(S(14)-T(14)))+(((8/3)*Z)*(((0.62*13)/13.25)*(TW-T(13))-((13
.5/13.25)*(T(13)-T(14)))))

'for infinite solution
FOR I = 14 TO 49
   S(I) = T(I) + Z * (T(I-1) - 2*T(I) + T(I+1) + (1/I) * (T(I+1)-T(I)))
NEXT I

'S(50) = T(50) + ((2 * Z) * ((49/50)*(T(49) - T(50)) - (0.020*(T(50)-TA))))

S(50)=T(50)-((1/3)*(S(49)-T(50)))+(((8/3)*Z)*((49.5/49.75)*(T(49)-T(50))-(0.0629
4*(T(50)-TA))))

'S(50) = TA

FOR I = 14 TO 50
   T(I) = S(I)
NEXT I

IF JREAD < 1 GOTO STEPTIME

FOR JJ = 149 TO 200
      IF RTIMEX% = 19 + (JJ * 20) THEN TK(JJ) = T(13) : TL(JJ) = T(17) :
TM(JJ) = T(21) : TN(JJ) = T(25)
NEXT JJ

PRINT USING "####.######"; RTIMEX% ,TORR,T(13),T(17),T(21),T(25),T(50)

IF RTIMEX% > 4020 THEN CONTINUE
IF TORR < V GOTO STEPTIME

CONTINUE:
OPEN "A:\infc_h.DAT" FOR OUTPUT AS #1
FOR KK = 149 TO 200
WRITE #1, TL(KK),TM(KK),TN(KK),TK(KK)
NEXT KK
CLOSE 1

END
```

```
'THIS PROGRAM CALCULATES THE FRACTINAL TEMPERATURE CHANGE
AFTER A STEP INPUT, EVERY 40 Sec.

'CALCULATION OF TEMPERATURE DISTRIBUTION IN AN FINITE NOZZLE
WALL

CLS
DIM S(200),T(200),TK(300),TL(300),TM(300),TN(300)
Z = 0.37556  'TIME RELATED STEP SIZE (MAX VALUE O.5)"; Z
X = 0        'MINIMUM VALUE OF TORR"; X
V = 1000     'MAXIMUM VALUE OF TORR"; V
TW = 0       'STEEL TEMPERATURE ";T(4)
Y = 0        'INITIAL WALL TEMPERATURE"; Y
TA = 0       'ROOM TEMPERATURE"; TA

PRINT " HEAT CONDUCTION IN A NOZZLE"

PRINT "   RTIME   TORR    T(4)    T(5)    T(6)    T(7)    T(8)    T(9)   T(10) "

TORR = 0
JREAD = 0

FOR I = 25 TO 97
   T(I) = Y
NEXT I

STEPTIME:

TORR = TORR + Z
RTIMEX% =  ( TORR * (0.002/8)^2 / (0.9398E-7))

IF RTIMEX% = 80 THEN
  TW = 0
END IF

IF RTIMEX% = 120 THEN
  TW = 1
END IF

IF RTIMEX% = 160 THEN
  TW = 0
END IF

JREAD = JREAD + 1
```

```
S(25)=T(25)-((1/3)*(S(26)-T(26)))+(((8/3)*Z)*(((0.60*25)/25.25)*(TW-T(25))-((25.
5/25.25)*(T(25)-T(26)))))

FOR I = 26 TO 96
   S(I) = T(I) + Z * (T(I-1) - 2*T(I) + T(I+1) + (1/I) * (T(I+1)-T(I)))
NEXT I


S(97)=T(97)-((1/3)*(S(96)-T(96)))+(((8/3)*Z)*((96.5/96.75)*(T(96)-T(97))-(0.062*(
97/96.75)*(T(97)-TA))))


FOR I = 25 TO 97
   T(I) = S(I)
NEXT I
IF JREAD < 1 GOTO STEPTIME

FOR JJ = 2 TO 45
      IF RTIMEX% = 39 + (JJ * 40) THEN TK(JJ) = T(25) : TL(JJ) = T(33) :
TM(JJ) = T(41) : TN(JJ) = T(49)
NEXT JJ

PRINT USING "####.######"; RTIMEX% ,TORR,T(25),T(33),T(41),T(49),T(97)

IF RTIMEX% > 1800 THEN CONTINUE
IF TORR < V GOTO STEPTIME

CONTINUE:
OPEN "A:\DAB2P.DAT" FOR OUTPUT AS #1
FOR KK = 2 TO 35
WRITE #1, TL(KK),TM(KK),TN(KK),TK(KK)
NEXT KK
CLOSE 1

FOR KK = 2 TO 45
PRINT TL(KK),TM(KK),TN(KK),TK(KK)
NEXT KK

END
```

```
'THIS PROGRAM READS THE TEMPERATURES LOGED WITH
'"WORKBENCH™" PACKAGE INTO THE INVERSE HEAT TRANSFER
'ALGORITHM TO ESTIMATE THE FLUID TEMPERATURE AT A POINT OF
'ENTRY TO THE TUNDISH.
'
'INPUT DATA FROM A DATA FILE.
'
DIM THETMES1(100),THETMES2(100),THETMES3(100),THETFIT(3,S),
THETFITS(S,S),SIGMA(1,0), FTHETA(75,1), PTHETA(1,100), TEMPPRED(S),
X(100), Y(100), Z(100),TEMPRED(50)
'
OPEN "I", #1, "c:\dab1m.dat"
      FOR I = 0 TO 29
      INPUT #1, X$, Y$, Z$

      THETMES1(I) = VAL (X$)
      THETMES2(I) = VAL (Y$)
      THETMES3(I) = VAL (Z$)
      PRINT THETMES1(I), THETMES2(I), THETMES3(I)
      NEXT I
CLOSE 1
N = 0

'LSF OF TEMPERATURES

CONTINUE:
'
X(1) = 0.301 : X(2) = 0.6020 : X(3) = 0.77815
Y(1) = THETMES1(N) : Y(2) = THETMES2(N) : Y(3) = THETMES3(N)

SumX = 0 : SumY = 0
SumX2 = 0 : SumY2 = 0
SumXY = 0

FOR I = 1 TO 3
   X = X(I)
   Y = Y(I)
   SumX = SumX + X
   SumY = SumY + Y
   SumXY = SumXY + X * Y
   SumX2 = SumX2 + X * X
   SumY2 = SumY2 + Y * Y
NEXT I

SXX = SumX2 - SumX * SumX /3
SXY = SumXY - SumX * SumY /3
```

```
SYY = SumY2 - SumY * SumY /3
B = SXY / SXX

THETFITS(S,S) = ((SumX2 * SumY - SumX * SumXY)/3)/SXX
FOR I = 1 TO 3
   THETFIT(I,S) = THETFITS(S,S) + B * X(I)
   PRINT THETFIT(I,S)
NEXT I

PRINT THETFITS(S,S),THETFIT(1,S)

'CALCULATE THE CURRENT PARTIAL TEMPERATURES FROM THE
MEASURED TEMPERATURE.

FTHETA(0,1) = 0.424640
FTHETA(1,1) = 0.119570
FTHETA(2,1) = 0.058880
FTHETA(3,1) = 0.036400
FTHETA(4,1) = 0.025800
FTHETA(5,1) = 0.019400
FTHETA(6,1) = 0.015330
FTHETA(7,1) = 0.012510
FTHETA(8,1) = 0.010480
FTHETA(9,1) = 0.00896
FTHETA(10,1) = 0.007799
FTHETA(11,1) = 0.006885
FTHETA(12,1) = 0.006141
FTHETA(13,1) = 0.005555
FTHETA(14,1) = 0.004678
FTHETA(15,1) = 0.004345
FTHETA(16,1) = 0.004061
FTHETA(17,1) = 0.003817
FTHETA(18,1) = 0.003605
FTHETA(19,1) = 0.003417
FTHETA(20,1) = 0.003251
R=0
TIMESTEP:

      SIGMA(1,0) = 0

      FOR J = 10 TO 1 STEP -1
         JP = J - 1
         PTHETA(S,J) = PTHETA(S,JP)
      NEXT J

      FOR J = 1 TO R
```

```
        SIGMA(1,0) = SIGMA(1,0) + PTHETA(S,JP) * FTHETA(J,1)
        NEXT J

        PTHETA(S,0) = (THETMES1(N) - THETFIT(1,S) - SIGMA(1,0)) /
FTHETA(0,1)

        PRINT THETMES1(N), THETFIT(1,S), SIGMA(1,0),FTHETA(0,1)

        TEMPPRED(S) = THETFITS(S,S) + PTHETA(S,0)

        PRINT TEMPPRED(S)

        TEMPRED(N) = TEMPPRED(S)

        OPEN "B:\AWD5FM.DAT" FOR OUTPUT AS #1
        FOR K = 0 TO 21
            WRITE #1,TEMPRED(K)
        NEXT K
        CLOSE 1

        R = R + 1
        N = N + 1 : INPUT JBS : PRINT N

              IF N < 29 THEN GOTO TIMESTEP

END
```